NASA TECHNICAL NOTE

NASA TN D-5971

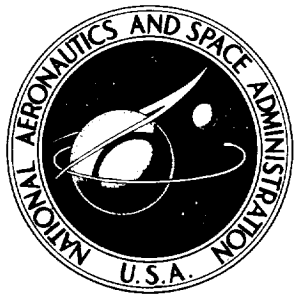

NASA TN D-5971

LONGITUDINAL AERODYNAMIC CHARACTERISTICS OF A TWIN-TURBOFAN SUBSONIC TRANSPORT WITH NACELLES MOUNTED UNDER THE WINGS

by Francis J. Capone

Langley Research Center
Hampton, Va. 23365

NATIONAL AERONAUTICS AND SPACE ADMINISTRATION • WASHINGTON, D. C. • OCTOBER 1970

1. Report No.	2. Government Accession No.	3. Recipient's Catalog No.
NASA TN D-5971		

4. Title and Subtitle	5. Report Date
LONGITUDINAL AERODYNAMIC CHARACTERISTICS OF A TWIN-TURBOFAN SUBSONIC TRANSPORT WITH NACELLES MOUNTED UNDER THE WINGS	October 1970
	6. Performing Organization Code
7. Author(s)	8. Performing Organization Report No.
Francis J. Capone	L-7141
	10. Work Unit No.
9. Performing Organization Name and Address	737-01-10-03
NASA Langley Research Center Hampton, Va. 23365	11. Contract or Grant No.
	13. Type of Report and Period Covered
12. Sponsoring Agency Name and Address	Technical Note
National Aeronautics and Space Administration Washington, D.C. 20546	14. Sponsoring Agency Code

15. Supplementary Notes

16. Abstract

An investigation has been conducted in the Langley 16-foot transonic tunnel to determine the longitudinal aerodynamic characteristics of a 0.062-scale, twin-turbofan subsonic transport at Mach numbers from 0.55 to 0.85 and angles of attack from about -2° to 6°. The Reynolds number based on wing mean aerodynamic chord varied from 2.25×10^6 to 2.70×10^6. The effects of model-component buildup, horizontal-tail effectiveness, boundary-layer transition, and wing and nacelle modifications were measured. The model was mounted by using a sting-strut arrangement with the strut entering the model through the underside of the fuselage approximately 65 percent of the fuselage length rearward of the model nose. Strut-interference effects were measured and applied as a correction to the data.

17. Key Words (Suggested by Author(s))	18. Distribution Statement
Subsonic aerodynamics Subsonic transport Strut interference	Unclassified – Unlimited

19. Security Classif. (of this report)	20. Security Classif. (of this page)	21. No. of Pages	22. Price*
Unclassified	Unclassified	93	$3.00

*For sale by the Clearinghouse for Federal Scientific and Technical Information
Springfield, Virginia 22151

LONGITUDINAL AERODYNAMIC CHARACTERISTICS OF A TWIN-TURBOFAN SUBSONIC TRANSPORT WITH NACELLES MOUNTED UNDER THE WINGS

By Francis J. Capone
Langley Research Center

SUMMARY

An investigation has been conducted in the Langley 16-foot transonic tunnel to determine the longitudinal aerodynamic characteristics of a 0.062-scale, twin-turbofan subsonic transport at Mach numbers from 0.55 to 0.85 and angles of attack from about -2° to 6°. The engine nacelles were mounted under the wings. The Reynolds number based on wing mean aerodynamic chord varied from 2.25×10^6 to 2.70×10^6. The effects of model-component buildup, horizontal-tail effectiveness, boundary-layer transition, and wing and nacelle modifications were measured. The model was mounted by using a sting-strut arrangement with the strut entering the model through the underside of the fuselage approximately 65 percent of the fuselage length rearward of the model nose. Strut-interference effects were measured and applied as a correction to the data.

For the small range of tail deflection (-0.5° to 0.5°), there was little or no effect of horizontal-tail deflection on lift-curve slope, model stability, drag coefficient, or maximum lift-drag ratio. The model with free boundary-layer transition had more lift at high angles of attack and less stability; and for tail deflections of 0° and 0.5°, the lift coefficient at which pitchup instabilities occurred was higher than that for the model with fixed transition. The configuration with a modified wing (reduced wing thickness ratio) and longer nacelles had greater lift at the same angle of attack and a higher lift coefficient at which pitchup instabilities occurred than did the basic configuration. The drag-rise Mach number for the modified configuration was increased by 0.02, and the modified configuration had much less drag due to lift at the higher Mach numbers than that of the basic configuration.

INTRODUCTION

The National Aeronautics and Space Administration has conducted a wind-tunnel investigation to obtain data for a correlation between wind-tunnel and flight-test results for a twin-turbofan, short-haul, subsonic transport with engines mounted under the wings. This airplane is capable of carrying about 100 passengers. This report presents only the results of the wind-tunnel investigation.

The wind-tunnel investigation was conducted with a 0.062-scale model in the Langley 16-foot transonic tunnel at Mach numbers from 0.55 to 0.85 and angles of attack from -2^{o} to about 6^{o}. The Reynolds number based on wing mean aerodynamic chord varied from 2.25×10^{6} to 2.70×10^{6}. The effects of model-component buildup, horizontal-tail effectiveness, boundary-layer transition, and wing and nacelle modifications were measured.

Subsonic transports are frequently designed with fuselage aftersections that are nonsymmetrical with a large amount of upsweep on the bottom of the afterbody. The pressure drag on this section of the fuselage can be a large part of the total fuselage drag. A recent investigation as reported in reference 1 was concerned with evaluating the sting-support interference effects of a conventional straight sting that entered through the rear of three subsonic transport models. However, the straight sting required a rather large cutout on the afterbody of the fuselage.

The model of the present investigation was mounted in the wind tunnel by using a sting-strut support arrangement with the strut entering the model through the underside of the fuselage approximately 65 percent of the fuselage length rearward of the model nose which minimized alterations to the fuselage. Strut-support interference effects were determined and applied as a correction to the measured aerodynamic characteristics.

SYMBOLS

Model forces and moments are referred to a stability axis system with the model moment reference center located 82.80 centimeters rearward of the model nose corresponding to 22.4 percent of the wing mean aerodynamic chord which is approximately at the nominal center-of-gravity position of the airplane. Dimensions are given in the International System of Units (SI).

A	aspect ratio
c	local wing chord
$\bar{c}$	wing or tail mean aerodynamic chord (Wing $\bar{c}$ = 21.17 centimeters)
$C_{A,i}$	nacelle internal axial-force coefficient
C_D	drag coefficient, $\frac{\text{Drag}}{qS}$
$C_{D,p}$	computed profile drag coefficient
$C_{D,min}$	minimum drag coefficient

$C_{D,trim}$ trim drag coefficient

C_L lift coefficient, $\frac{Lift}{qS}$

$C_{L,M}$ lift coefficient at $C_{D,min}$

$C_{L,trim}$ trim lift coefficient (lift coefficient at $C_m = 0$)

C_{L_α} lift-curve slope per degree

C_m pitching-moment coefficient, $\frac{\text{Pitching moment}}{qS\bar{c}}$

$C_{m_{C_L}}$ static-longitudinal-stability parameter, $\frac{\partial C_m}{\partial C_L}$

$C_{m,o}$ pitching-moment coefficient at zero lift

$\Delta C_{D,av}$ average drag-coefficient increment due to strut interference, $(C_D)_{\text{with strut}} - (C_D)_{\text{without strut}}$

$\Delta C_{D,HV}$ drag-coefficient increment due to adding horizontal and vertical tails

$\Delta C_{D,N_1}$ drag-coefficient increment due to adding nacelle 1 and pylon

$\Delta C_{L,av}$ average lift-coefficient increment due to strut interference, $(C_L)_{\text{with strut}} - (C_L)_{\text{without strut}}$

$\Delta C_{m,av}$ average pitching-moment-coefficient increment due to strut interference, $(C_m)_{\text{with strut}} - (C_m)_{\text{without strut}}$

k_M drag-due-to-lift factor, $\frac{dC_D}{d(C_L - C_{L,M})^2}$

L/D lift-drag ratio

$(L/D)_{max}$ maximum lift-drag ratio

$(L/D)_{trim}$ lift-drag ratio at trim conditions

M free-stream Mach number

q	free-stream dynamic pressure
R	Reynolds number per meter
S	wing reference area (3674.30 centimeters^2)
T_t	stagnation temperature
x,z	wing coordinates
α_w	wing angle of attack (1^o with respect to body center line)
δ_h	incidence angle of horizontal tail, positive when trailing edge is down

Subscripts:

l	lower
u	upper

Abbreviations:

LER	leading-edge radius
WL	water line

Model-component designations:

B	fuselage plus wing-root-flap actuator fairing
H	horizontal tail
N_1	basic nacelle and pylon
N_2	basic nacelle and pylon with rear-end extension
T	wing trailing-edge-flap actuator fairings (two each located outboard on wing)
V	vertical tail

W_1 basic wing

W_2 basic wing plus leading- and trailing-edge chord extensions

W_3 basic wing plus trailing-edge chord extension

APPARATUS

Model

The complete 0.062-scale basic model is shown in the sketch and photographs of figures 1 and 2, respectively. The model represented a twin-turbofan, short-haul, subsonic transport weighing about 45 000 kilograms that was capable of carrying about 100 passengers at a cruise Mach number between 0.78 and 0.80. The design lift coefficient is 0.30. Details of the various model components are presented in figure 3.

Fuselage.- Fuselage geometry and cross sections are shown in figures 3(a) and 3(b), respectively. The fuselage was 171.19 centimeters long and had a fineness ratio of 6.9 based on the maximum body depth. The wing root fairing was located between fuselage stations 54.33 and 109.76. A fairing on the fuselage used to house a wing trailing-edge flap track and actuator mechanism extended from station 85.04 to 105.03. (See fig. 3(b).) The wing trailing-edge flaps were not simulated during this investigation.

Basic wing.- The planform geometry of the basic wing (W_1) is shown in figure 3(c). The basic wing had an aspect ratio of 8.41, a span of 175.59 centimeters, an incidence angle of 1°, and a dihedral angle of 6°. Both the leading and trailing edges had discontinuous sweep. Airfoil ordinates for the basic wing are presented in table I(a). The model with the basic wing is shown in the photographs of figure 2.

Two modifications were made to the basic wing as shown in figure 3(d). The modification for wing 2 (W_2) consisted of a 1-percent-chord leading-edge extension and a 15-percent-chord trailing-edge extension, both outboard of span station 32.19 which was the spanwise location of the break in the leading and trailing edges of the basic wing. The trailing edge also extended inboard to the nacelle pylon. Photographs of the model with this wing are presented in figure 4. The modification for wing 3 (W_3) involved only a trailing-edge extension from 15 percent chord at span station 32.19 to 0 percent chord at span station 65.67. The model with this wing is shown in the photographs of figure 5. Airfoil ordinates for wings 2 and 3 are presented in table I(b). These ordinates were nondimensionalized with respect to the local chords of wing 1. Therefore, these modifications reduce the wing thickness ratio when based on the chord of the modified wing. For example, at span station 32.19, the maximum wing thickness ratio for wing 1 (based on the chord of wing 1) is 0.108, and for wing 3 the maximum thickness ratio is 0.095 (based on

the chord of wing 3). It should be noted that wings 2 and 3 were tested with a different nacelle from that on wing 1 and without the flap-track fairings on the wings. The flap-track fairing at the wing root, however, was present.

Only the complete model using wing 1 included fairings on the wing for the wing flap tracks and actuators. A sketch of the fairings is presented in figure 3(e). These fairings were located at span stations 40.64 and 56.82 and are shown in the photographs of figure 2.

Nacelles.- Sketches of the two nacelles tested are presented in figure 3(f). Nacelle 1 (N_1) was 34.54 centimeters long and was tested only with wing 1. Nacelle 2 (N_2) was similar to nacelle 1 except that the rear portion was extended 7.08 centimeters resulting in a total length of 41.62 centimeters. This nacelle was tested only with wings 2 and 3. Both nacelle inlets had the same geometry and were located at the same body station.

Horizontal and vertical tails.- Figures 3(g) and 3(h) show the planform geometry of the horizontal and vertical tails, respectively. Airfoil ordinates are presented in tables II and III. The horizontal tail was all-movable with the hinge axis located at fuselage station 160.93.

Model Support System

The present investigation utilized a sting-strut mount in order to minimize the alterations made to the fuselage for a support system. A sketch showing the various support systems is presented in figure 6. For determining the aerodynamic characteristics of the model, the model was supported with the strut entering through the underside of the fuselage at a location approximately 65 percent of the fuselage length to the rear of the nose as shown by the sting-strut arrangement of figure 6(a). This mounting system is also shown in the photographs of figures 2, 4, and 5. This type of strut allowed for the minimum amount of cutout to the model (as compared with the large amount of cutout to the models of ref. 1) since the strut chord length at the body juncture was about 25.4 centimeters with a maximum thickness of about 2.54 centimeters.

In order to assess the magnitude of the strut interference, two additional support systems were used as shown in figures 6(b), 6(c), and the photographs of figure 7. Figures 6(b) and 7(a) show the model with the strut entering through the top of the model. A dummy sting strut was attached to the live sting strut through a blade downstream of the model base. The dummy strut entered through the bottom of the model (at the same location as the live strut). A positioning pin that was part of the dummy strut fit loosely into the balance support block and was the only point of contact inside the model. The loose fit of the pin allowed model deflection with the same aeroelastic support stiffness as existed with only the live strut present. The support system of figures 6(c) and 7(b)

shows the model with only the live strut entering through the top of the model (dummy sting strut removed). The gaps between the struts and model were sealed with synthetic sponge rubber. Pressure inside the model was continuously monitored in order to detect and warn of possible leakage through the seal if it occurred. Calibrations of normal force, axial force, and pitching moment with the model assembled showed no restraint due to this method of sealing. It should be noted that the vertical tail could not be attached while using the top mount system.

Because of the mounting arrangements, the model was tested above and below the wind-tunnel center line (fig. 6). Therefore, it was necessary to test the wing-body combination upright and inverted in both wind-tunnel positions in order to determine the magnitude of the wind-tunnel flow angularity. This was accomplished by using the sting-strut—dummy-strut combination with the live strut coming into the model from either the top or bottom as shown in the following table:

Model position to tunnel center line	Live strut	Dummy strut	Model attitude
Below	Top	Bottom	Upright
Below	Bottom	Top	Inverted
Above	Top	Bottom	Inverted
Above	Bottom	Top	Upright

Wind Tunnel and Instrumentation

This investigation was conducted in the Langley 16-foot transonic wind tunnel which is a single-return, atmospheric wind tunnel with a slotted octagonal test section and continuous air exchange. For models mounted along the tunnel center line, the model-support angle-of-attack mechanism pivots the sting support in such a manner that the model is close to the center line. However, for the present investigation with its sting-strut arrangement, that puts the model either above or below the tunnel center line, there is some translation of the model along with the rotation. The center of model rotation is indicated in figure 6.

Aerodynamic forces were measured with an internally located, six-component strain-gage balance. Angle of attack was determined with a pendulum-type strain-gage inclinometer located inside the model nose. For the determination of nacelle internal axial force, stagnation pressures at the nacelle-duct exit were measured on a pressure-scanning unit; whereas static pressures at the nacelle-duct exit were measured with individual pressure transducers.

TESTS

This investigation was conducted at Mach numbers from 0.55 to 0.85 and at wing angles of attack from -2° to about 6°. The Reynolds number based on the mean aerodynamic chord varied from 2.25×10^6 to 2.70×10^6. All model configurations except as noted were tested with boundary-layer transition strips consisting of No. 120 silicon carbide grit particles sparsely distributed in a thin film of lacquer that was 0.25 centimeter wide. These strips were located on both the upper and lower surfaces of the wings and tails at 10 percent of the local streamwise chord, on the nacelles (outside and inside) at 0.76 centimeter from the nacelle leading edge, and on the fuselage nose at 2.54 centimeters from the tip of the nose. The grit size and the location of the strips were determined according to the recommendations of reference 2.

The aerodynamic characteristics of the various model configurations were determined with the model mounted in the wind tunnel as shown in figures 2, 4, 5, and 6(a), that is, with the strut entering the model from the bottom. The effects of model-component buildup, horizontal-tail deflections ($\delta_h = 0^{\circ}$ and $\pm 0.5^{\circ}$), boundary-layer transition not artificially fixed, and two wing and nacelle modifications were studied.

Sting-strut interference effects were measured by testing configuration BW_1H ($\delta_h = -0.5^{\circ}$) which was supported by the three methods shown in figure 6. Wind-tunnel flow angularity was determined by conducting tests of configuration BW_1, upright and inverted, both above and below the wind-tunnel center line. Both configurations BW_1H and BW_1 were tested with transition fixed. The methods of support for this portion of the tests were summarized in a previous section entitled "Apparatus." Nacelle internal axial force was determined from measurements of both static and stagnation pressure at the exit of one nacelle by means of a pressure survey rake that was rigidly attached to the nacelle.

CORRECTIONS AND ACCURACY

General Corrections

The wind-tunnel flow angularity as determined by tests of the model upright and inverted, both above and below the wind-tunnel center line, was found to be 0°. The measured balance axial force was corrected for nacelle internal axial force shown in figure 8. The effects of nacelle incidence and the variation of $C_{A,i}$ with angle of attack were accounted for in applying the correction to the balance axial force.

No corrections have been made for roughness drag due to the grit applied for the boundary-layer transition strips. These corrections are considered unnecessary at subsonic speeds since the general guideline for the application of transition strips (ref. 3)

and a grit height based on a transitional Reynolds number of 600 were used. (See also ref. 2.) Corrections to the lift data from either solid-blockage interference or tunnel-boundary interference effects are not considered necessary. Theoretical calculations presented in reference 4 for a model with approximately the same wing span and cross-sectional area have shown that the tunnel-wall lift-interference correction reduced the angle of attack by $0.02C_L$. For the model of reference 4, the reduced angle of attack at $C_L = 0.5$ reduced the drag coefficient by 0.0001. Since there is no Mach number gradient in the Langley 16-foot transonic tunnel, no corrections for buoyancy are made.

Since the gap between the strut and the model was sealed with the synthetic sponge rubber, no corrections are necessary for either the base or balance cavity. An advantage of this type of mounting over that of reference 1 can be seen in the application of corrections to the measured aerodynamic characteristics due to the effects of the sting cavity. It was necessary in the investigation of reference 1 to measure the longitudinal variation of cavity pressure along the sting and fuselage-sting cavity. In addition to correcting the axial force (to the condition of free-stream static pressure acting across the sting cavity), an adjustment is necessary to both normal force and pitching moment. This was done by integrating the pressures along the sting longitudinally and obtaining incremental corrections.

Sting-Strut Interference Correction

The technique used to determine the sting-strut interference effects was similar to that described in reference 1. Force and moment measurements made with the model supported with the strut through the bottom of the model (fig. 6(a)) will, of course, contain an interference term of the bottom strut on the model that must be subtracted from the measurements made. This interference term can be evaluated from measurements made when the model is supported as shown in figures 6(b) and 6(c).

When the model is supported with the strut through the top and the dummy strut in place from the bottom (fig. 6(b)), the measured forces contain interference terms caused by both the top and bottom struts. The interference term due to only the top strut is contained in the measured data when the model is supported as shown in figure 6(c). Therefore, subtracting the coefficient data measured when the model is supported as shown in figure 6(c) from that of figure 6(b) will result in the desired strut-interference term.

The variation of strut-interference terms for lift, drag, and pitching moment with wing angle of attack for the Mach numbers investigated is presented in figure 9. Shown are average faired values for each of these components. Corrections to the measured aerodynamic data were made automatically when processing the data by computer by inputing a table of the strut-interference terms as a function of the wing angle of attack at 0.25° increments and linearly interpolating between input points.

Accuracy

The accuracy of data presented herein prior to making corrections for strut interference, based primarily on expected instrumentation accuracies, is presented as follows:

M	±0.007
α_w, deg	±0.10
C_L	±0.004
C_D	±0.0005
C_m	±0.003
δ_h, deg	±0.03

PRESENTATION OF RESULTS

The basic longitudinal aerodynamic force and moment coefficients are presented in figures 10 to 14 as follows:

Configuration	δ_h, deg	Transition	Figure
BW_1 and BW_1HV	-0.5	Fixed	10
BW_1HVN_1T	-.5	Fixed and free	11
BW_1HVN_1T	0	Fixed and free	12
BW_1HVN_1T	.5	Fixed and free	13
BW_1HVN_1, BW_2HVN_2, and BW_3HVN_2	-.5	Fixed	14

Various summary plots of the longitudinal aerodynamic characteristics are presented in figures 15 to 19 as follows:

	Figure
Effect of model-component buildup	15
Computed profile drag coefficients	16
Effect of horizontal-tail deflection	17
Effect of fixing boundary-layer transition	18
Effect of wing and nacelle modifications	19

DISCUSSION

Effect of Model-Component Buildup

The effects of model-component buildup can be seen by comparing the basic data presented in figures 10, 11, and 14 and the summary data of figure 15 for configurations BW_1, BW_1HV, BW_1HVN_1, and BW_1HVN_1T with $\delta_h = -0.5^\circ$ and the transition fixed. The

lift curves for these configurations are linear over the angle-of-attack range investigated at Mach numbers of 0.55 and 0.625. At $M = 0.725$ or greater, nonlinearities in the lift curves occurred at lower lift coefficients as Mach number was increased.

The pitching-moment curves exhibited nonlinearities at approximately the same value of C_L as the lift curves with the model either becoming neutrally stable (except BW_1) or having a pitchup instability.

Lift-curve slope C_{L_α} increased by about 10 percent up to $M = 0.825$ with the addition of the tail surfaces (fig. 15(a)). The nacelles caused a further small increase in C_{L_α} up to $M = 0.80$, whereas there was no effect on C_{L_α} of adding the flap-track fairings.

The nacelles and flap-track fairings together (compare configurations BW_1HV and BW_1HVN_1T) are seen to cause a reduction in both the stability $C_{m_{C_L}}$ and in $C_{m,o}$ (fig. 15(a)). This reduction in $C_{m,o}$ is 0.026 at $M = 0.55$ and 0.039 at $M = 0.80$. This reduction in $C_{m,o}$ results in $C_{L,trim}$ being reduced from 0.355 to 0.320 at $M = 0.55$, whereas $C_{L,trim}$ is reduced from 0.5 to 0.3 at $M = 0.80$. (See figs. 10 and 11.)

The effects on minimum drag and drag at lifting conditions caused by the various model components are shown in figure 15(b). Computed profile drag coefficients and measured incremental drag coefficients for the tail surfaces and the nacelles are presented in figure 16. Skin-friction drag coefficients were computed by the methods of references 5 and 6. Wetted areas, reference lengths, average Reynolds number per meter, wind-tunnel stagnation temperature, and computed $C_{D,p}$ are presented in table IV. Form factors given in chapter XXIV of reference 7 were used to obtain the profile drag coefficients from the skin-friction drag coefficients. The incremental drag due to a particular model component is nearly constant with Mach number up to $M = 0.775$ at each of the lift coefficients presented (fig. 15(b)). Addition of the tails caused an increase in $C_{D,min}$ from 0.0049 at $M = 0.55$ to 0.0060 at $M = 0.85$ (fig. 16). This drag increment was 0.0008 to 0.0020 higher than the computed profile drag coefficient, probably due to some tail drag due to lift and interference of the tails on the fuselage afterbody.

The same observations can be made for the addition of the nacelles where an interference drag of about 0.0006 is indicated up to about $M = 0.775$ at minimum drag conditions (fig. 16). Both of the incremental drag coefficients caused from adding either the tails or nacelles indicate drag-rise Mach numbers of about 0.775. The drag-rise Mach number $\left(\text{where } dC_{D,min}/dM = 0.1\right)$ is between 0.78 and 0.80 for the complete configuration BW_1HVN_1T (fig. 15(b)).

The maximum lift-drag ratio for configuration BW_1 was 20.2. (See fig. 15(c).) A loss in L/D of about 4 occurred due to the addition of the remainder of the model components and resulted in a value of $(L/D)_{max}$ of 16.2 for configuration BW_1HVN_1T.

Effect of Horizontal-Tail Deflection

The effect of horizontal-tail deflection for the complete configuration BW_1HVN_1T with transition fixed or free can be seen by comparing the basic data of figures 11, 12, and 13 and the summary data of figure 17 for the condition of transition fixed.

Horizontal-tail deflection had little or no effect on lift-curve slope and only a small effect on the model stability (fig. 17(a)). The effects due to this small range of tail deflection on $C_{D,min}$ or C_D at lifting conditions (fig. 17(b)) and on $(L/D)_{max}$ (fig. 17(c)) were small as expected. Trimmed drag polars are presented in figure 17(d) where the symbols represent the trim points obtained from the pitching-moment data of figures 11, 12, and 13 for the transition-fixed conditions.

Effect of Boundary-Layer Transition

The basic aerodynamic data for configuration BW_1HVN_1T for three horizontal-tail deflections with boundary-layer transition fixed and free are presented in figures 11, 12, and 13, and summary data are presented in figure 18. Generally, fixing transition had little or no effect on C_{L_α} up to M = 0.825. Lift-curve slopes shown in figure 18(a) for $\delta_h = -0.5^o$ are a typical example. The model with free transition had more lift at high angles of attack at Mach numbers greater than 0.75 for the three tail deflections.

For the model with $\delta_h = -0.5^o$ (fig. 11), the pitching-moment curves were more linear over a greater range of lift coefficient with transition fixed. Pitchup occurs at approximately the same lift coefficient. However, for the model with $\delta_h = 0^o$ or 0.5^o (figs. 12 and 13, respectively), the pitching-moment curves were linear over the same range of lift coefficient with transition both free and fixed, and the lift coefficient at which the pitchup instability occurred was substantially higher.

Shown in figure 18(a) is $C_{m_{C_L}}$ for the three tail deflections with transition free and also $C_{m_{C_L}}$ for $\delta_h = -0.5^o$ with transition both fixed and free. The variation $C_{m_{C_L}}$ with transition fixed and free at the other two tail deflections (0^o and 0.5^o) is similar to that shown in figure 17(a). Figure 18(b) presents $C_{m,o}$ data with transition fixed and free for the three tail deflections. The model with transition free exhibited lower stability and higher values of pitching-moment coefficient at zero lift. A comparison of $C_{m_{C_L}}$ curves with transition fixed and free (figs. 18(a) and 18(b)) shows a rearward shift in the center of pressure due to fixing transition from 5 to 10 percent of the mean aerodynamic chord at Mach numbers up to 0.75.

The effects on drag and lift-drag ratio of fixing transition are compared only for $\delta_h = -0.5^o$ in figures 18(c) and 18(d). The results for the other two tail settings are similar. As expected, the free-transition condition exhibited lower drag and higher $(L/D)_{max}$ than the fixed-transition condition.

Effect of Wing Modification

A comparison of the aerodynamic effects due to the two wing modifications for the complete model without the flap-track fairings, with transition fixed and $\delta_h = -0.5^o$, is shown by the basic data of figure 14 and the summary data of figure 19. These modifications, made to the basic wing (W_1) outboard of the nacelle (span station 30.07), were intended to increase aerodynamic performance between the cruise Mach numbers of 0.78 and 0.80 and possibly to increase the cruise Mach number. Wing 2 (W_2) had both a 1-percent-chord leading-edge extension and a 15-percent-chord trailing-edge extension which resulted in the leading-edge sweep being increased from 27.58^o to 27.68^o. Wing 3 (W_3) had only a 15-percent-chord trailing-edge extension at span station 32.19 which tapered to 0 percent chord at span station 65.67. (See figs. 3(c), 3(d), 4, and 5.) Both wings 2 and 3 were tested with the longer nacelle. (See fig. 3(f).)

Configuration BW_2HVN_2 had a higher lift-curve slope C_{L_α} over the entire Mach number range than that of BW_1HVN_1, whereas C_{L_α} for configuration BW_3HVN_2 was higher only at Mach numbers greater than 0.775 (fig. 19(a)).

Except at the lower Mach numbers and at $M = 0.85$, the three wings had about the same stability (fig. 19(a)). However, the modifications to the basic wing increased the lift coefficient at which pitchup instabilities occurred (fig. 14). Configuration BW_2HVN_2 showed no pitchup tendencies until $M = 0.775$.

The drag characteristics of figure 19(b) show configuration BW_2HVN_2 to have lower drag as Mach number and lift coefficient are increased. At $C_L = 0.3$ and $M = 0.8$ the drag coefficient of this configuration is 0.0058 less than that of configuration BW_1HVN_1. The drag-rise Mach number for configuration BW_2HVN_2 is about 0.82 as compared with a Mach number range from 0.78 to 0.80 for configuration BW_1HVN_1. It should be noted that the aerodynamic coefficients presented in figures 14 and 19 were computed based upon the reference wing area of configuration BW_1HVN_1. Using the actual wing area, for example, of configuration BW_2HVN_2 would decrease the drag coefficients by some 7 percent.

From the lift-drag polars of figure 14 it is obvious that significant changes in drag-due-to-lift factor, especially at high Mach numbers, were a result of the wing modifications. Therefore, the drag-due-to-lift factor k_M for each configuration has been determined by fitting the equation

$$C_D = C_{D,min} + k_M(C_L - C_{L,m})^2$$

to the lift-drag polars. (See refs. 8 and 9.) The resulting drag-due-to-lift factors are presented in figure 19(c) in product form k_MA. In this form, k_MA is independent of the wing reference area used in calculating the two parameters. This equation was fitted over a range of lift coefficients from about -0.1 to the lift coefficient just below C_L for $(L/D)_{max}$. Also presented in figure 19(c) are the conditions for zero suction A/C_{L_α}, and for 100 percent suction $1/\pi$.

The abrupt rise in the drag-due-to-lift factor for configuration BW_2HVN_2 occurs at $M = 0.80$ which is 0.05 higher than that for the other two configurations. This probably results from the lower thickness ratio of the modified wing and the higher critical Mach number of the airfoil.

Lift-drag-ratio characteristics are shown in figure 19(d). Up to $M = 0.725$, wing modifications have little or no effect on $(L/D)_{max}$. However, at higher Mach numbers, the modified wings display higher values of $(L/D)_{max}$ than those of the unmodified wing. For example, at $M = 0.80$, $(L/D)_{max}$ for configuration BW_2HVN_2 was 3.4 higher than that for BW_1HVN_1.

SUMMARY OF RESULTS

An investigation has been conducted in the Langley 16-foot transonic tunnel to determine the longitudinal aerodynamic characteristics of a 0.062-scale, twin-turbofan subsonic transport at Mach numbers from 0.55 to 0.85 and angles of attack from about -2^o to 6^o. The Reynolds number based on wing mean aerodynamic chord varied from 2.25×10^6 to 2.70×10^6. The effects of model-component buildup, horizontal-tail effectiveness, boundary-layer transition, and wing and nacelle modifications were measured. The model was mounted by using a sting-strut arrangement with the strut entering the model through the underside of the fuselage approximately 65 percent of the fuselage length rearward of the model nose. Strut-interference effects were measured and applied as a correction to the data. The investigation indicated the following results:

1. For the small range of tail deflection (-0.5^o to 0.5^o), there was little or no effect of horizontal-tail deflection on lift-curve slope, model stability, drag coefficient, or maximum lift-drag ratio.

2. The model with free boundary-layer transition had more lift at high angles of attack and less stability; and for tail deflections of 0^o and 0.5^o, the lift coefficient at which pitchup instability occurred was higher than that for the model with fixed transition. The model with free transition had lower stability over the Mach number range tested.

3. The configuration with a modified wing (reduced wing thickness ratio) and longer nacelles had greater lift at the same angle of attack and a higher lift coefficient at which pitchup instabilities occurred than that of the basic configuration. The drag-rise Mach number for the modified configuration was 0.02 higher than that of the basic configuration, and the modified configuration had much less drag due to lift at the higher Mach numbers.

Langley Research Center,
National Aeronautics and Space Administration,
Hampton, Va., June 19, 1970.

REFERENCES

1. Loving, Donald L.; and Luoma, Arvo A.: Sting-Support Interference on Longitudinal Aerodynamic Characteristics of Cargo-Type Airplane Models at Mach 0.70 to 0.84. NASA TN D-4021, 1967.

2. Braslow, Albert L.; and Knox, Eugene C.: Simplified Method for Determination of Critical Height of Distributed Roughness Particles for Boundary-Layer Transition at Mach Numbers From 0 to 5. NACA TN 4363, 1958.

3. Braslow, Albert L.; Hicks, Raymond M.; and Harris, Roy V., Jr.: Use of Grit-Type Boundary-Layer-Transition Trips on Wind-Tunnel Models. NASA TN D-3579, 1966.

4. Luoma, Arvo A.; Re, Richard J.; and Loving, Donald L.: Subsonic Longitudinal Aerodynamic Measurements on a Transport Model In Two Slotted Tunnels Differing in Size. NASA TM X-1660, 1968.

5. Schoenherr, Karl E.: Resistance of Flat Surfaces Moving Through a Fluid. Trans. Soc. Naval Architects Marine Eng., 1932, pp. 279-313.

6. Sommer, Simon C.; and Short, Barbara J.: Free-Flight Measurements of Turbulent-Boundary-Layer Skin Friction in the Presence of Severe Aerodynamic Heating at Mach Numbers From 2.8 to 7.0. NACA TN 3391, 1955.

7. Schlichting, Hermann (J. Kestin, transl.): Boundary Layer Theory. Fourth ed., McGraw-Hill Book Co., Inc., c.1960.

8. Igoe, William B.; Re, Richard J.; and Cassetti, Marlowe D.: Transonic Aerodynamic Characteristics of a Wing-Body Combination Having a 52.5° Sweptback Wing of Aspect Ratio 3 With Conical Camber and Designed for a Mach Number of $\sqrt{2}$. NASA TN D-817, 1961.

9. Re, Richard J.; and Stumbris, Gunars: An Investigation at Mach Numbers From 0.40 to 1.00 of a Model With a Wing Having Inboard Sections Cambered for Mach 1.2. NASA TN D-3419, 1966.

TABLE I.- WING AIRFOIL ORDINATES

(a) Wing 1

Wing 1 span stations at –															
11.219				16.441				25.484				32.189 to 82.204			
x_u/c	z_u/c	x_l/c	z_l/c	x_u/c	z_u/c	x_l/c	z_l/c	x_u/c	z_u/c	x_l/c	z_l/c	x/c	z_u/c	z_l/c	
0	0.0177	0	0.0177	0	0.0088	0	0.0088	0	0	0	0	0	0	0	
.0023	.0309	.0022	.0038	.0026	.0198	.0021	.0004	.0019	.0057	.0022	-.0040	.0025	.0070	-.0051	
.0050	.0372	.0049	-.0018	.0047	.0236	.0051	-.0037	.0060	.0105	.0049	-.0057	.0050	.0100	-.0066	
.0076	.0415	.0072	-.0053	.0075	.0275	.0078	-.0062	.0078	.0120	.0070	-.0066	.0075	.0123	-.0077	
.0143	.0499	.0119	-.0106	.0129	.0332	.0139	-.0103	.0129	.0157	.0125	-.0076	.0125	.0160	-.0091	
.0249	.0582	.0243	-.0204	.0229	.0408	.0230	-.0147	.0237	.0218	.0209	-.0101	.0250	.0232	-.0116	
.0495	.0730	.0486	-.0342	.0530	.0552	.0509	-.0244	.0505	.0324	.0555	-.0147	.0500	.0335	-.0148	
.0740	.0814	.0716	-.0437	.0736	.0613	.0725	-.0301	.0794	.0402	.0816	-.0174	.0750	.0410	-.0174	
.0990	.0866	.0979	-.0516	.0996	.0666	.0961	-.0352	.0975	.0441	.1078	-.0201	.1000	.0468	-.0200	
.1530	.0907	.1488	-.0607	.1513	.0728	.1513	-.0432	.1511	.0524	.1571	-.0247	.1500	.0549	-.0246	
.1961	.0905	.1953	-.0632	.2080	.0756	.2080	-.0477	.2036	.0576	.2036	-.0286	.2000	.0606	-.0291	
.2504	.0887	.2501	-.0632	.2500	.0761	.2500	-.0493	.2500	.0606	.2500	-.0319	.2500	.0643	-.0331	
.3094	.0858	.2945	-.0626	.2972	.0756	.3095	-.0500	.2964	.0623	.2964	-.0347	.3000	.0662	-.0359	
.3520	.0833	.3579	-.0610	.3602	.0734	.3449	-.0498	.3468	.0629	.3549	-.0370	.3500	.0678	-.0388	
.3919	.0804	.3965	-.0595	.4075	.0705	.3981	-.0486	.3990	.0625	.3996	-.0375	.4000	.0678	-.0402	
.4477	.0756	.4543	-.0563	.4547	.0667	.4512	-.0463	.4447	.0608	.4532	-.0366	.4500	.0668	-.0404	
.5034	.0696	.5050	-.0527	.5101	.0614	.5066	-.0428	.4904	.0597	.4911	-.0352	.5000	.0646	-.0393	
.5593	.0626	.5556	-.0482	.5525	.0567	.5490	-.0397	.5486	.0529	.5434	-.0328	.5500	.0611	-.0371	
.5965	.0575	.6063	-.0427	.6001	.0512	.5966	-.0357	.6091	.0470	.6269	-.0282	.6000	.0563	-.0339	
.6488	.0498	.6485	-.0375	.7003	.0388	.6889	-.0275	.6571	.0422	.7396	-.0220	.7000	.0437	-.0257	
.8331	.0224	.8317	-.0149	.8266	.0233	.8505	-.0131	.8741	.0183	.7832	-.0190	.8000	.0291	-.0172	
.9109	.0132	.9410	-.0053	.9021	.0142	.9313	-.0060	.9470	.0076	.9354	-.0056	.9000	.0145	-.0086	
1.0000	.0003	1.0000	-.0003	1.0000	.0004	1.0000	-.0004	1.0000	.0005	1.0000	-.0005	1.0000	.0008	-.0008	
c, cm . . .	37.229			33.439				26.881				22.017 at 32.189; 10.815 at 82.204			
LER/c . . .	0.0380			0.0180				0.0042				0.0049			

TABLE I.- WING AIRFOIL ORDINATES – Concluded

(b) Wings 2 and 3

x/c	Wing 2 span stations at 32.189 and outboard –	
	z_u/c	z_l/c
-0.0100	0	0
0	.0040	-.0040
.0025	.0105	-.0035
.0050	.0135	-.0050
.0100	.0190	-.0070
.0250	.0284	-.0100
.0500	.0385	-.0135
.1000	.0489	-.0190
.1500	.0559	
.2000	.0608	
.3000	.0670	-.0365
.3500	.0685	-.0390
.4000	.0694	-.0405
.4500	.0700	-.0400
.5000	.0710	-.0394
.5500	.0710	-.0375
.6000	.0710	-.0340
.6500	.0700	-.0300
.7000	.0675	-.0259
.7500	.0640	-.0223
.8000	.0590	-.0177
.8500	.0530	-.0143
.9000	.0465	-.0102
.9500	.0400	-.0035
1.0000	.0329	-.0023
1.0500	.0258	.0018
1.1000	.0183	.0054
1.1500	.0110	.0110
Span station 32.189, c = 22.017 cm Span station 71.928, c = 13.129 cm		

x/c	Wing 3 span stations at –			
	32.189		48.928	
	z_u/c	z_l/c	z_u/c	z_l/c
0	0	0	0	0
.0025	.0070	-.0051	.0070	-.0051
.0050	.0100	-.0066	.0100	-.0066
.0250	.0232	-.0116	.0232	-.0116
.0500	.0335	-.0148	.0335	-.0145
.1000	.0468	-.0200	.0464	-.0206
.1500	.0549	-.0246	.0551	-.0248
.2000	.0606	-.0291	.0601	-.0286
.3000	.0670	-.0365	.0670	-.0365
.3500	.0685	-.0390	.0680	-.0389
.4000	.0694	-.0405	.0687	-.0407
.4500	.0700	-.0400	.0687	-.0407
.5000	.0710	-.0394	.0687	-.0395
.5500	.0710	-.0375	.0673	-.0375
.6000	.0710	-.0340	.0650	-.0340
.6500	.0700	-.0300	.0602	-.0303
.7000	.0675	-.0259	.0576	-.0260
.7500	.0640	-.0223	.0526	-.0220
.8000	.0590	-.0177	.0464	-.0175
.8500	.0530	-.0143	.0400	-.0129
.9000	.0465	-.0102	.0330	-.0092
.9500	.0400	-.0035	.0267	-.0056
1.0000	.0329	-.0023	.0189	-.0017
1.0500	.0258	.0018	.0120	.0019
1.0900			.0043	.0043
1.1500	.0110	.0110		
c, cm . . .	22.017		18.263	
LER/c . . .	0.0049		0.0049	

TABLE II.- HORIZONTAL-TAIL AIRFOIL ORDINATES

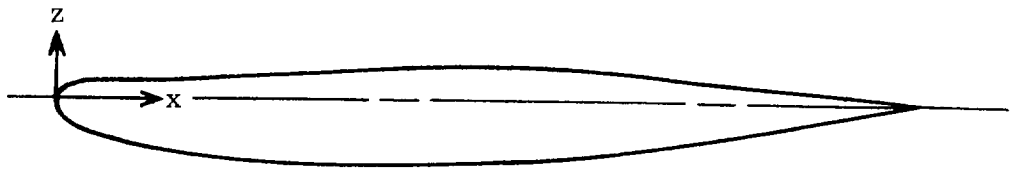

x/c	Horizontal-tail span stations at –					
	0.0		7.010		15.354 to 33.381	
	z_u/c	z_l/c	z_u/c	z_l/c	z_u/c	z_l/c
0	0	-0.0140	0	-0.0114	0	-0.0104
.0050	.0093	-.0230	.0085	-.0197	.0080	-.0184
.0075	.0118	-.0260	.0111	-.0223	.0100	-.0213
.0125	.0156	-.0306	.0143	-.0267	.0128	-.0254
.0250	.0209	-.0387	.0182	-.0347	.0164	-.0324
.0500	.0251	-.0489	.0208	-.0448	.0186	-.0422
.0750	.0270	-.0564	.0222	-.0516	.0200	-.0485
.1000	.0286	-.0619	.0238	-.0567	.0213	-.0534
.1500	.0321	-.0697	.0267	-.0639	.0237	-.0603
.2000	.0355	-.0753	.0296	-.0687	.0264	-.0650
.2500	.0391	-.0796	.0324	-.0726	.0288	-.0685
.3000	.0424	-.0827	.0353	-.0756	.0313	-.0711
.3500	.0448	-.0846	.0375	-.0774	.0333	-.0727
.4000	.0464	-.0854	.0389	-.0779	.0344	-.0732
.5000	.0447	-.0822	.0379	-.0751	.0349	-.0716
.6000	.0363	-.0694	.0334	-.0668	.0323	-.0652
.7000	.0268	-.0537	.0246	-.0539	.0235	-.0538
.9000	.0089	-.0177	.0082	-.0178	.0078	-.0176
1.0000	.0005	-.0005	.0006	-.0006	.0010	-.0010
c, cm . . .	23.843		20.838		17.262 at 15.354 9.538 at 33.381	
LER/c . . .	0.0226		0.0188		0.0155	

TABLE III.- VERTICAL-TAIL AIRFOIL ORDINATES

Vertical-tail water line at stations –						
23.90		x/c	27.62	30.97	39.37	62.01
x/c	$\pm \frac{z}{c}$		$\pm \frac{z}{c}$	$\pm \frac{z}{c}$	$\pm \frac{z}{c}$	$\pm \frac{z}{c}$
0	0	0	0	0	0	0
.0017	.0051	.0025	.0067	.0066	.0060	.0060
.0034	.0069	.0050	.0092	.0090	.0083	.0083
.0050	.0083	.0075	.0109	.0108	.0099	.0099
.0084	.0104	.0100	.0124	.0122	.0112	.0112
.0167	.0139	.0125	.0136	.0132	.0126	.0126
.0334	.0190	.0250	.0184	.0181	.0173	.0173
.0501	.0233	.0500	.0253	.0248	.0237	.0237
.0668	.0270	.0750	.0311	.0304	.0285	.0285
.1002	.0325	.1000	.0358	.0351	.0328	.0328
.1336	.0366	.1500	.0428	.0423	.0396	.0396
.1670	.0397	.2000	.0480	.0475	.0448	.0448
.2004	.0419	.2500	.0515	.0513	.0486	.0486
.2338	.0433	.3000	.0539	.0540	.0514	.0514
.2672	.0440	.3500	.0551	.0556	.0530	.0530
.2859	.0441	.4000	.0554	.0563	.0539	.0539
.6144	.0441	.4250	.0554	.0563	.0539	.0539
.6326	.0437	.4500	.0554	.0563	.0539	.0539
.6660	.0415	.5000	.0552	.0555	.0531	.0531
.6994	.0383	.5500	.0532	.0534	.0516	.0516
.7328	.0346	.6000	.0496	.0499	.0490	.0490
.7662	.0306	.6500	.0449	.0452	.0450	.0450
.7996	.0263	.7000	.0393	.0394	.0394	.0394
.8330	.0220	.7500	.0329	.0328	.0328	.0328
1.0000	.0003	1.0000	.0004	.0004	.0005	.0013
c, cm . . .	48.330		33.670	29.174	23.139	9.764
LER/c . . .	0.0060		0.0100	0.0100	0.0083	0.0083

TABLE IV.- DATA FOR CALCULATION OF PROFILE DRAG COEFFICIENTS

(a) Wetted areas and reference lengths

Model component	Wetted area, cm^2	Reference length, cm
Fuselage and wing-root flap track fairings . . .	10 257.9	171.20
Wing	5 733.9	19.50
Horizontal tails	1 820.7	14.30
Vertical tail	1 651.2	21.66
Pylons	213.2	34.45
Nacelles	1 479.2	34.54
Outboard flap-track fairing	261.7	17.60

(b) Reynolds number per meter, wind-tunnel stagnation temperature, and calculated profile drag coefficients

M	R	T_t, °K	Values of $C_{D,p}$ for configurations –			
			BW_1	BW_1HV	BW_1HVN_1	BW_1HVN_1T
0.550	10.62×10^6	301	0.01508	0.01929	0.02093	0.02113
.625	11.35	307	.01481	.01894	.02055	.02074
.725	11.94	315	.01453	.01858	.02016	.02035
.750	12.13	323				
.775	12.25	322	.01439	.01839	.01996	.02015
.800	12.40	316				
.825	12.50	328				
.850	12.76	325	.01416	.01810	.01964	.01983

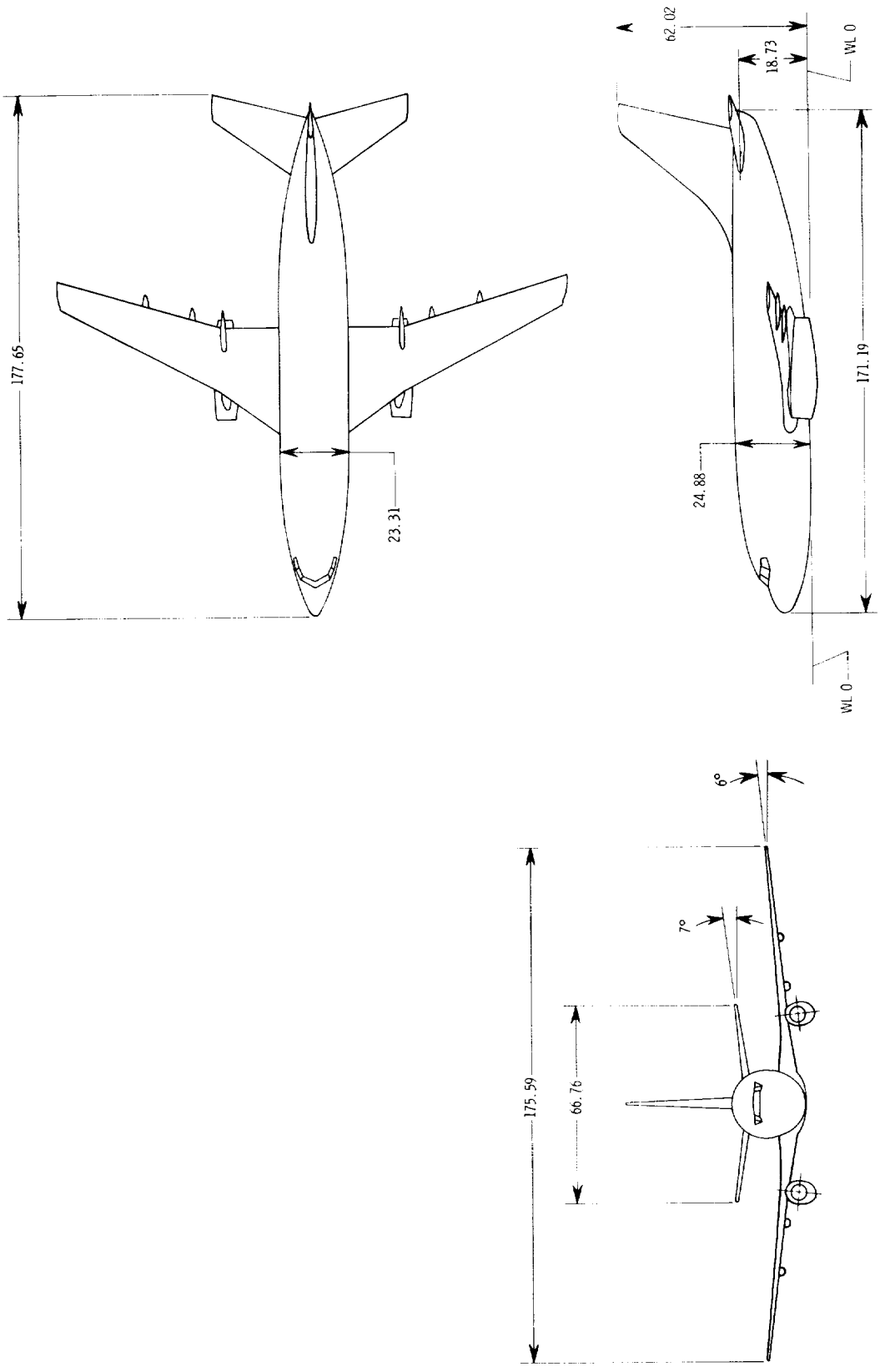

Figure 1.- Sketch of transport model. All dimensions are in centimeters unless otherwise noted.

L-68-988

Figure 2.- Photographs of configuration BW_1HVN_1T with sting strut mounted from the bottom. L-68-987

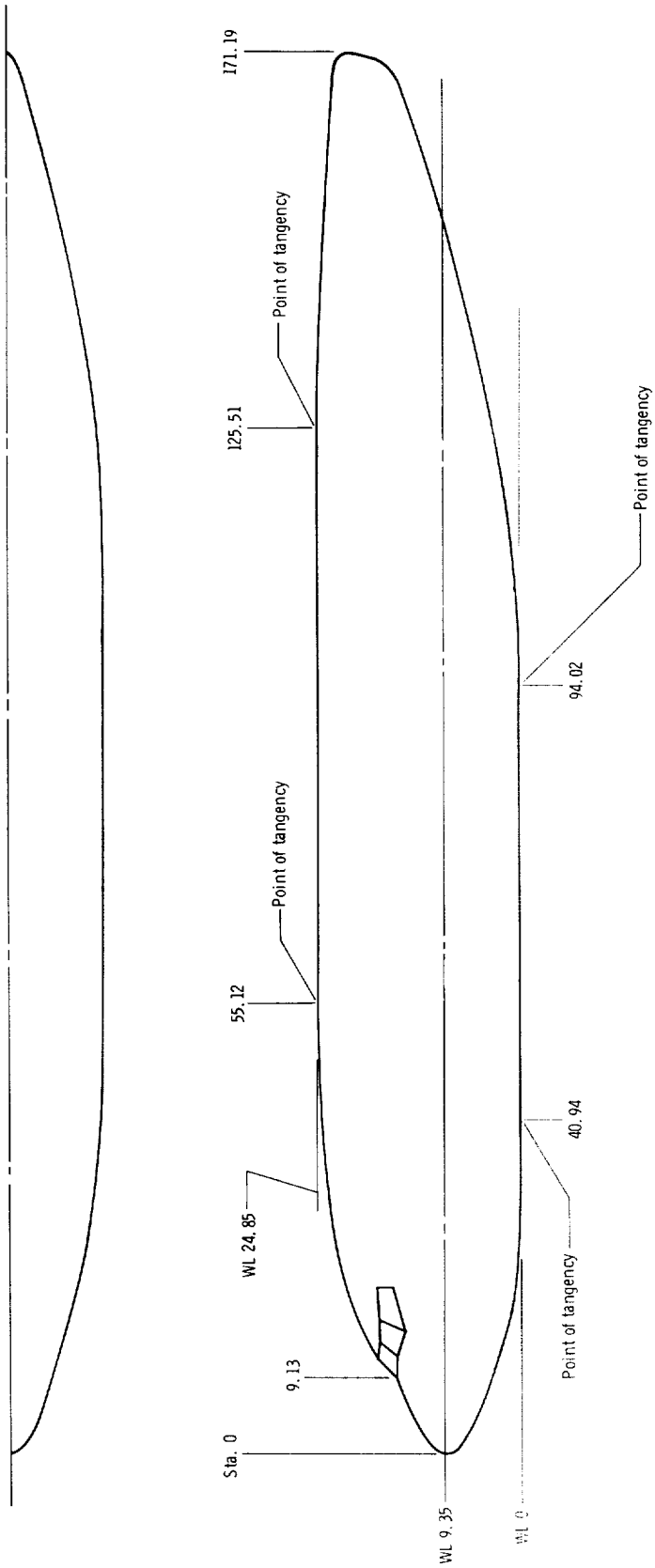

(a) Fuselage geometry.

Figure 3.- Details of various model components. All dimensions are in centimeters unless otherwise noted.

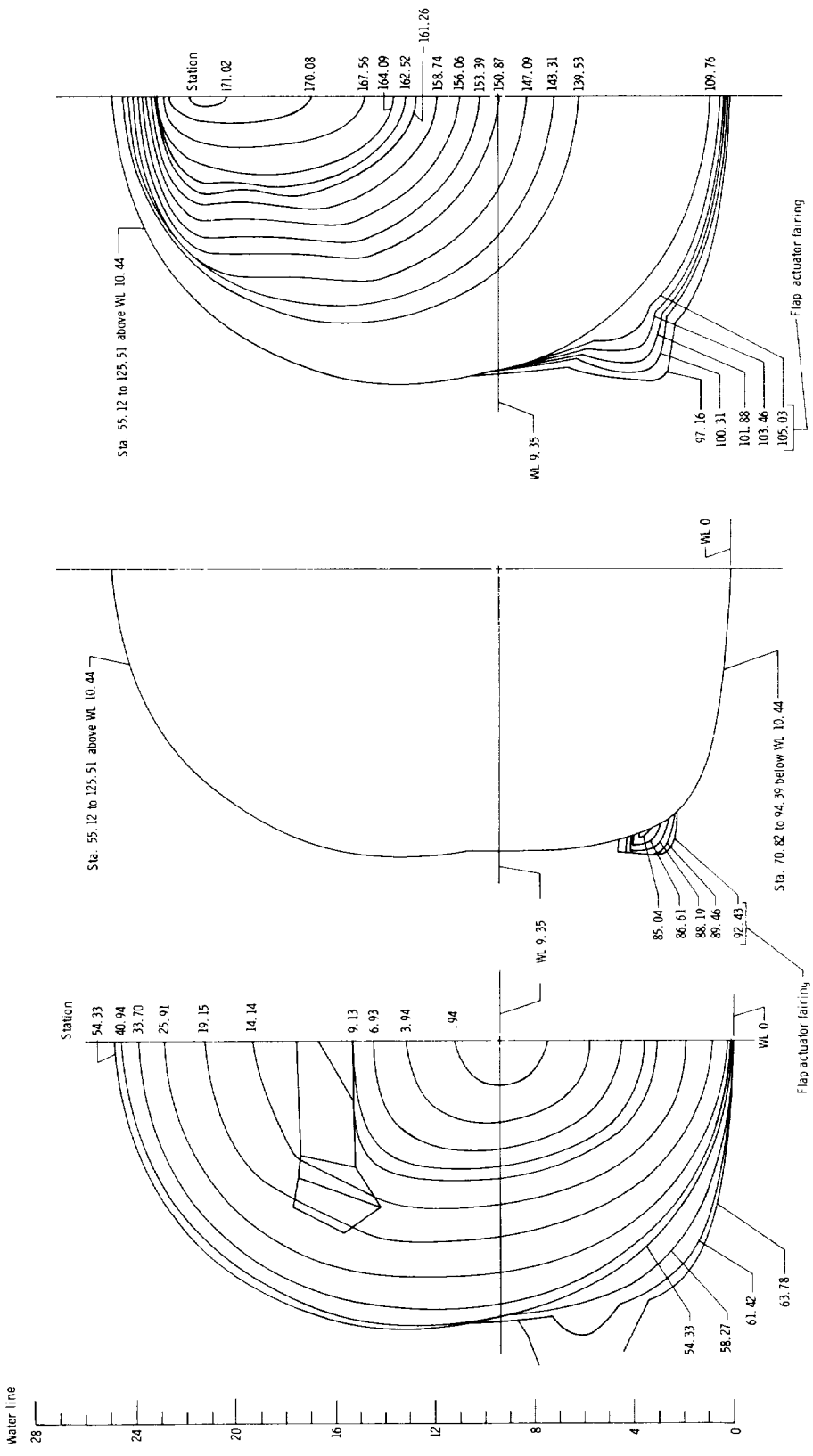

(b) Fuselage cross sections.

Figure 3.- Continued.

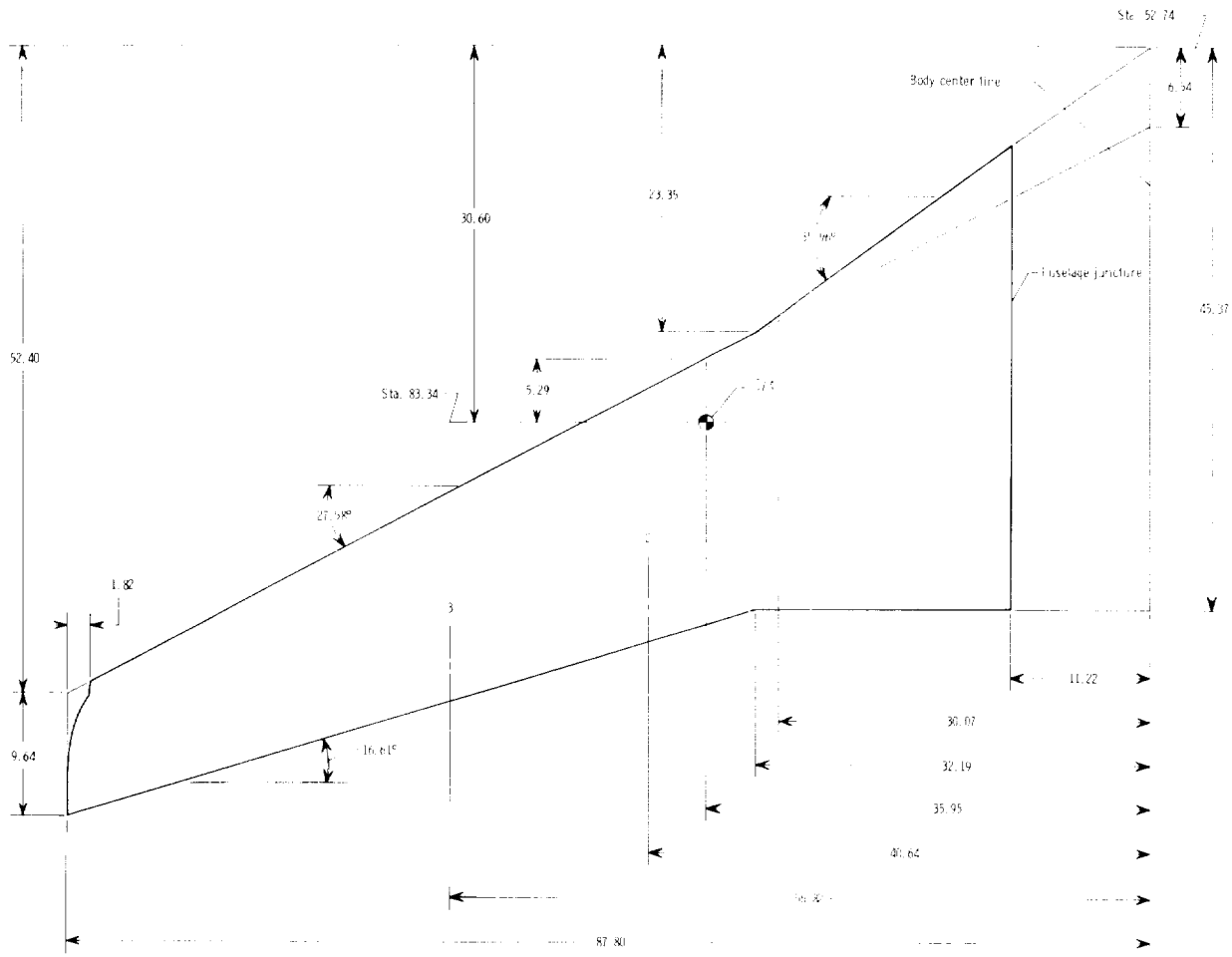

(c) Planform geometry of basic wing 1.

Figure 3.- Continued.

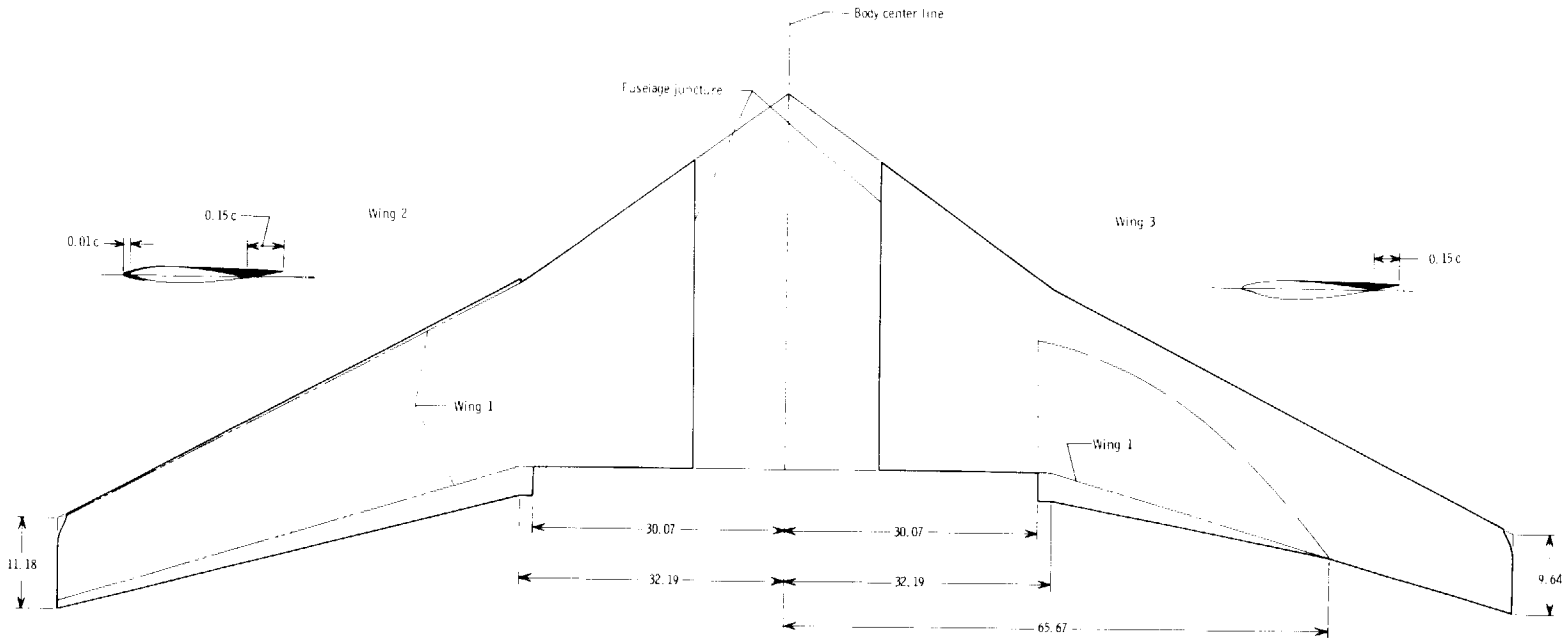

Note: 1. Wing span station 30.07 corresponds to nacelle center line.
2. Wing span station 32.19 corresponds to break in wing leading edge.
3. Modifications to both wings made outboard of nacelles only.
4. Modifications to lower surface stopped at outboard side of the nacelle strut.
5. Modifications to upper surface faired into original wing in the vicinity of the nacelle center-line span station.

(d) Wings 2 and 3.

Figure 3.- Continued.

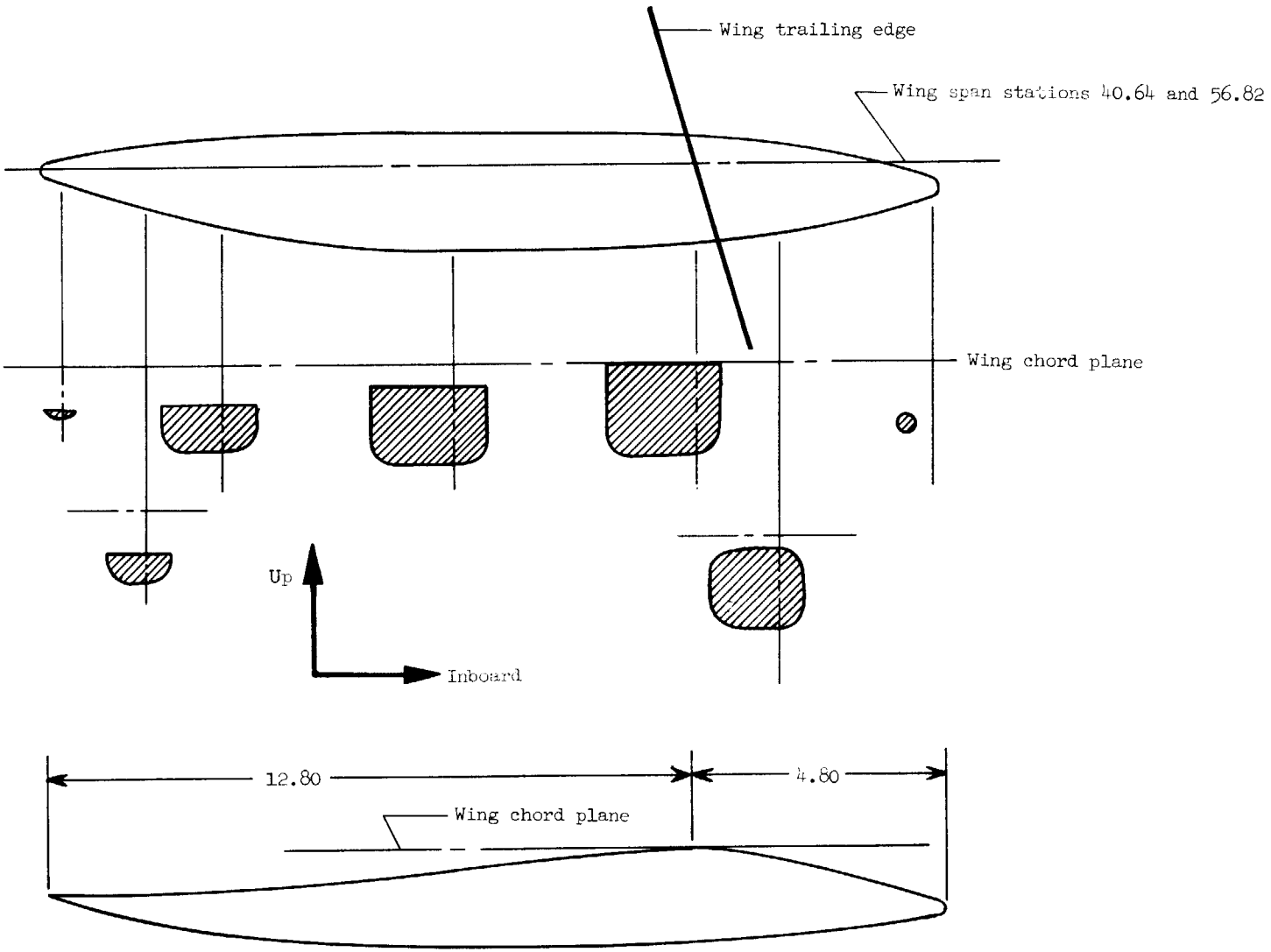

(e) Flap-track fairings.

Figure 3.- Continued.

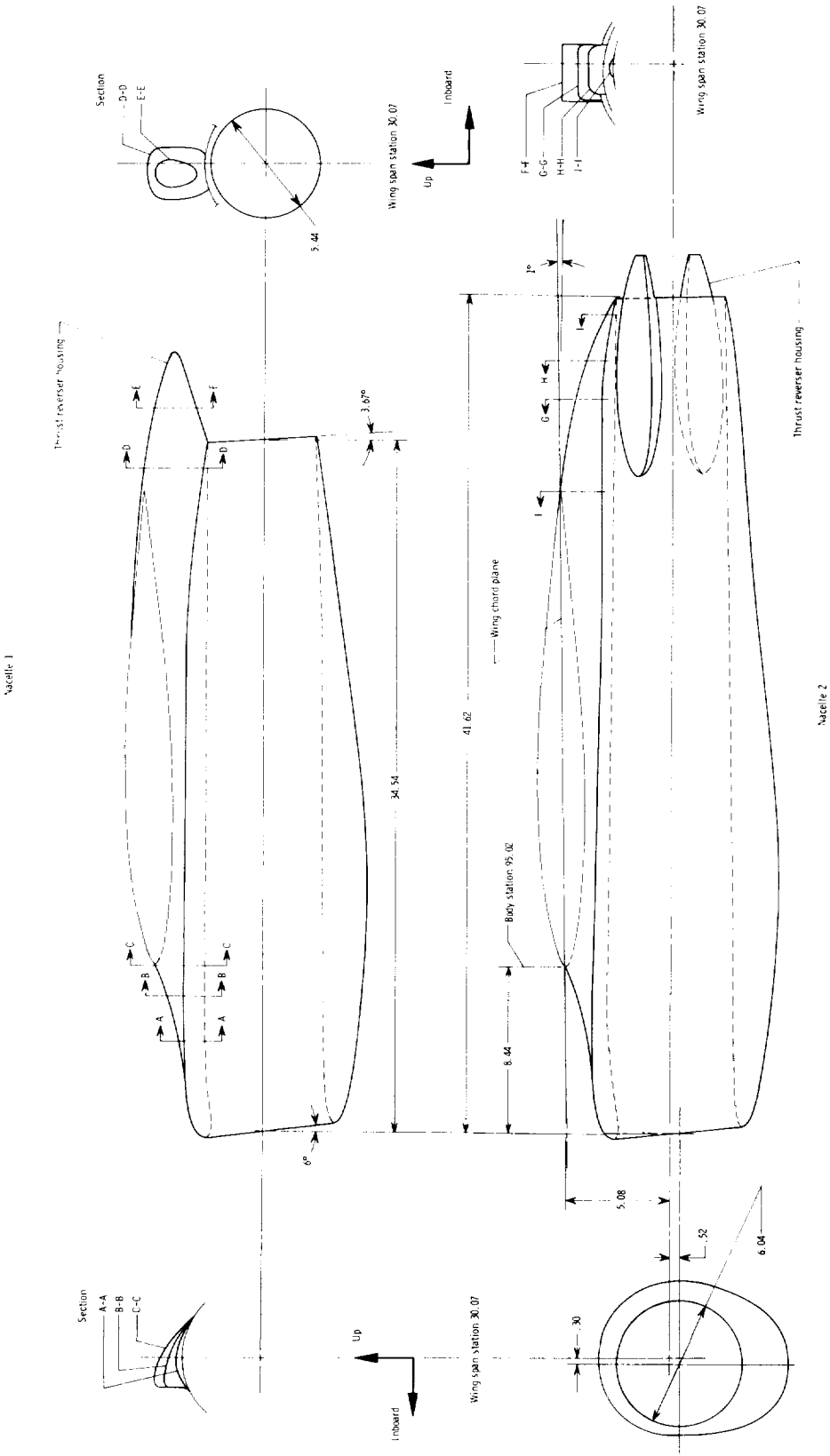

(f) Nacelles 1 and 2. Nacelle incidence 2^0 with respect to body center line.

Figure 3.- Continued.

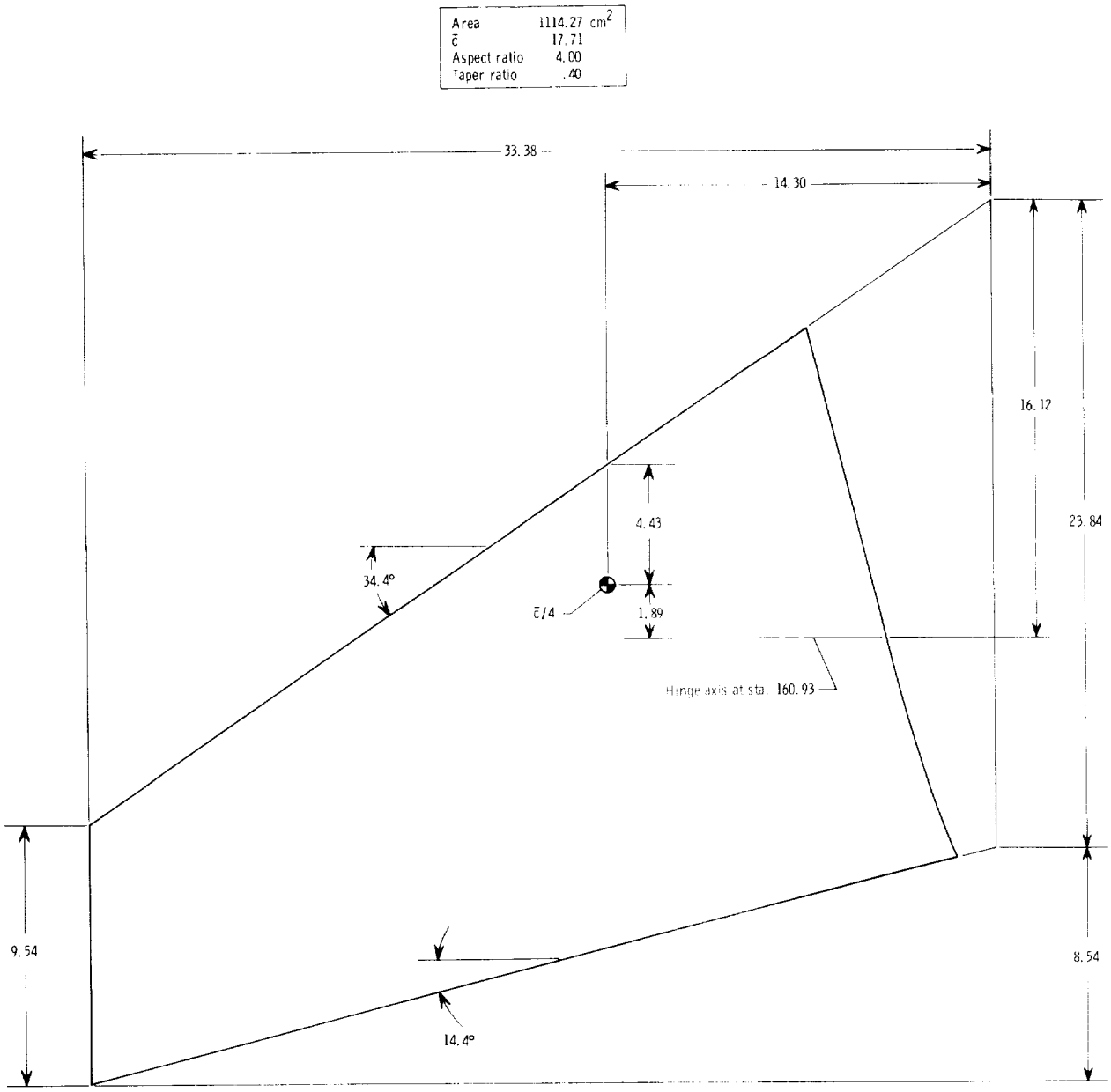

(g) Horizontal tail.

Figure 3.- Continued.

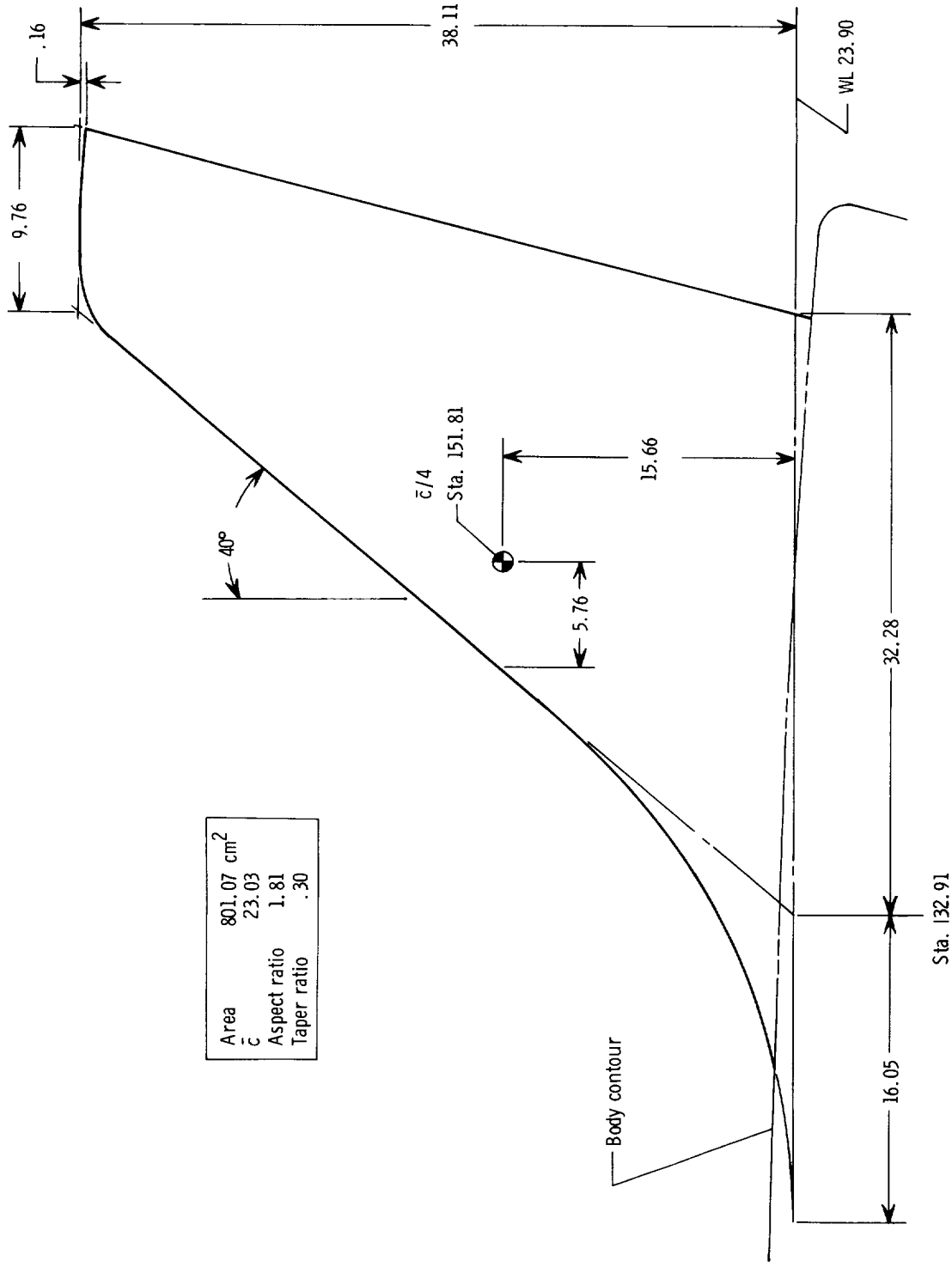

(h) Vertical tail.

Figure 3.- Concluded.

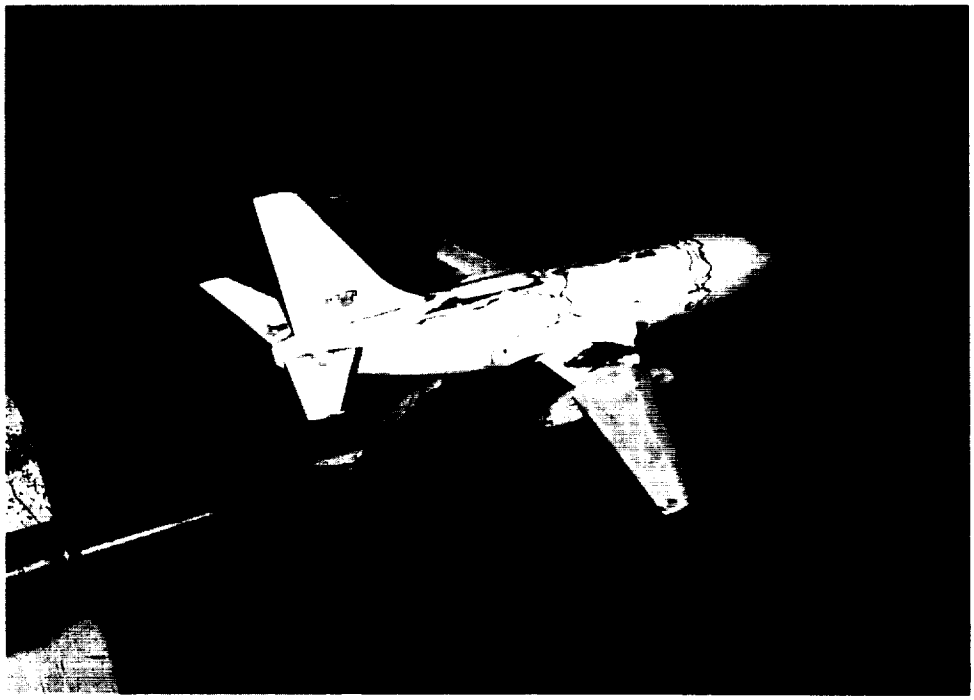

L-68-1129

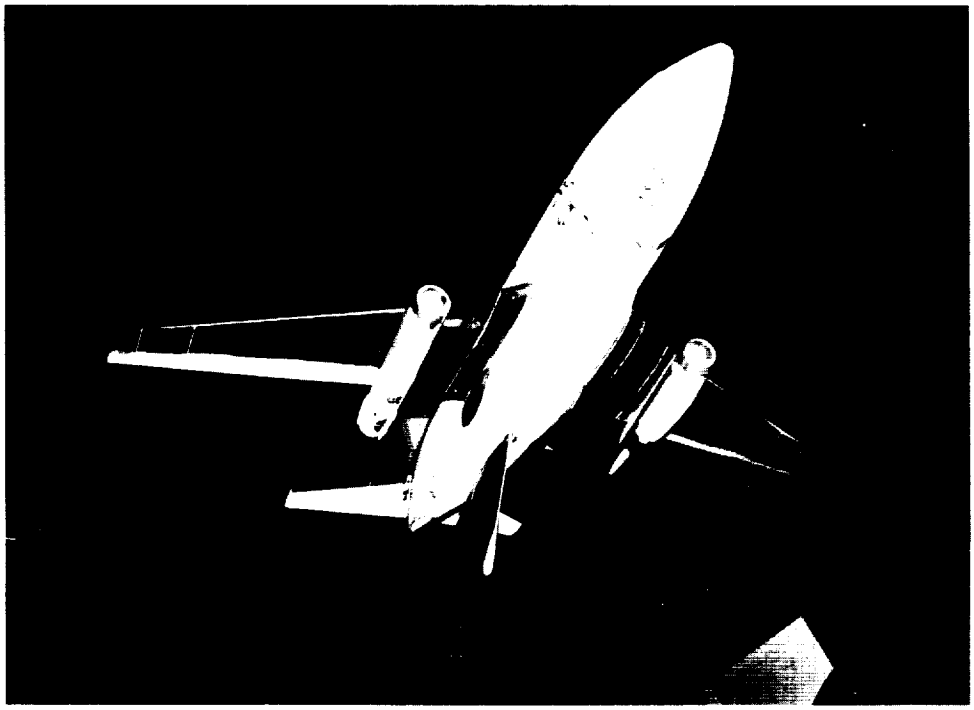

Figure 4.- Photographs of configuration BW_2HVN_2 with sting strut mounted from the bottom. L-68-1130

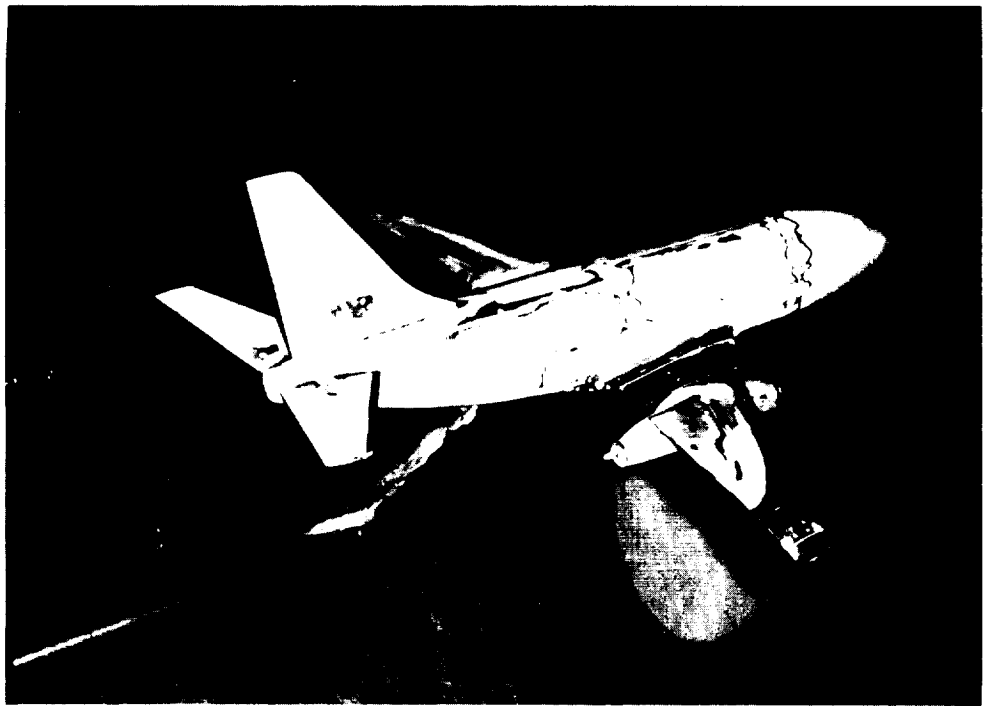

L-68-1174

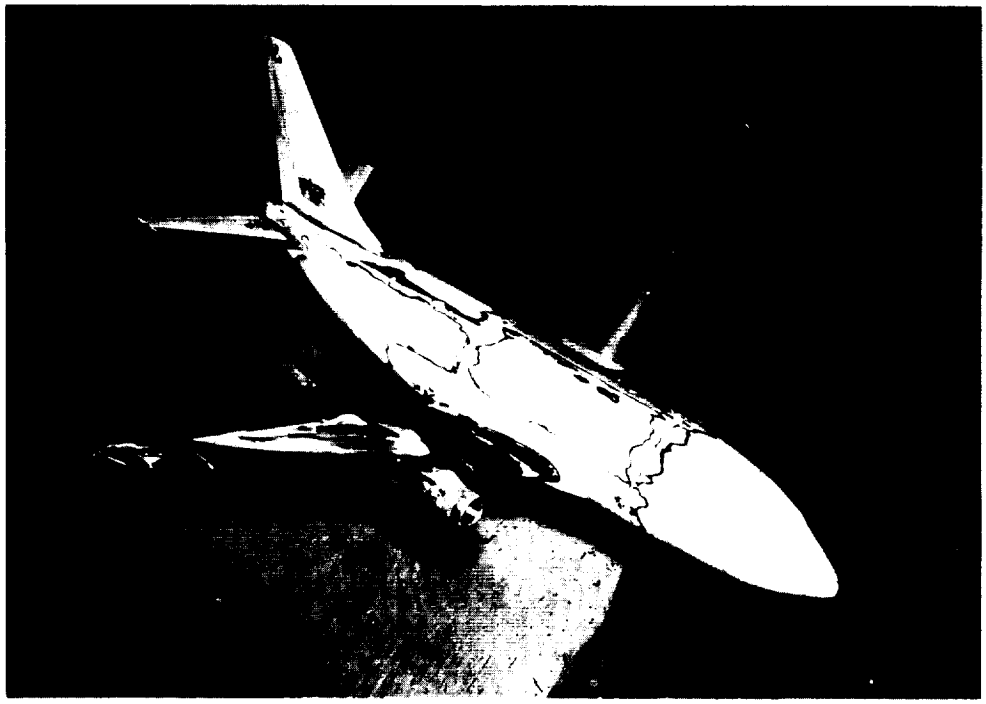

Figure 5.- Photographs of configuation BW_3HVN_2 with sting strut mounted from the bottom. L-68-1172

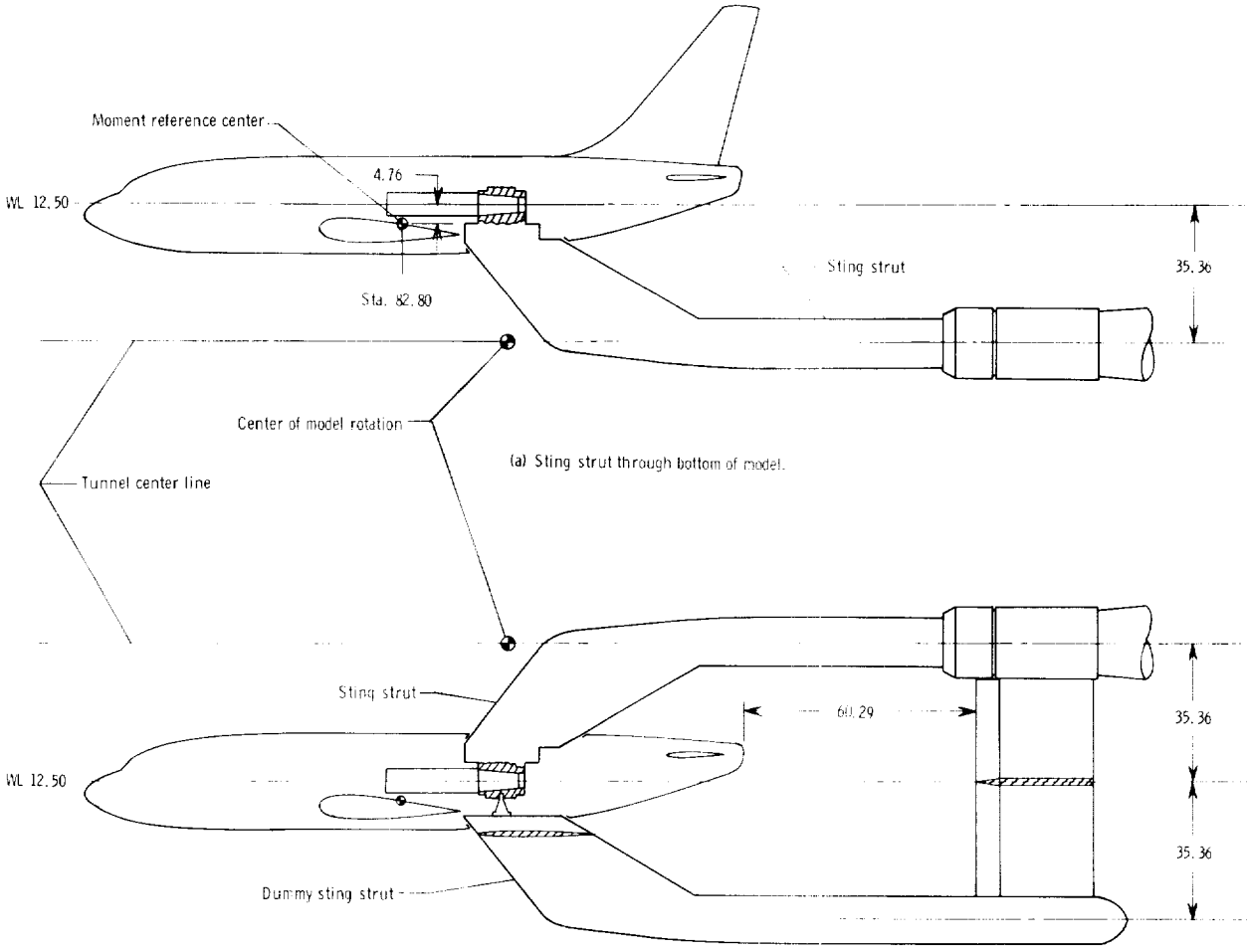

Figure 6.- Sketch of support systems. All dimensions are in centimeters.

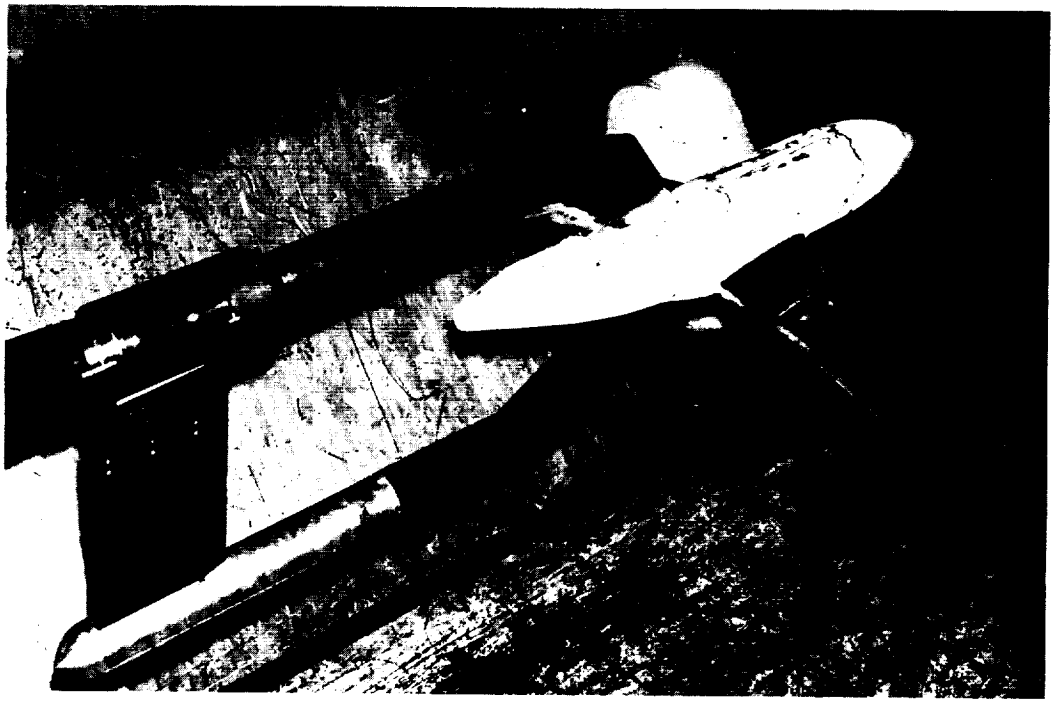

(a) Sting strut through top with dummy on the bottom. L-68-781

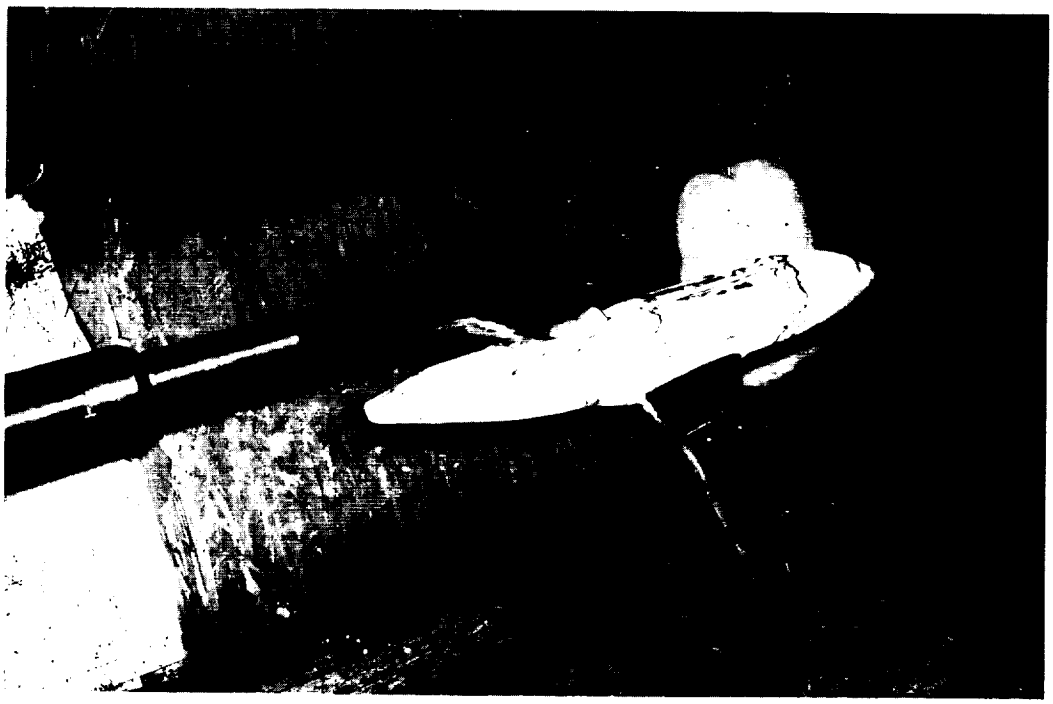

(b) Sting strut through the top. L-68-782

Figure 7.- Photographs of configuation BW_1 showing alternate mounting systems.

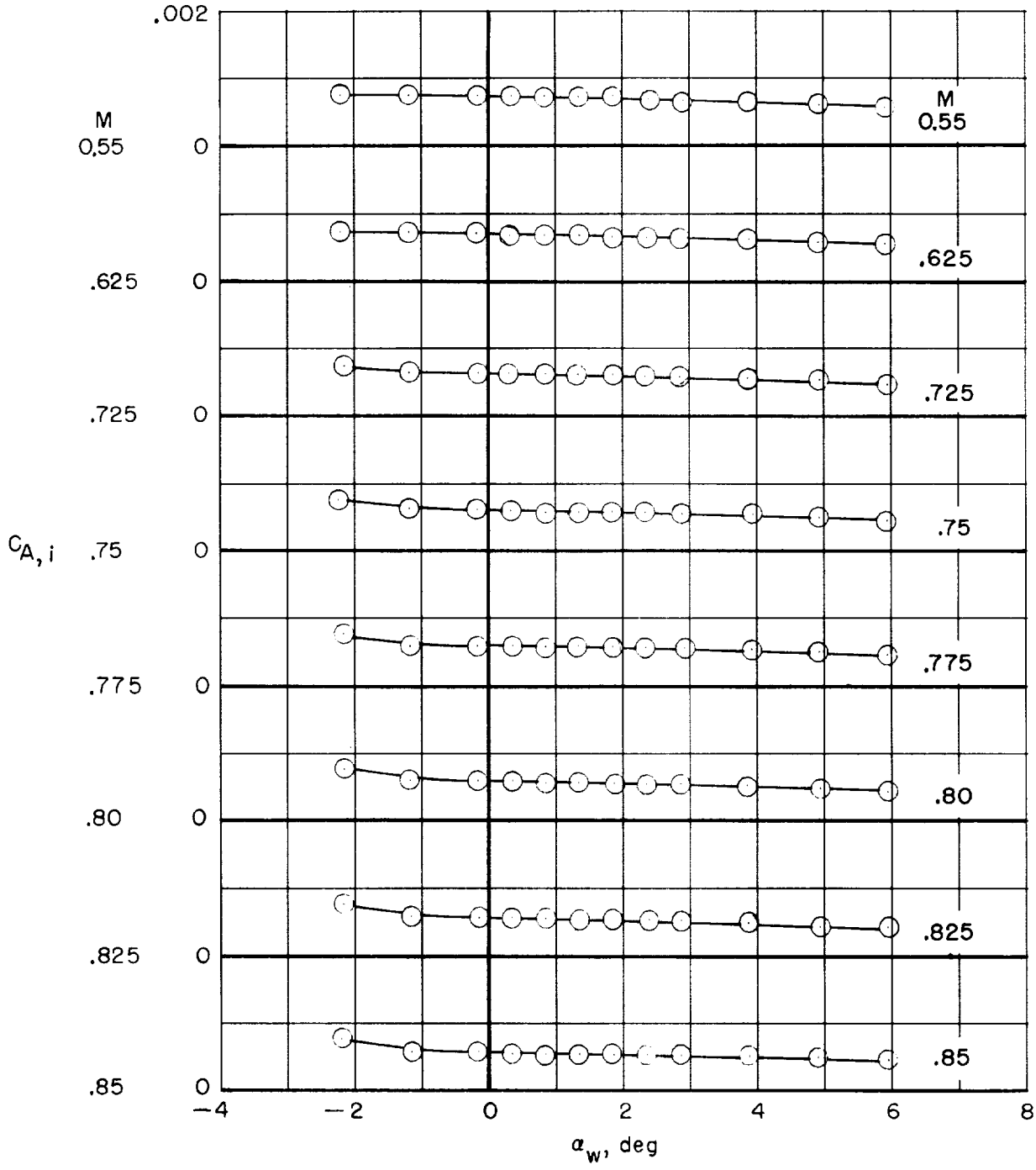

Figure 8.- Variation of nacelle internal axial forces with wing angle of attack. Internal axial force referred along fuselage center line.

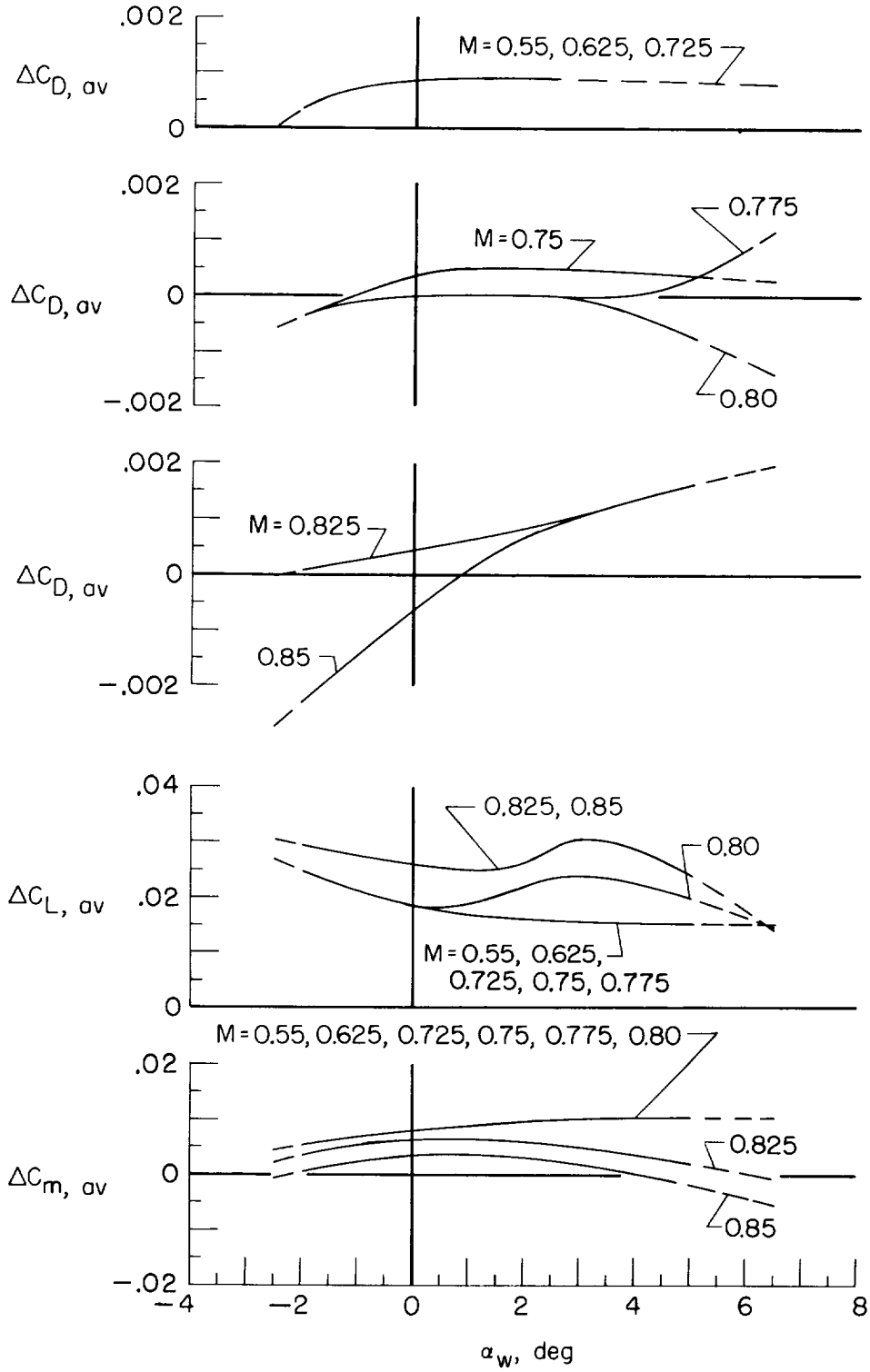

Figure 9.- Variation of incremental strut-interference forces with wing angle of attack. Extrapolation of measured data is represented by dashed portion of the curves.

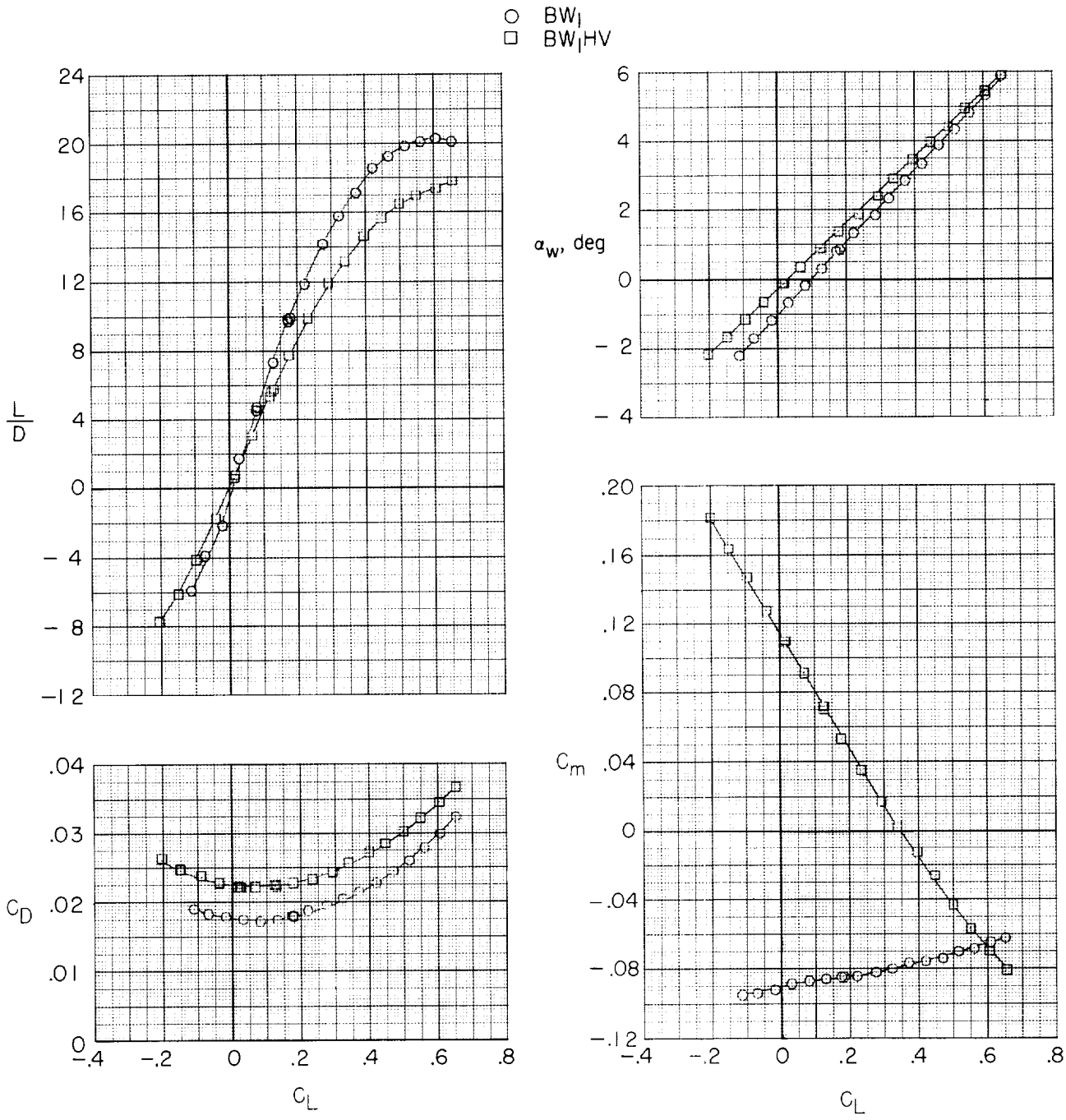

(a) M = 0.55.

Figure 10.- Longitudinal aerodynamic characteristics for configurations BW_1 and BW_1HV with $\delta_h = -0.5^0$. Transition fixed.

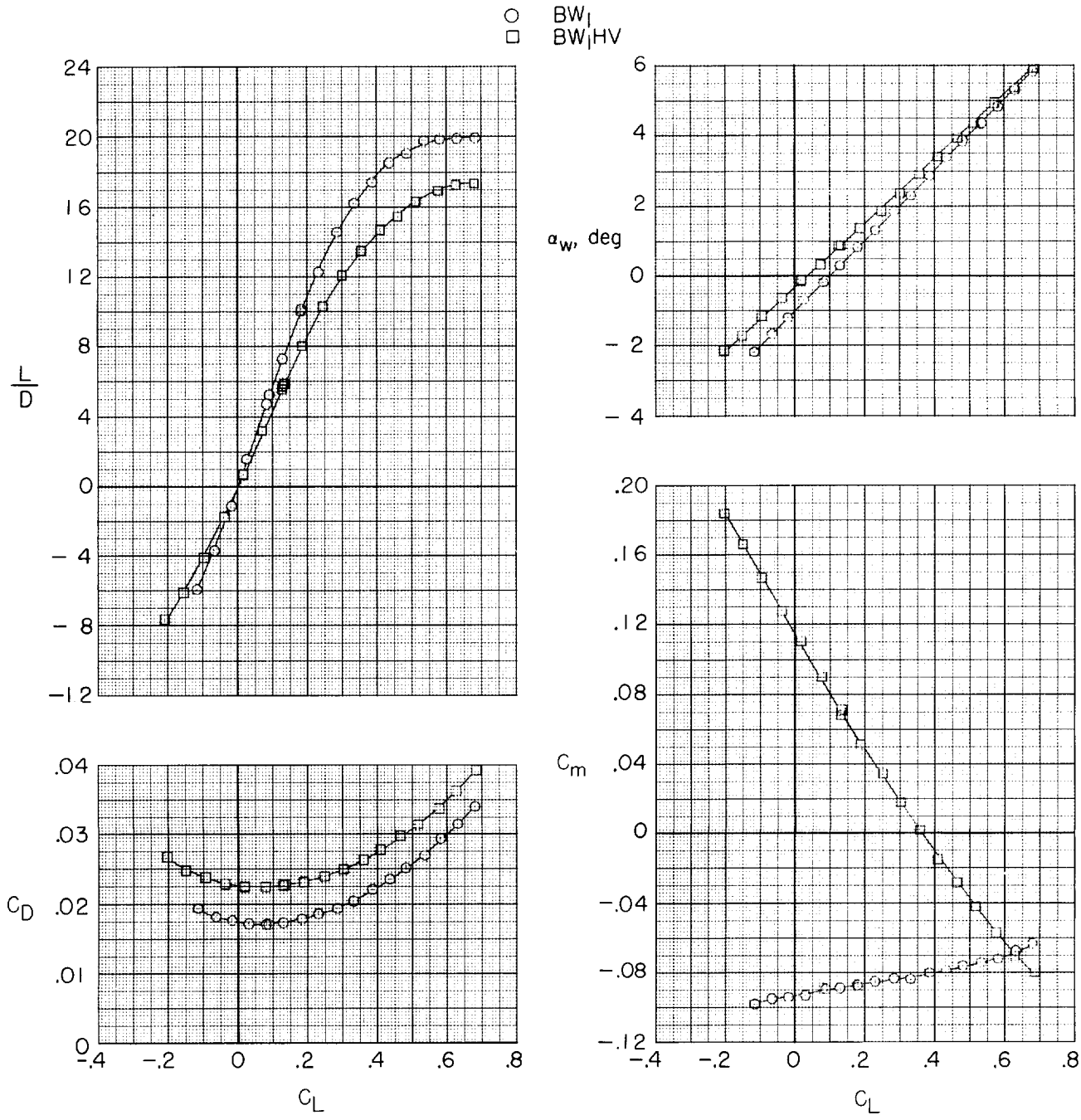

(b) M = 0.625.

Figure 10.- Continued.

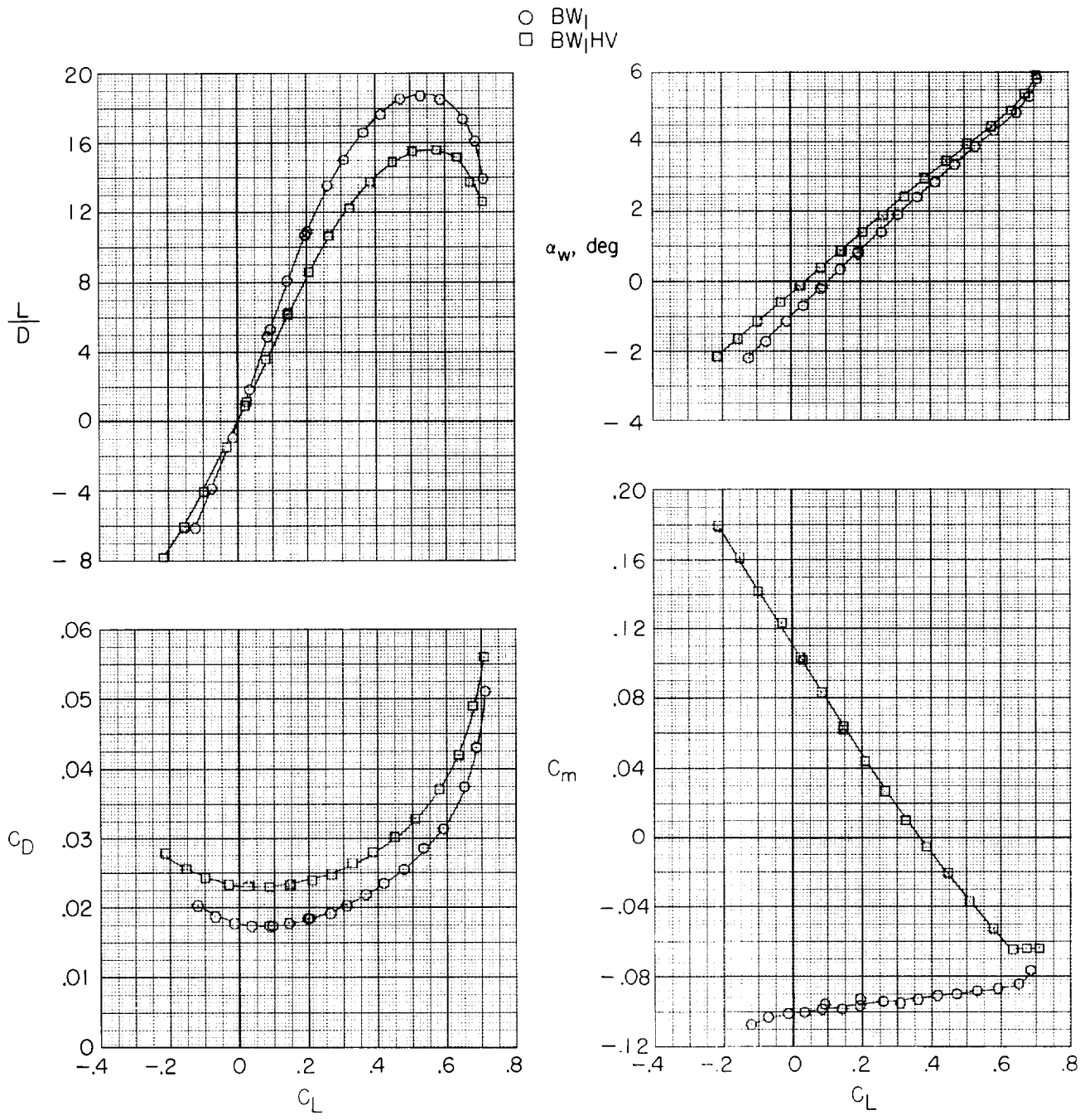

(c) M = 0.725.

Figure 10.- Continued.

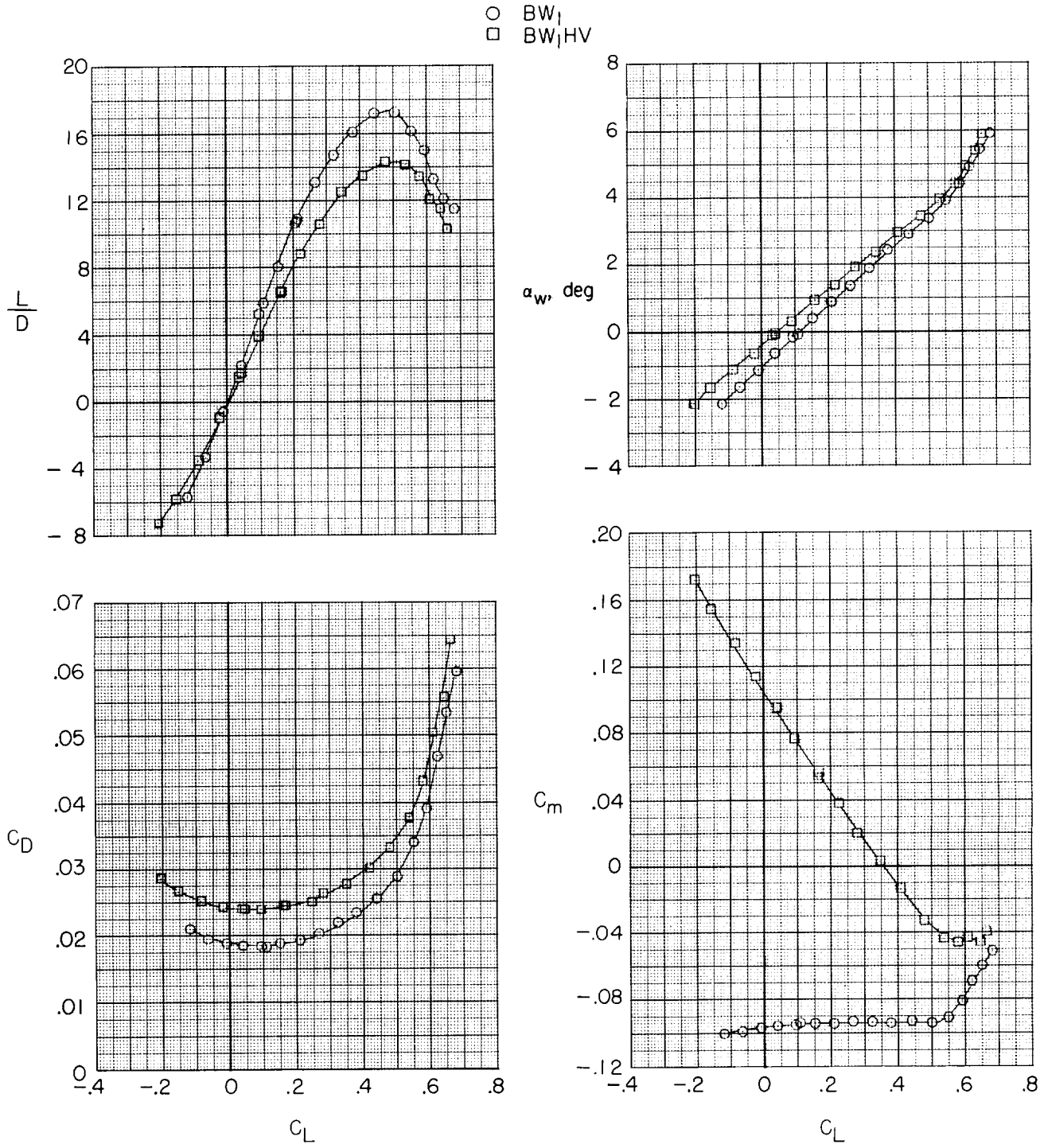

(d) M = 0.75.

Figure 10.- Continued.

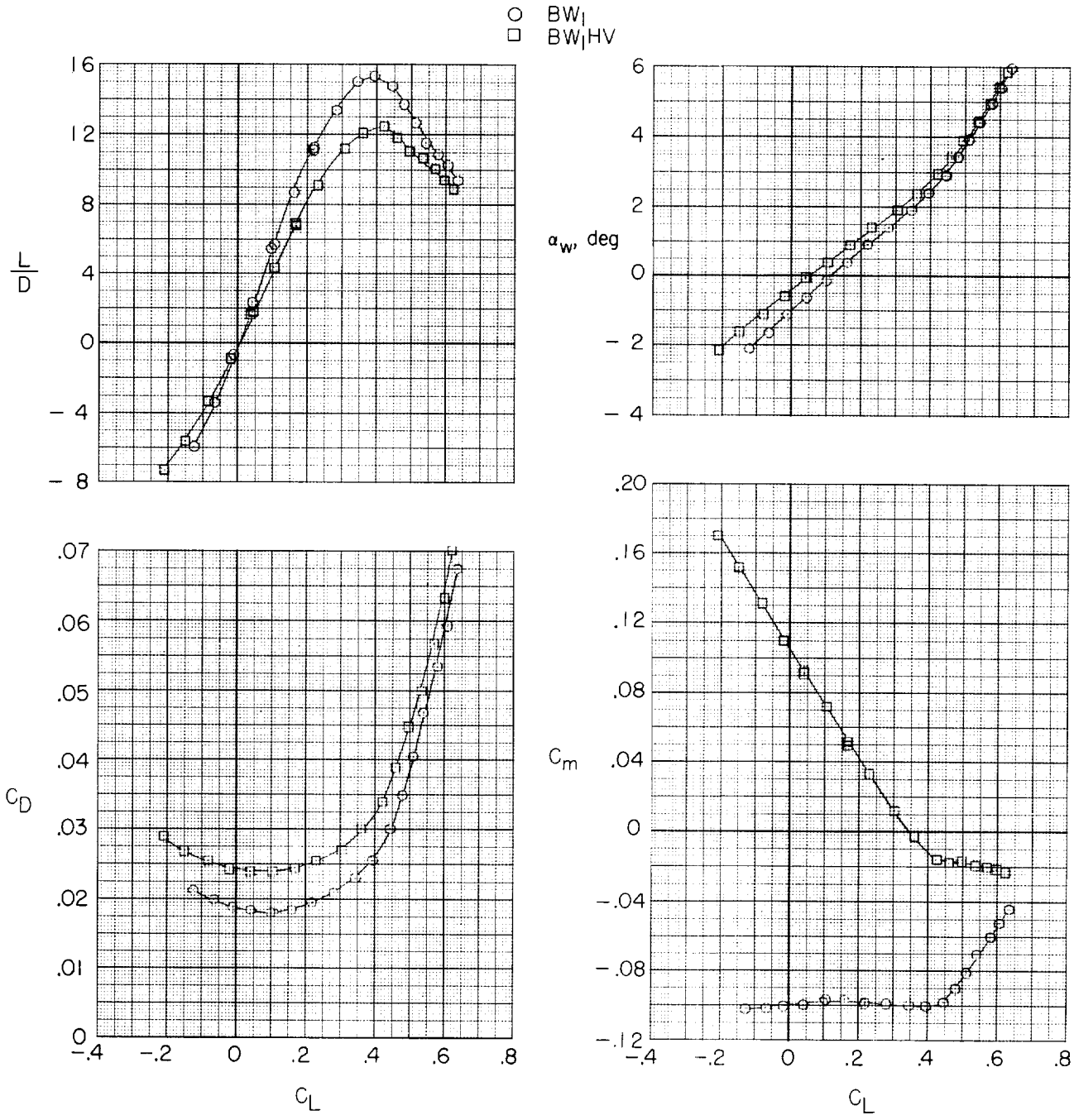

(e) M = 0.775.

Figure 10.- Continued.

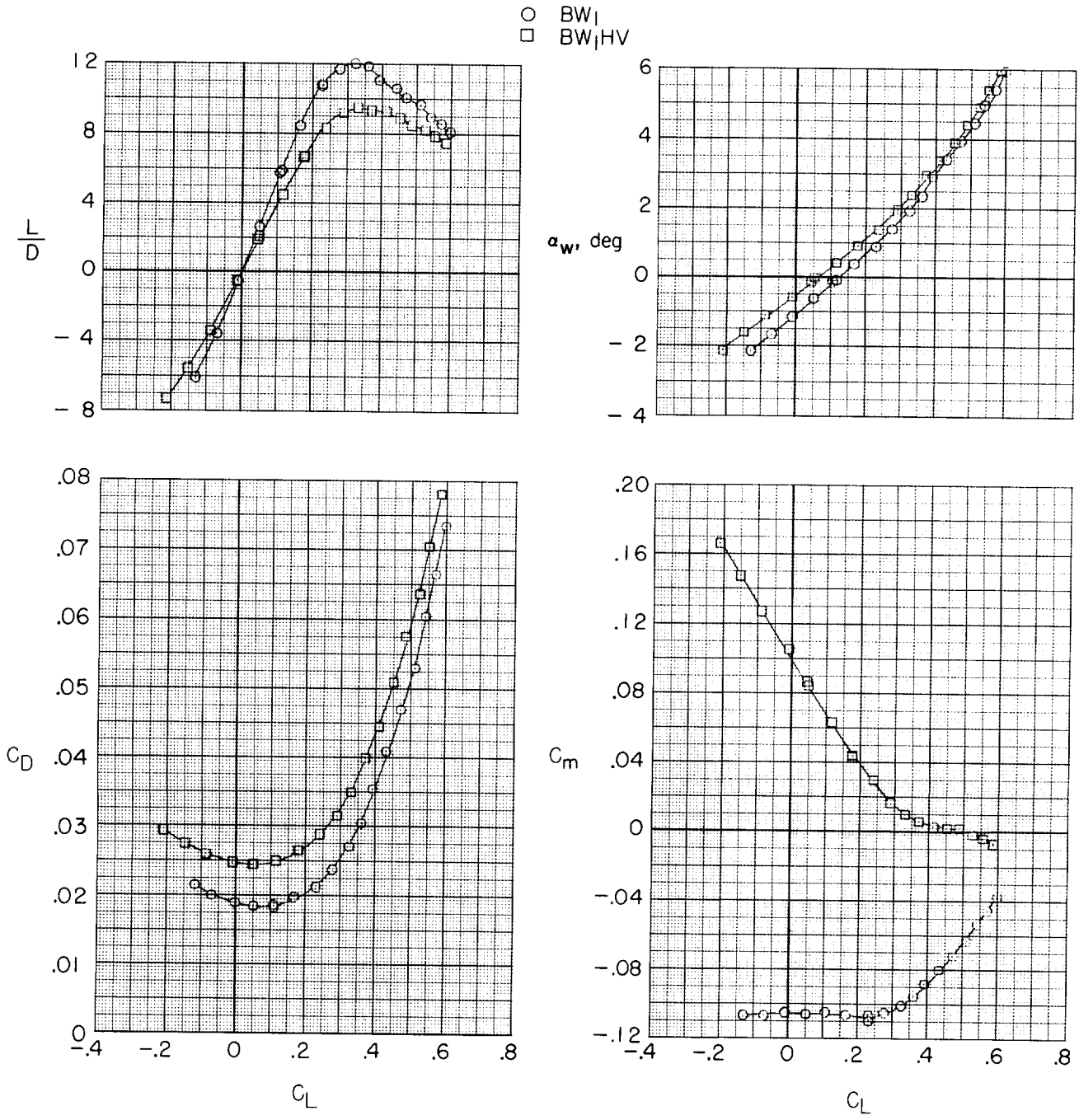

(f) M = 0.80.

Figure 10.- Continued.

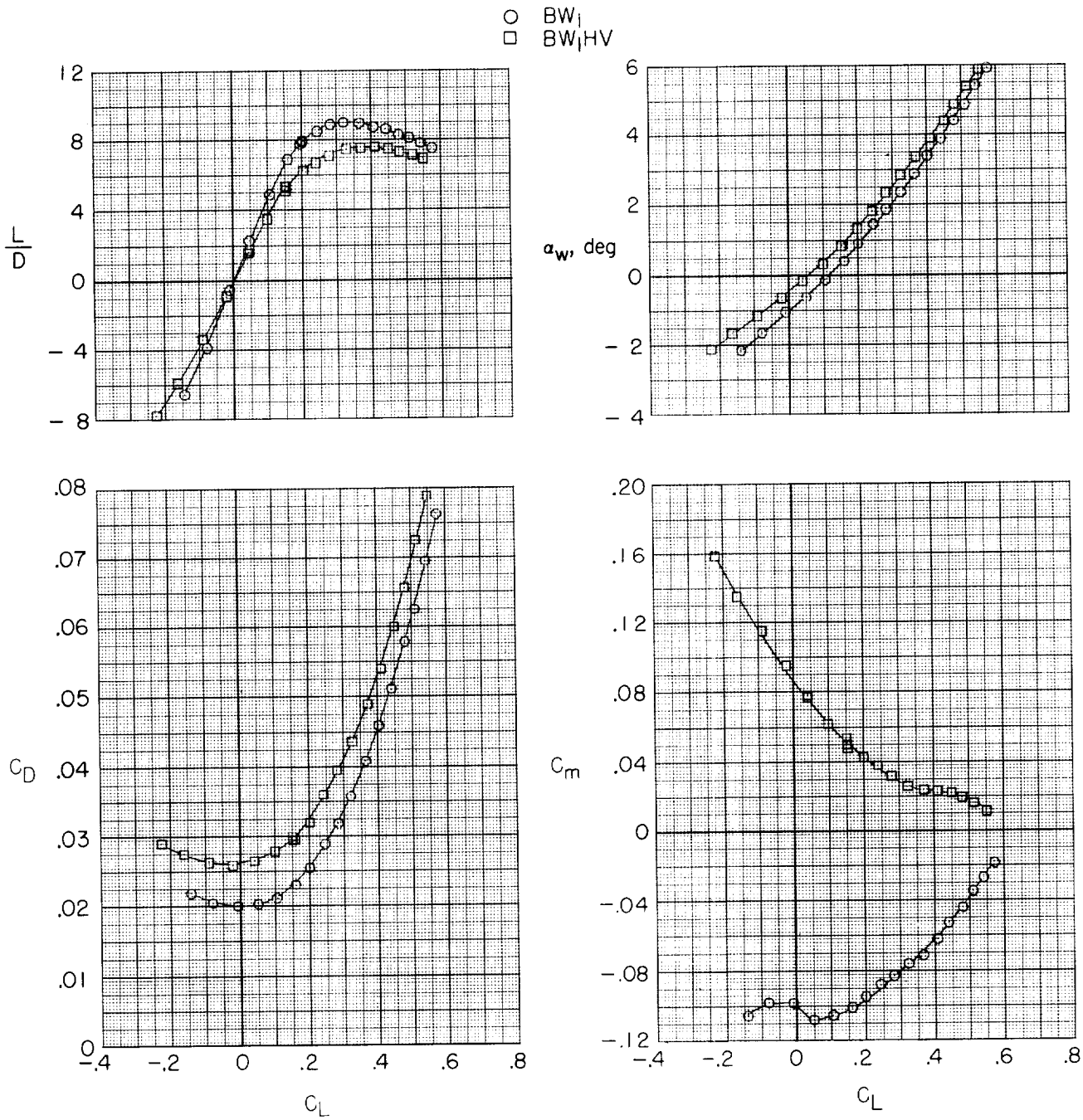

(g) M = 0.825.

Figure 10.- Continued.

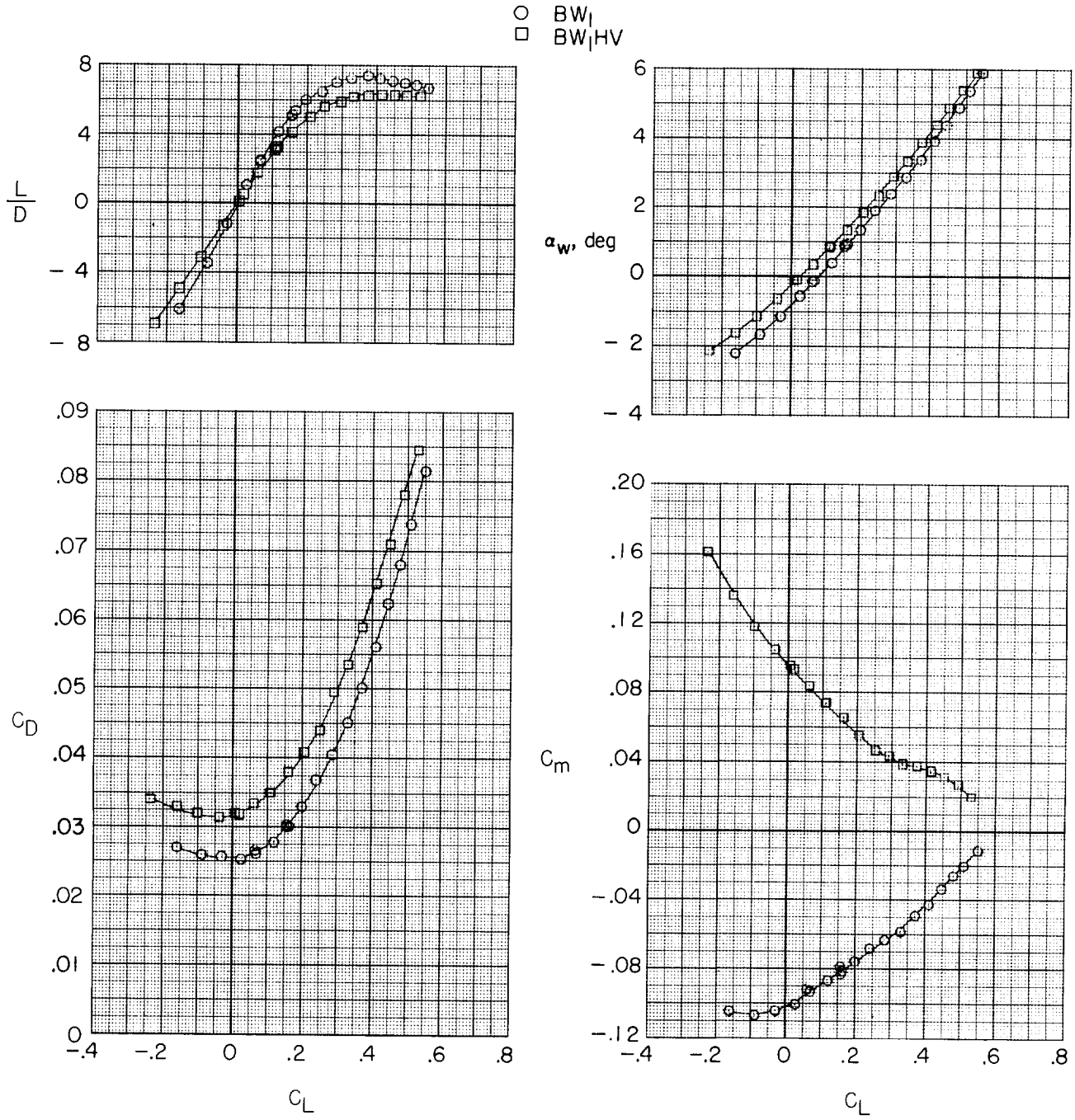

(h) M = 0.85.

Figure 10.- Concluded.

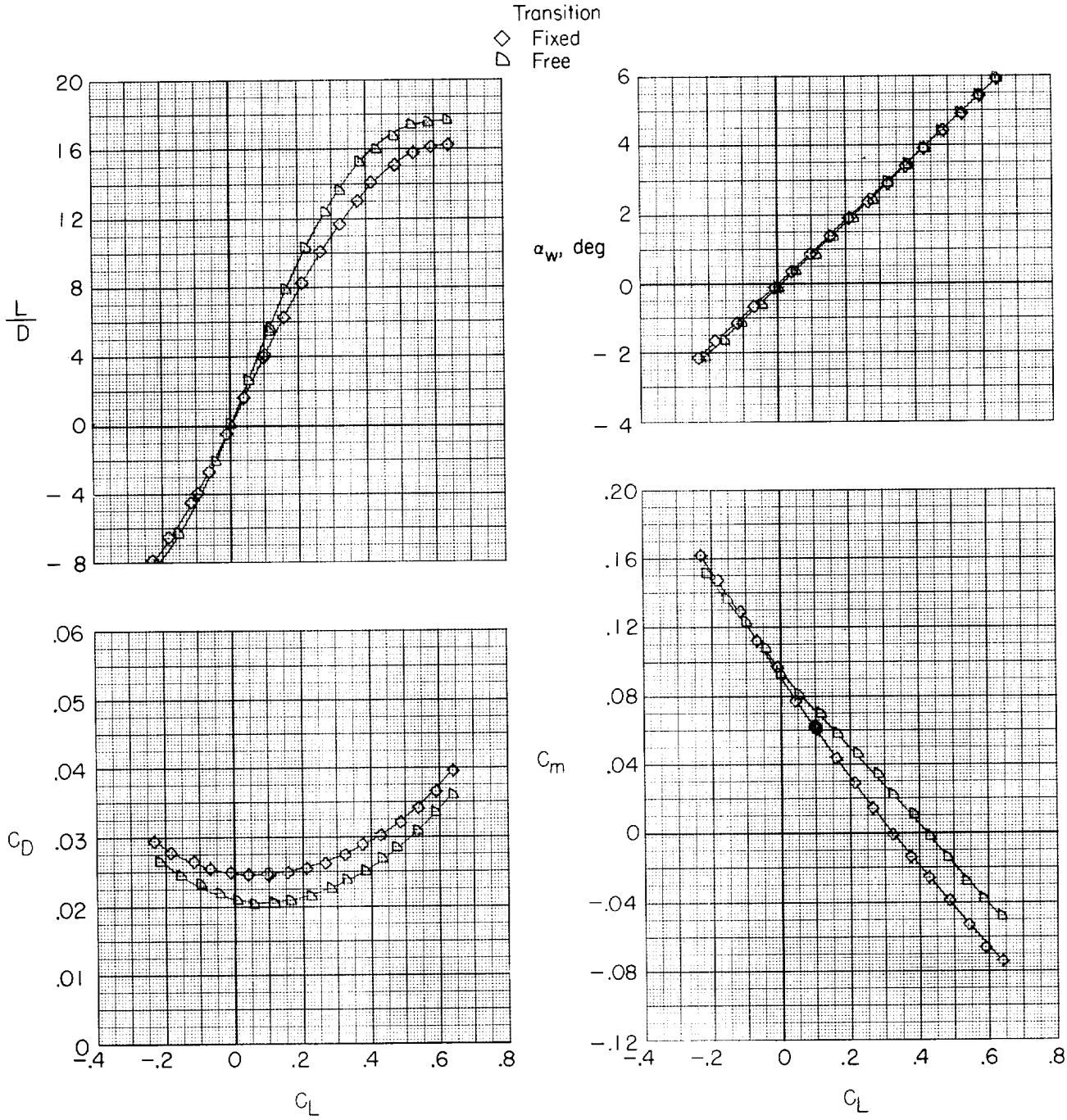

(a) M = 0.55.

Figure 11.- Longitudinal aerodynamic characteristics for configuration BW_1HVN_1T with $\delta_h = -0.5^0$. Transition fixed and free.

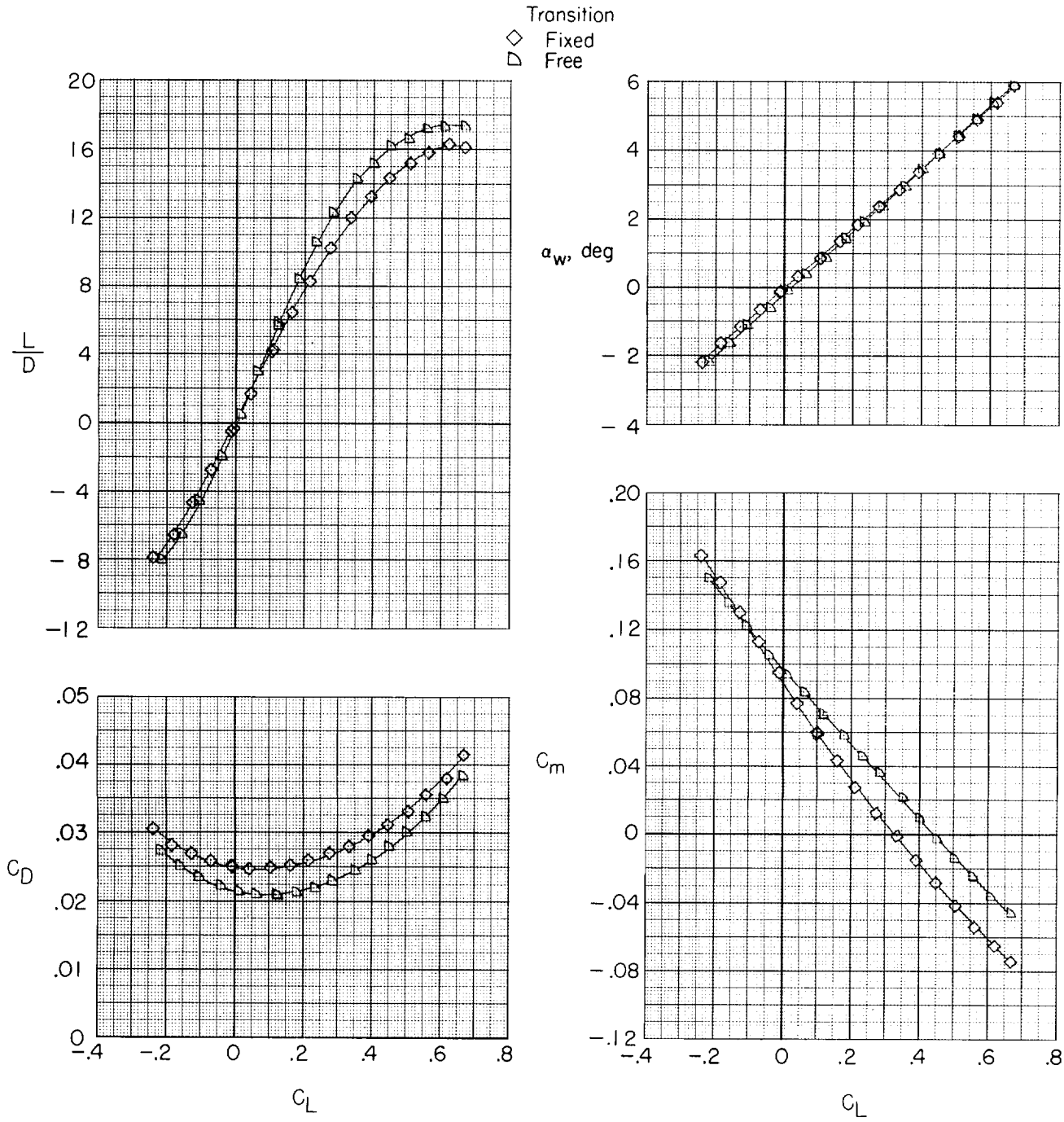

(b) M = 0.625.

Figure 11.- Continued.

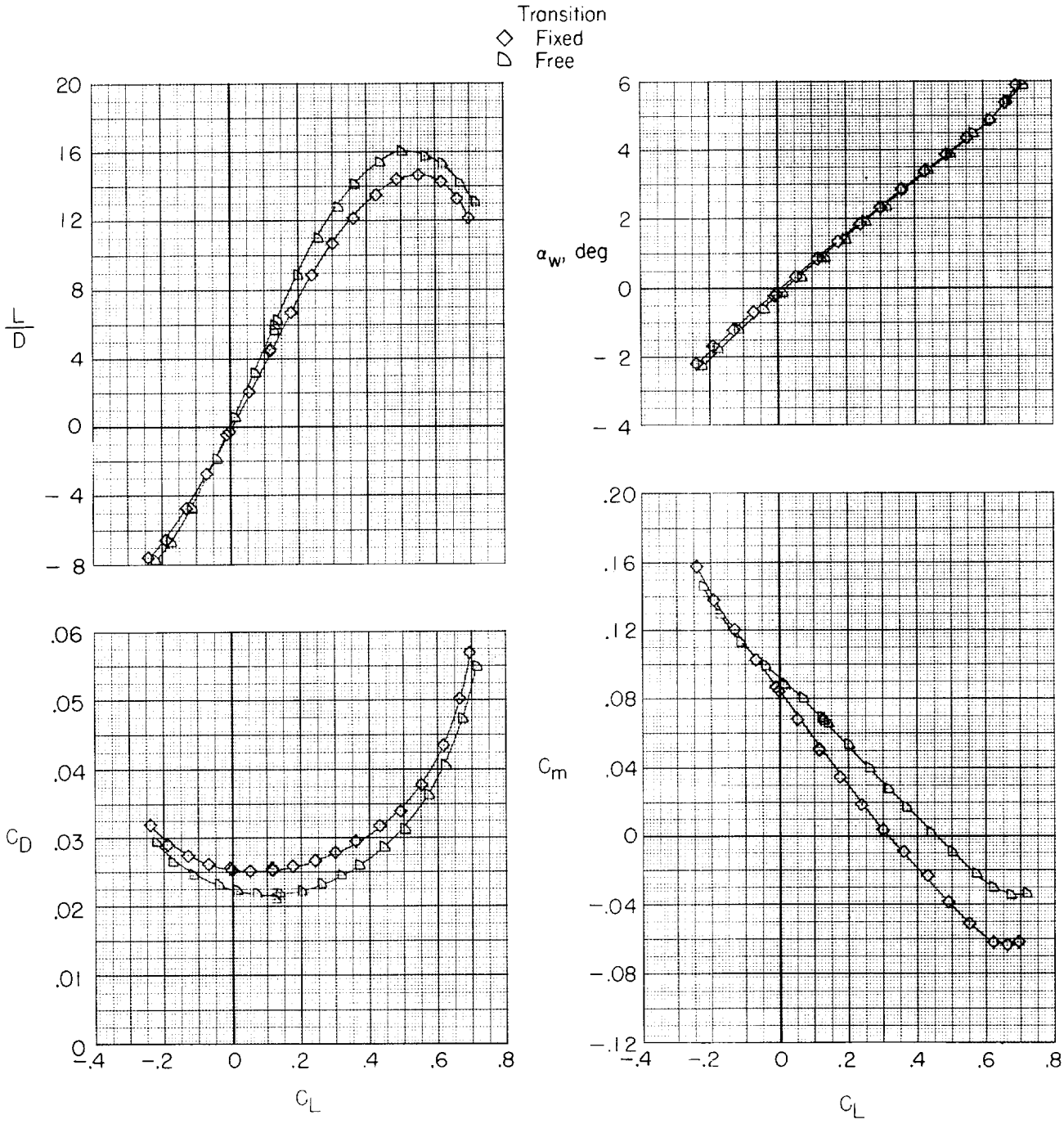

(c) M = 0.725.

Figure 11.- Continued.

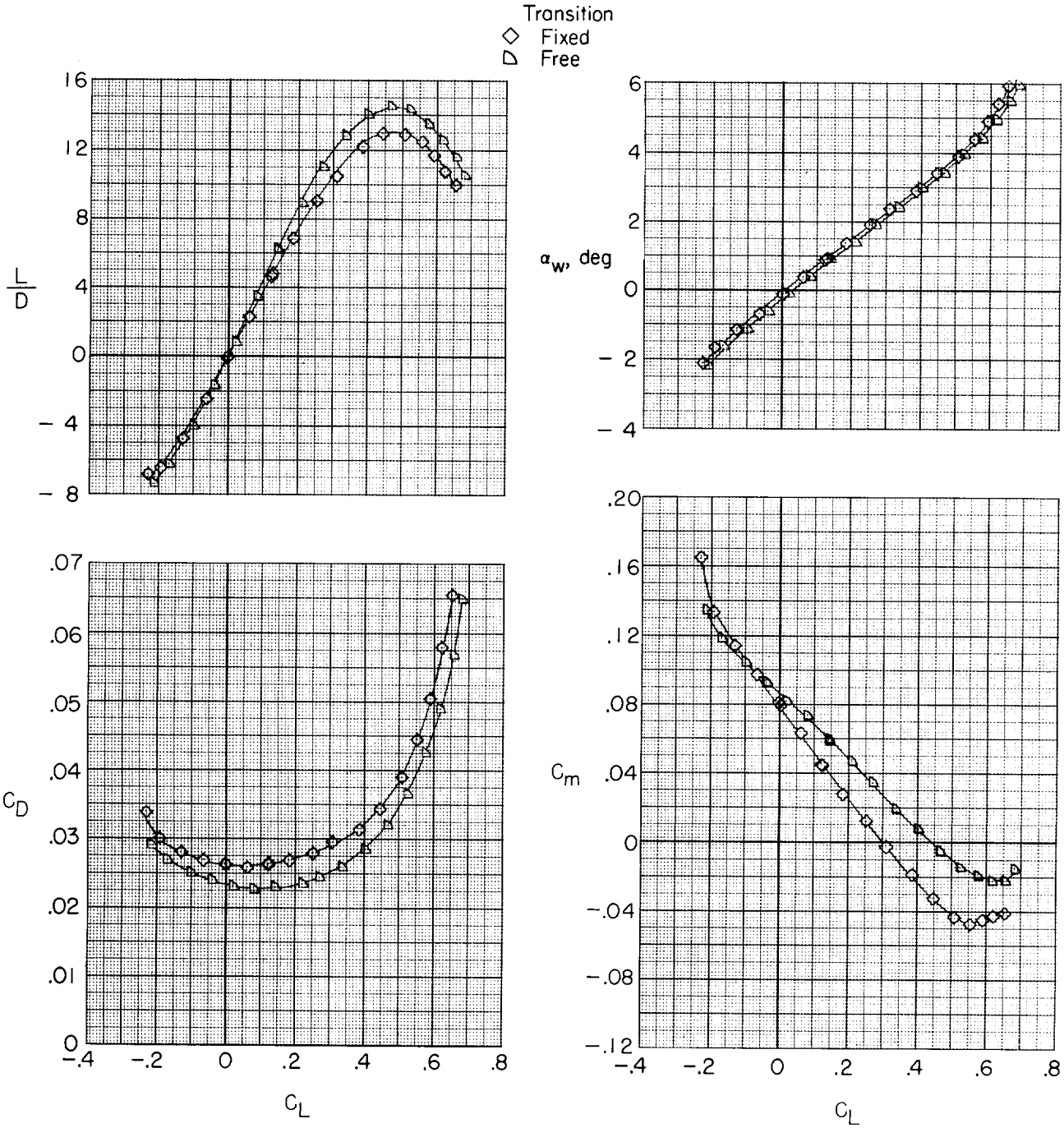

(d) M = 0.75.

Figure 11.- Continued.

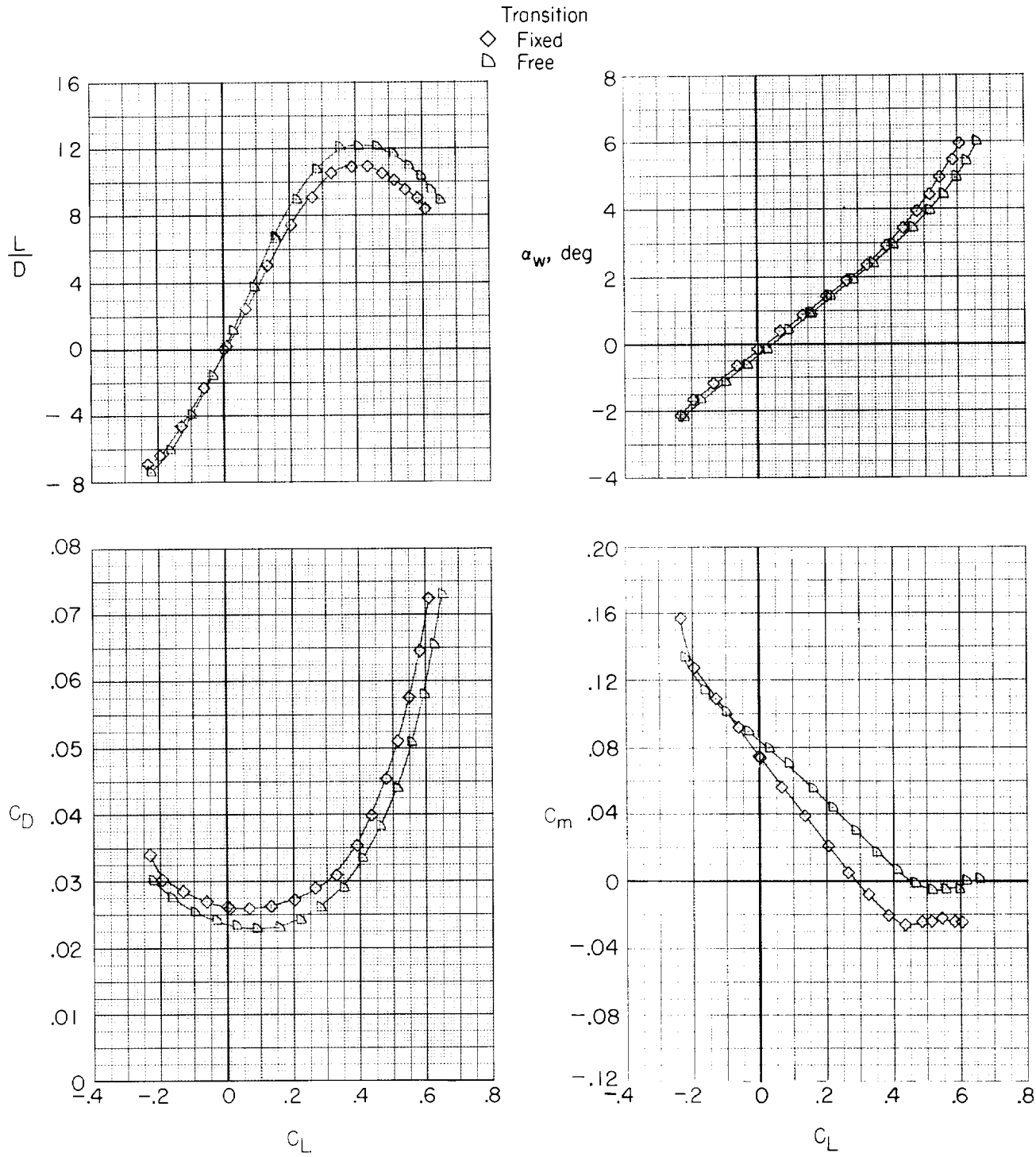

(e) M = 0.775.

Figure 11.- Continued.

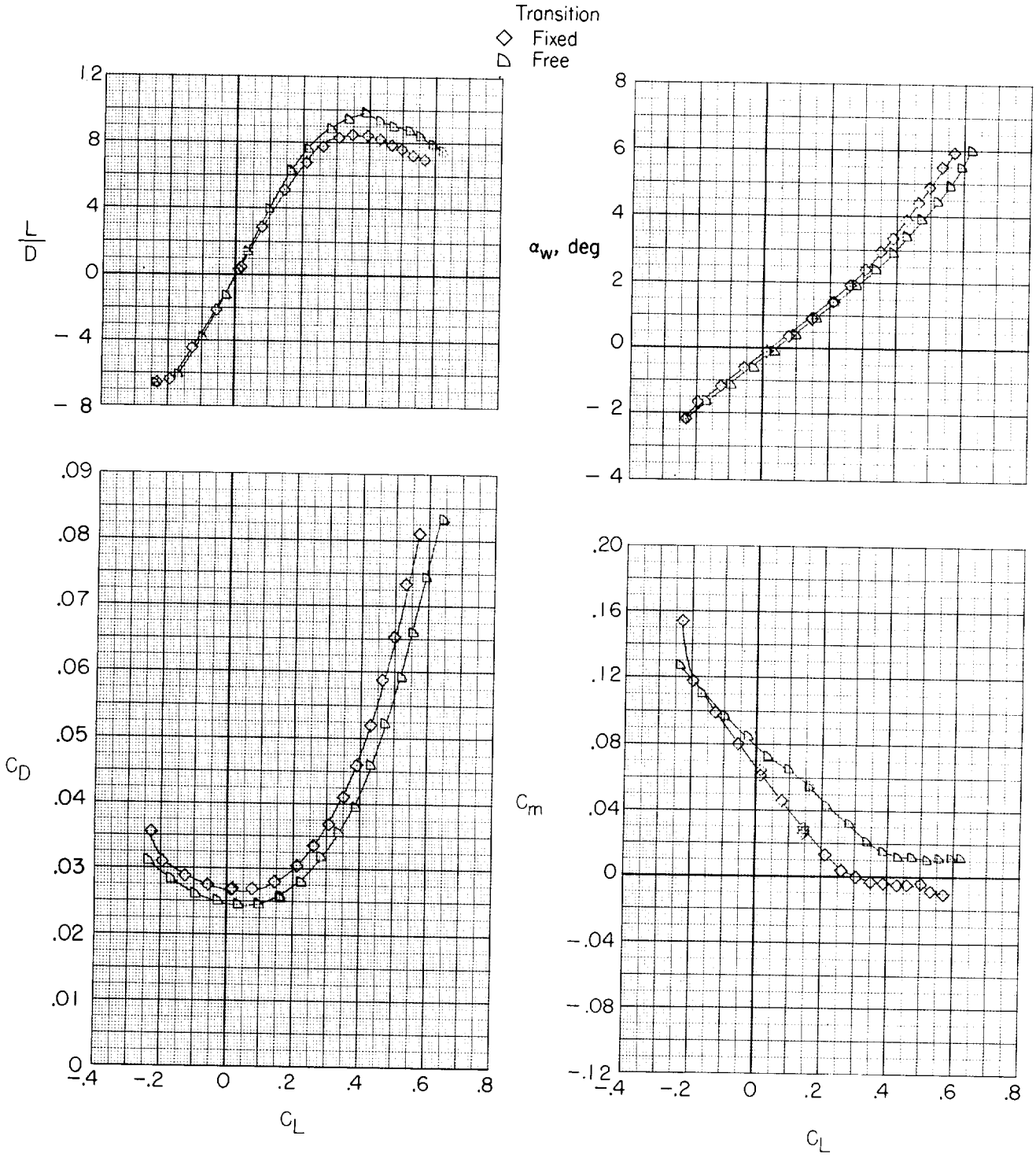

(f) M = 0.80.

Figure 11.- Continued.

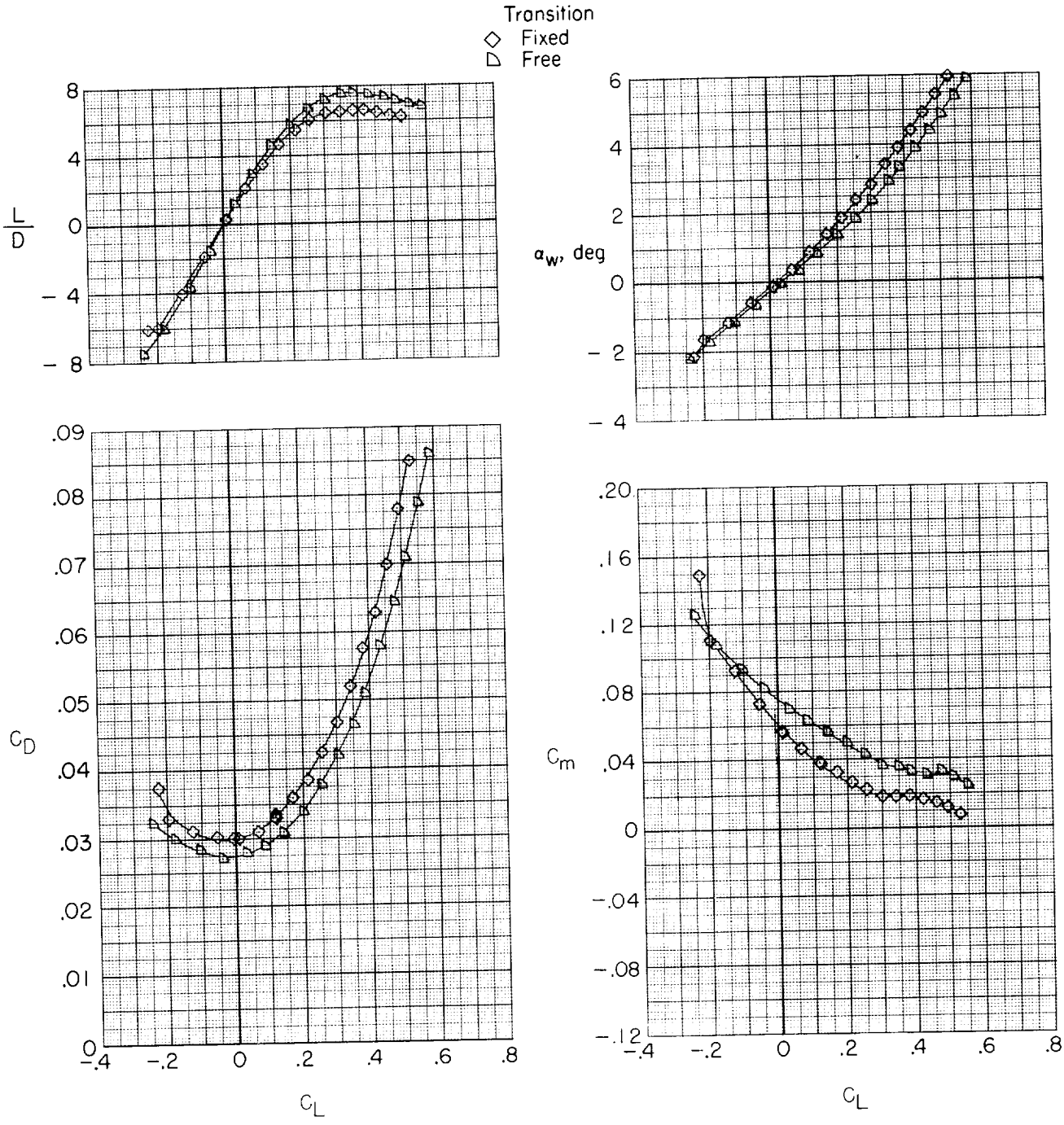

(g) M = 0.825.

Figure 11.- Continued.

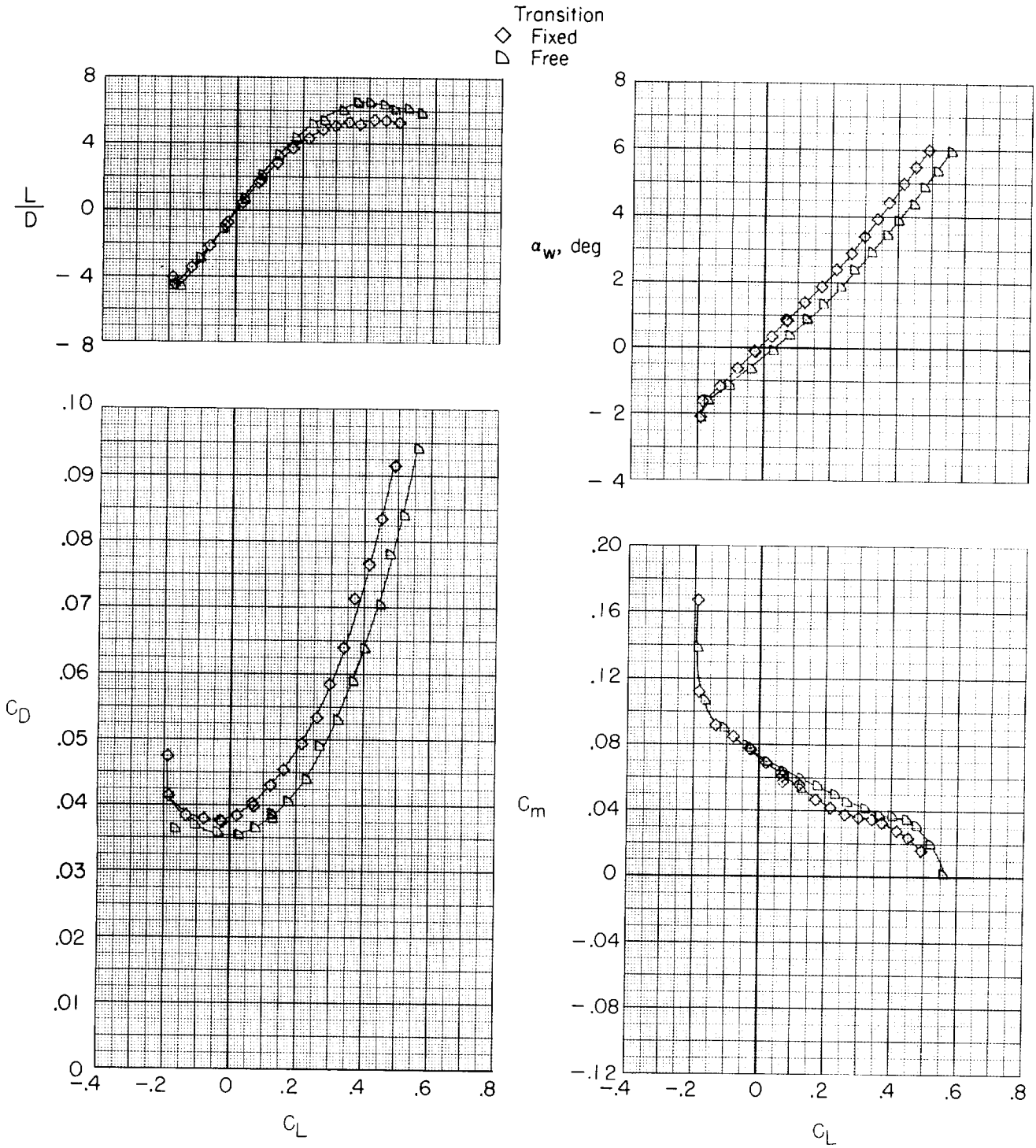

(h) M = 0.85.

Figure 11.- Concluded.

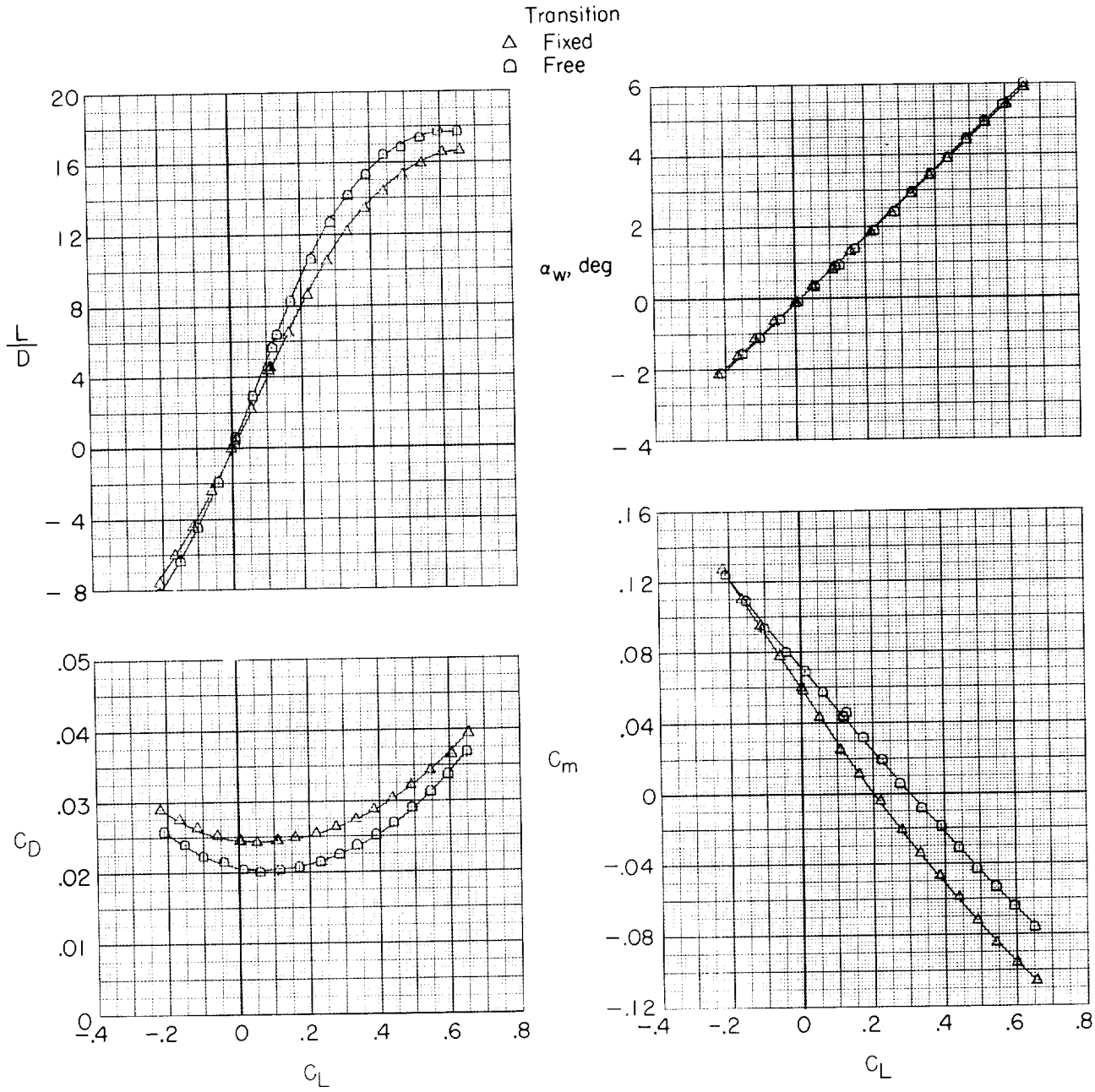

(a) M = 0.55.

Figure 12.- Longitudinal aerodynamic characteristics for configuration BW_1HVN_1T with $\delta_h = 0^0$. Transition fixed and free.

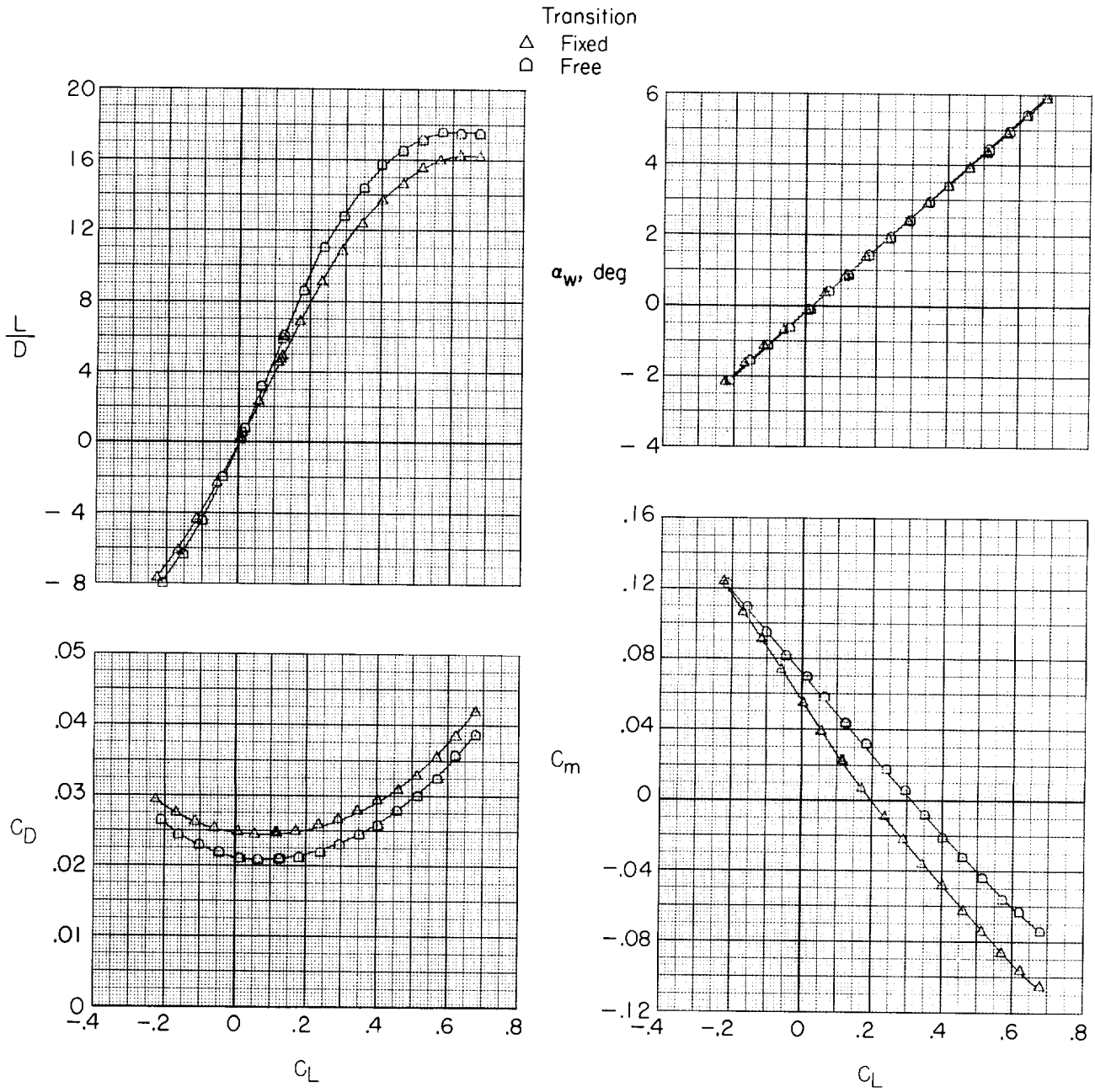

(b) M = 0.625.

Figure 12.- Continued.

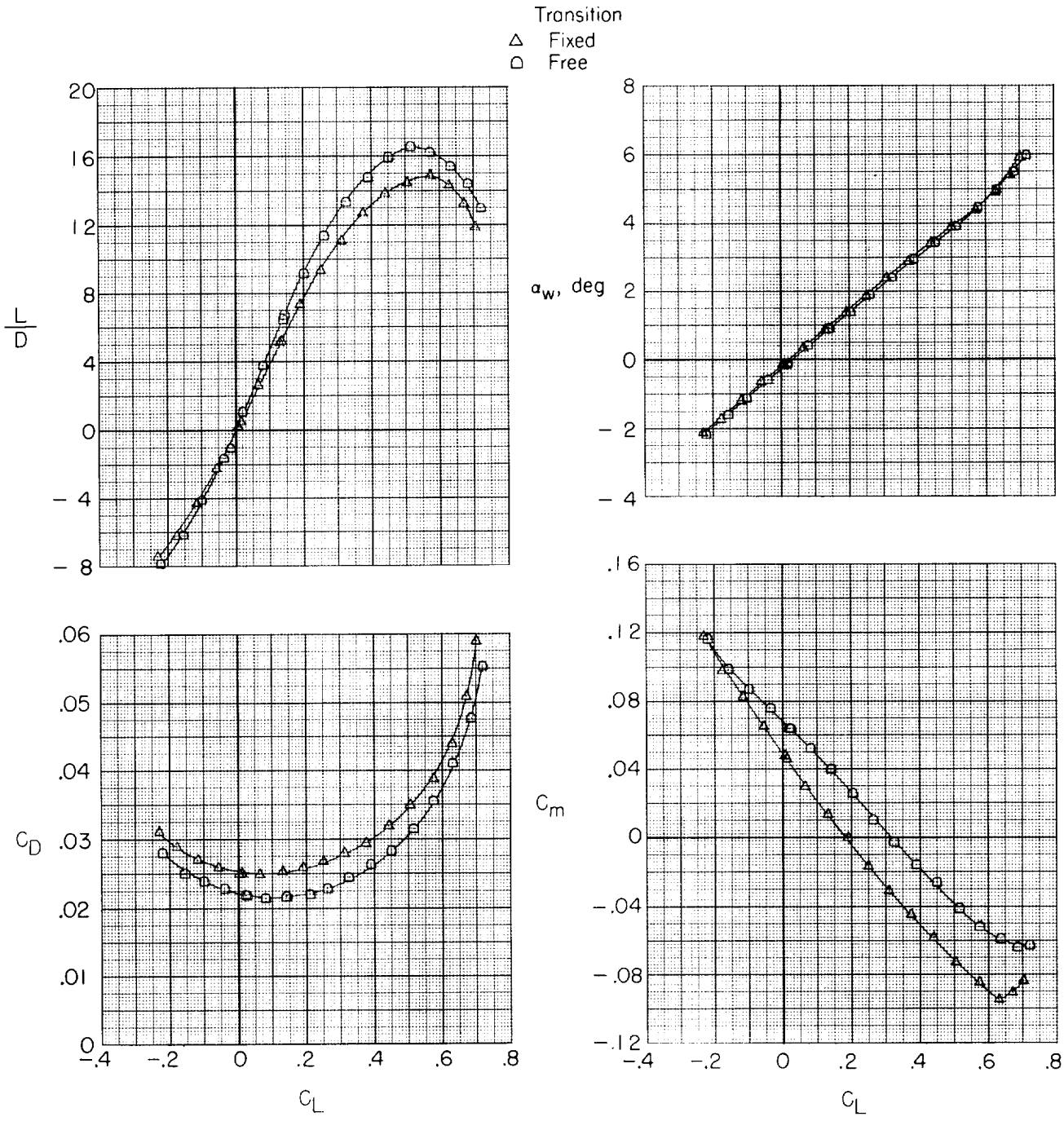

(c) M = 0.725.

Figure 12.- Continued.

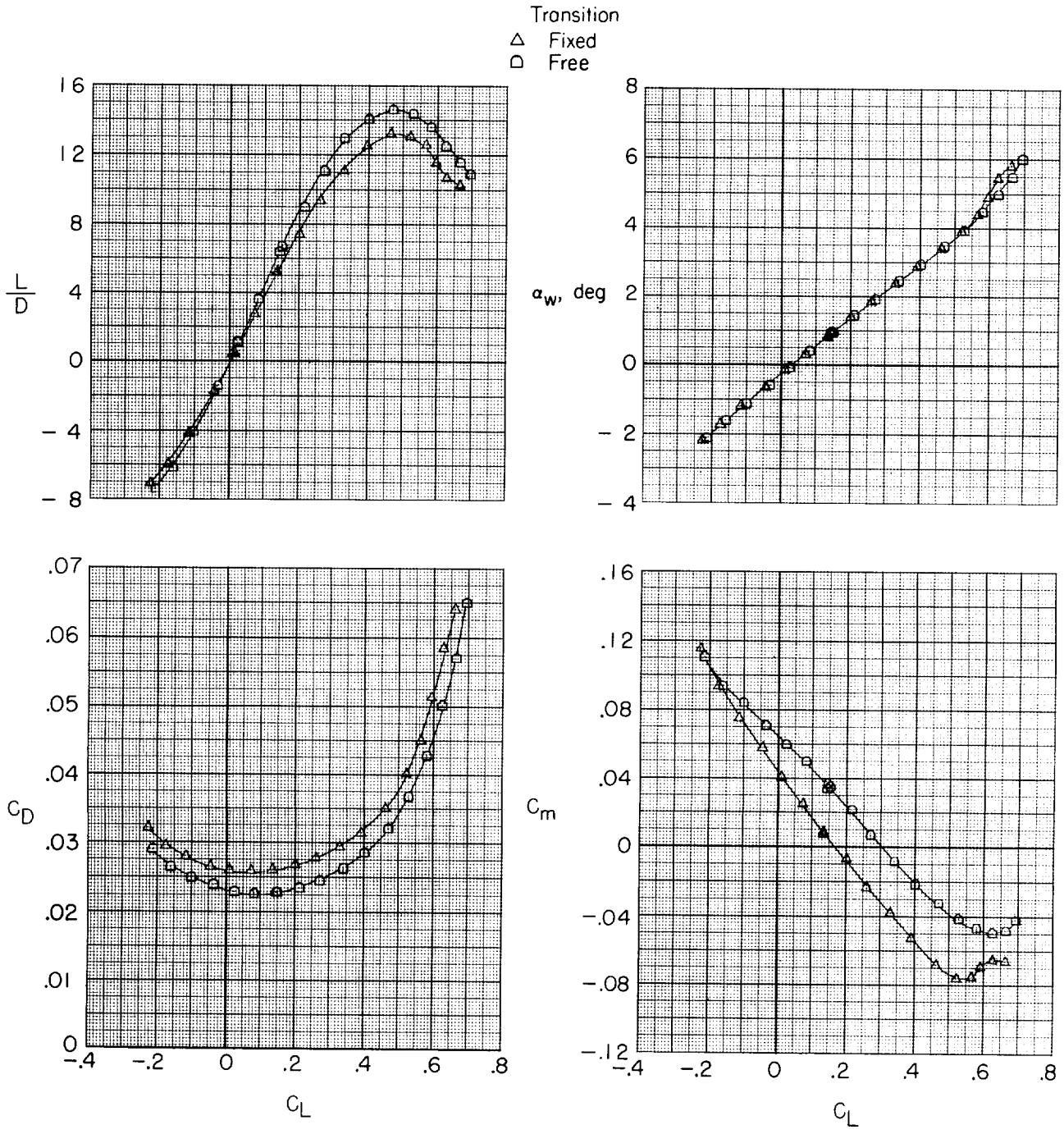

(d) M = 0.75.

Figure 12.- Continued.

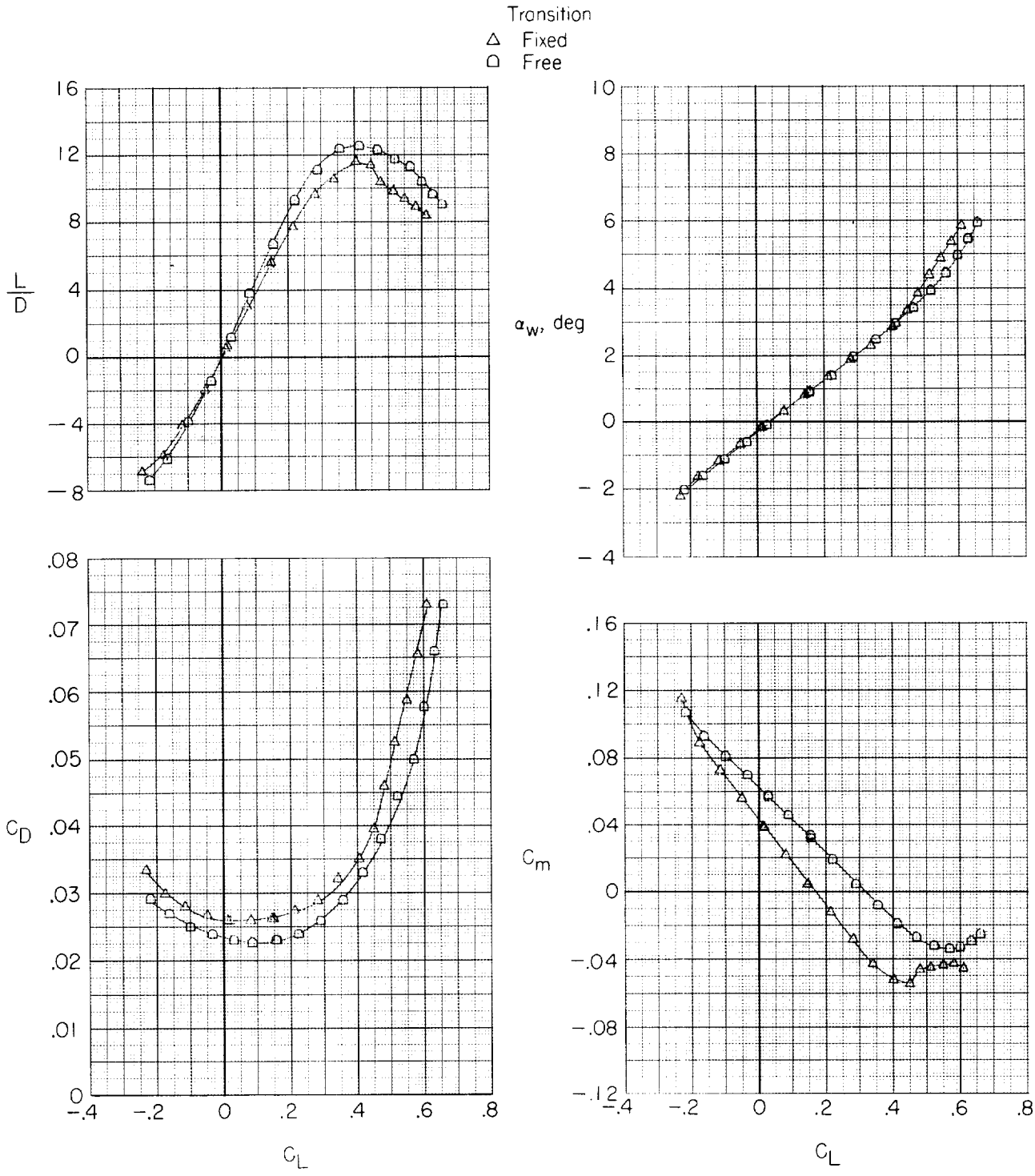

(e) M = 0.775.

Figure 12.- Continued.

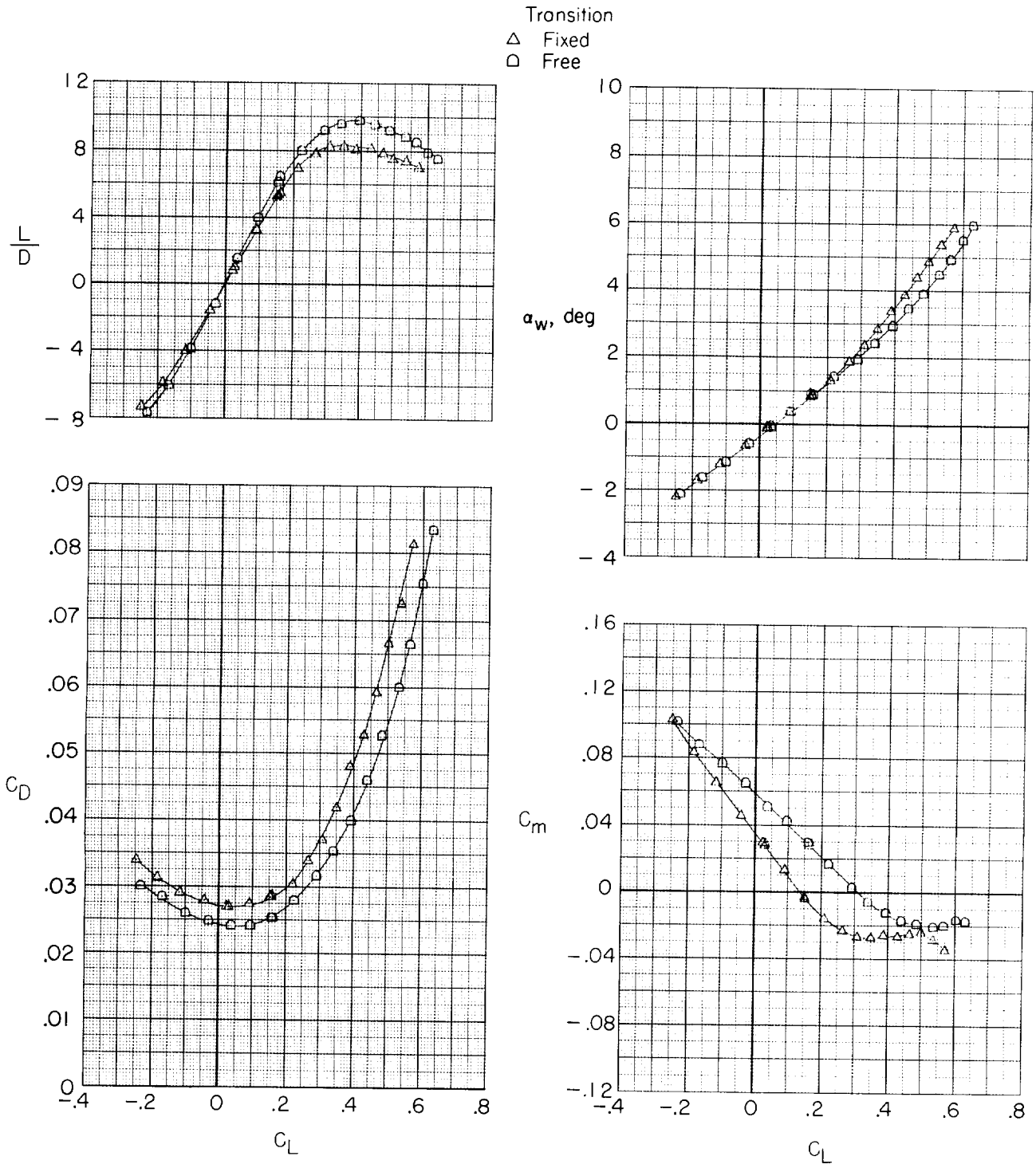

(f) M = 0.80.

Figure 12.- Continued.

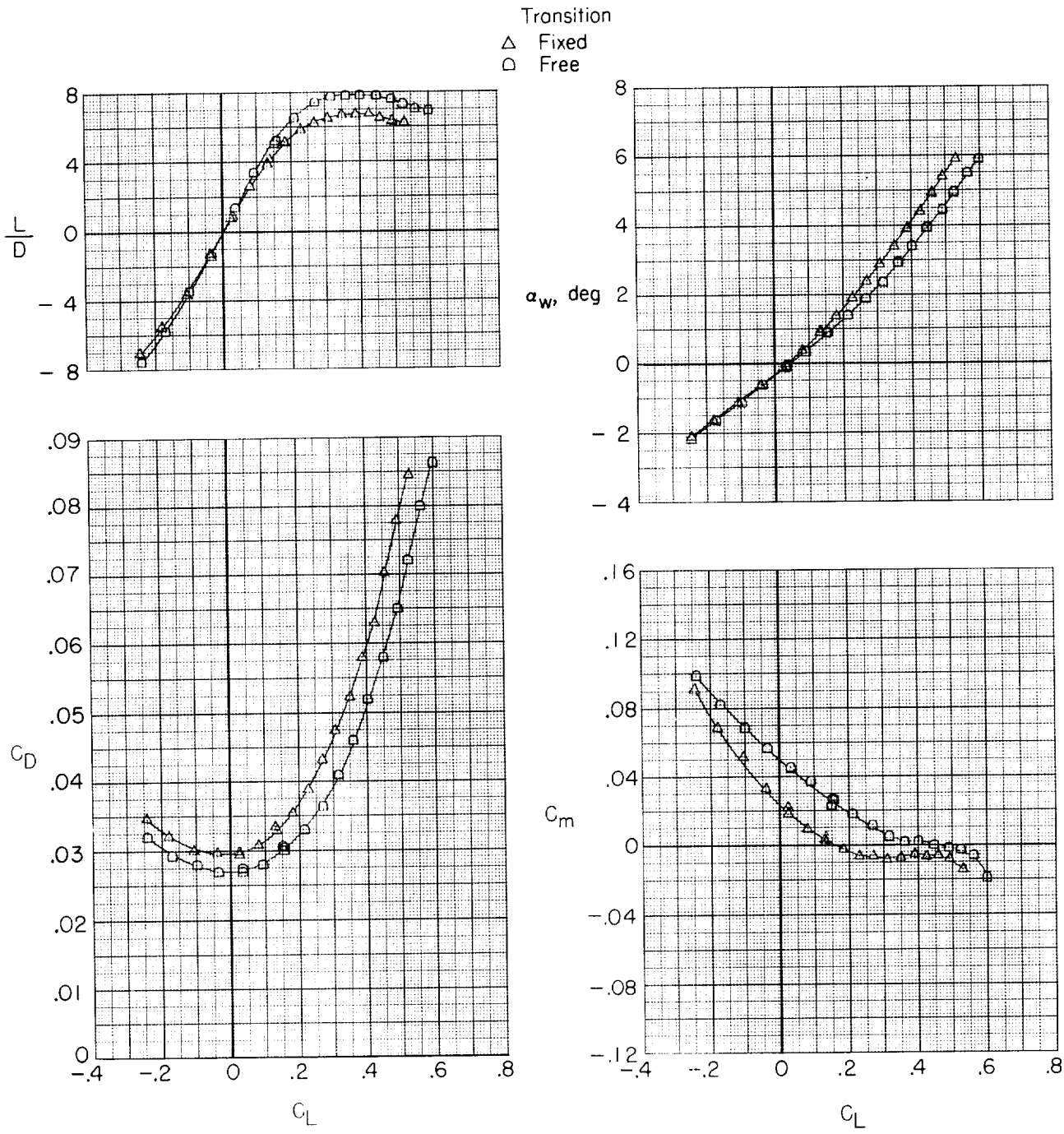

(g) M = 0.825.

Figure 12.- Continued.

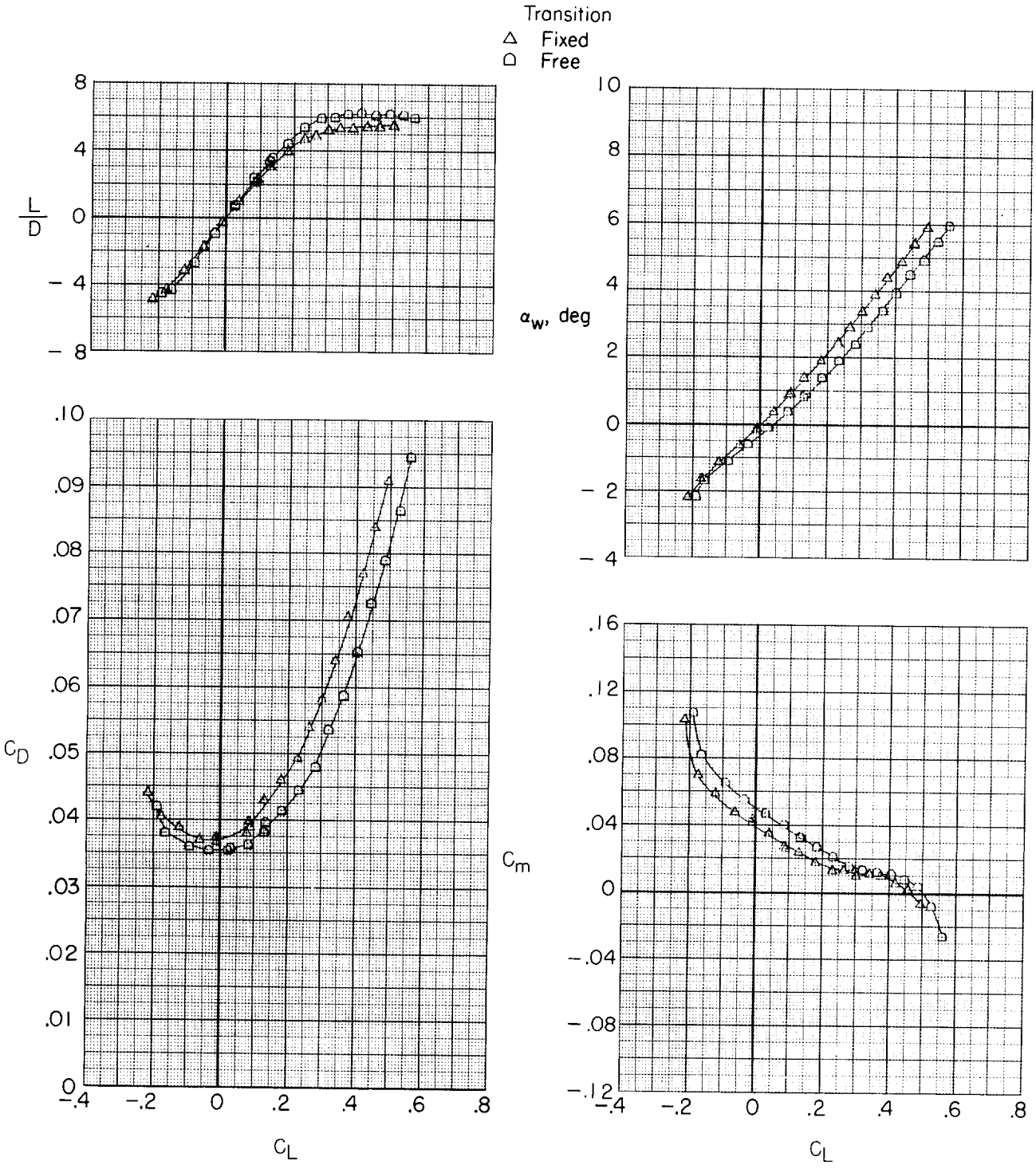

(h) M = 0.85.

Figure 12.- Concluded.

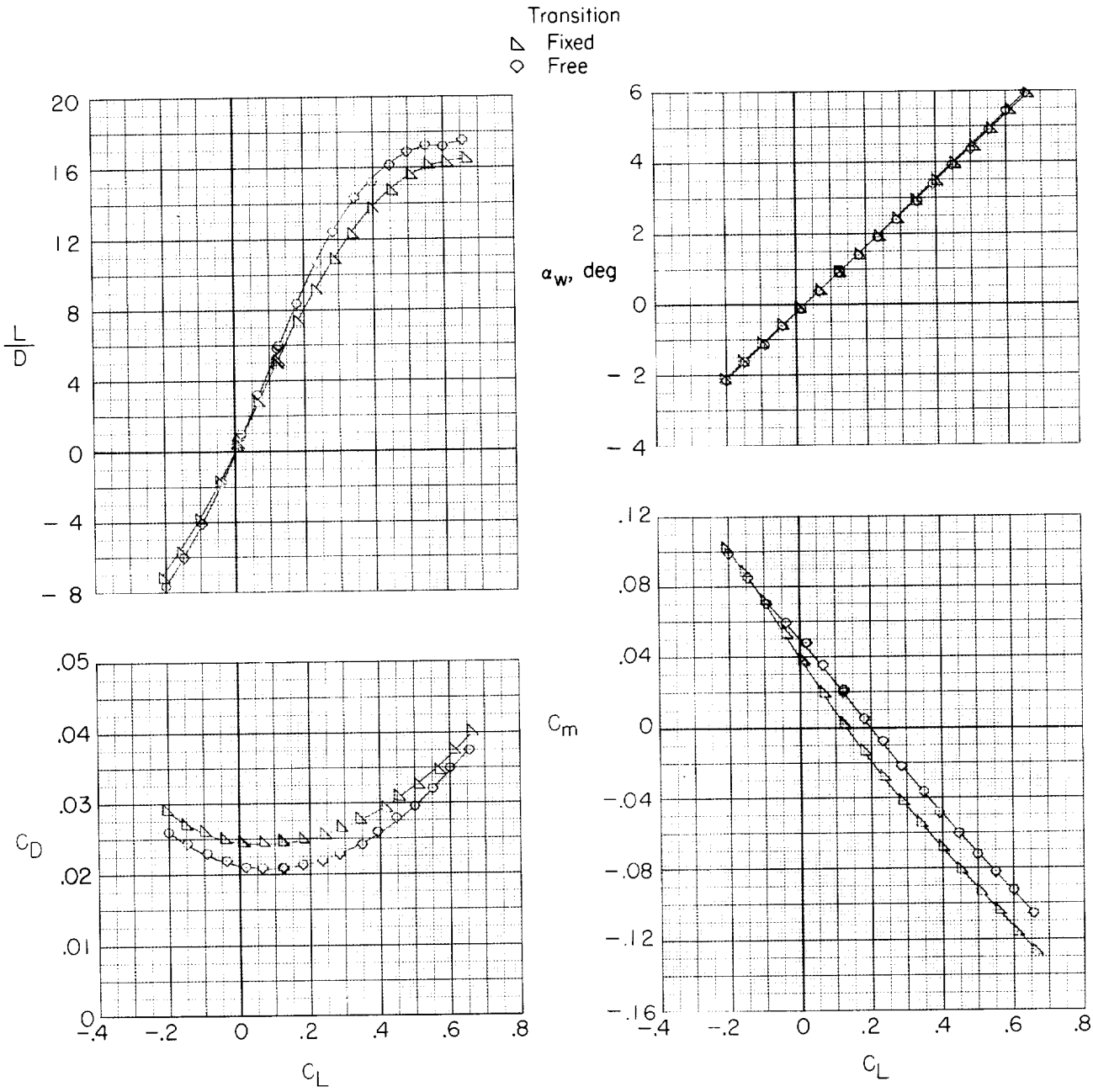

(a) M = 0.55.

Figure 13.- Longitudinal aerodynamic characteristics for configuration BW_1HVN_1T with $\delta_h = 0.5^0$. Transition fixed and free.

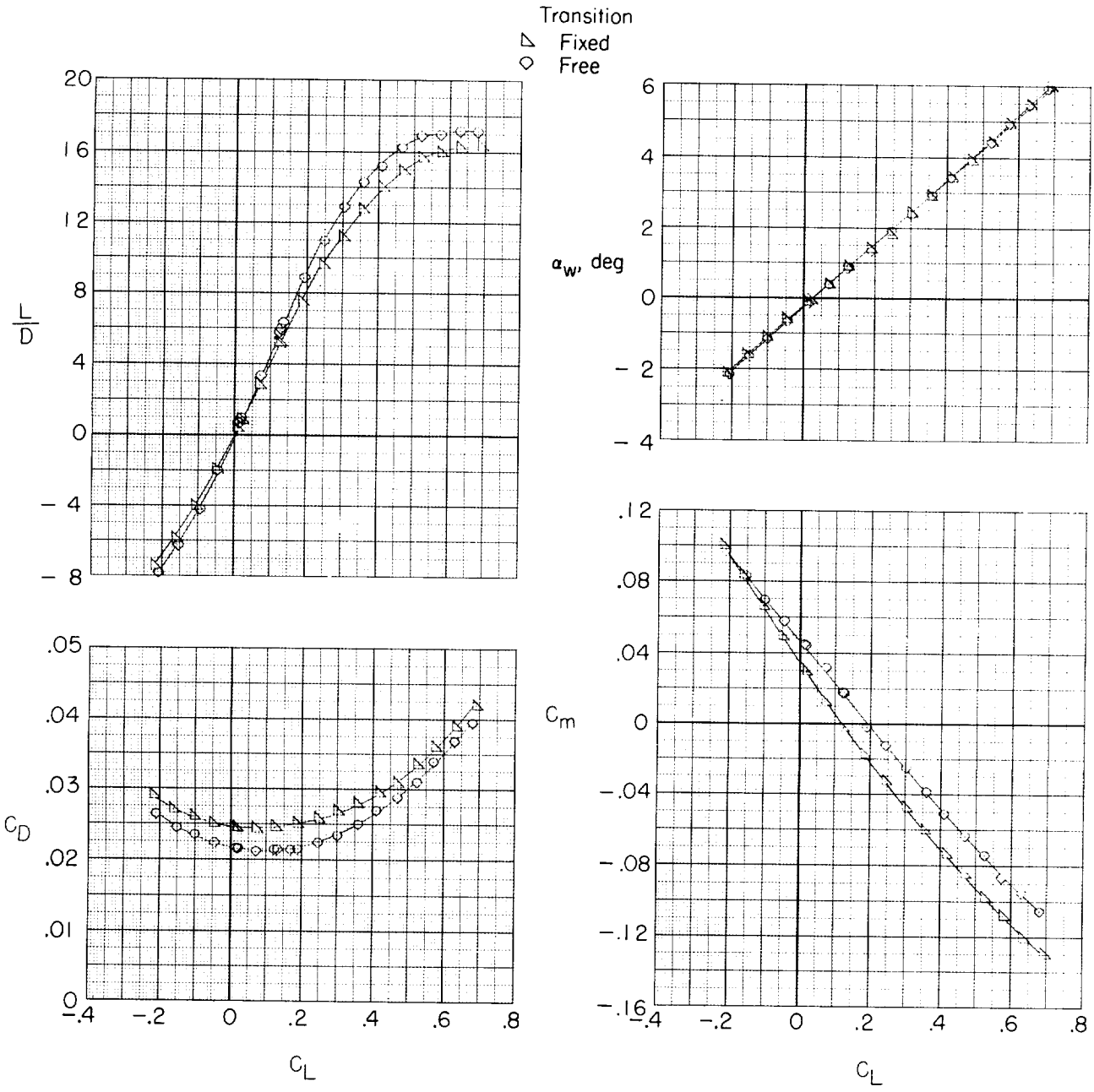

(b) M = 0.625.

Figure 13.- Continued.

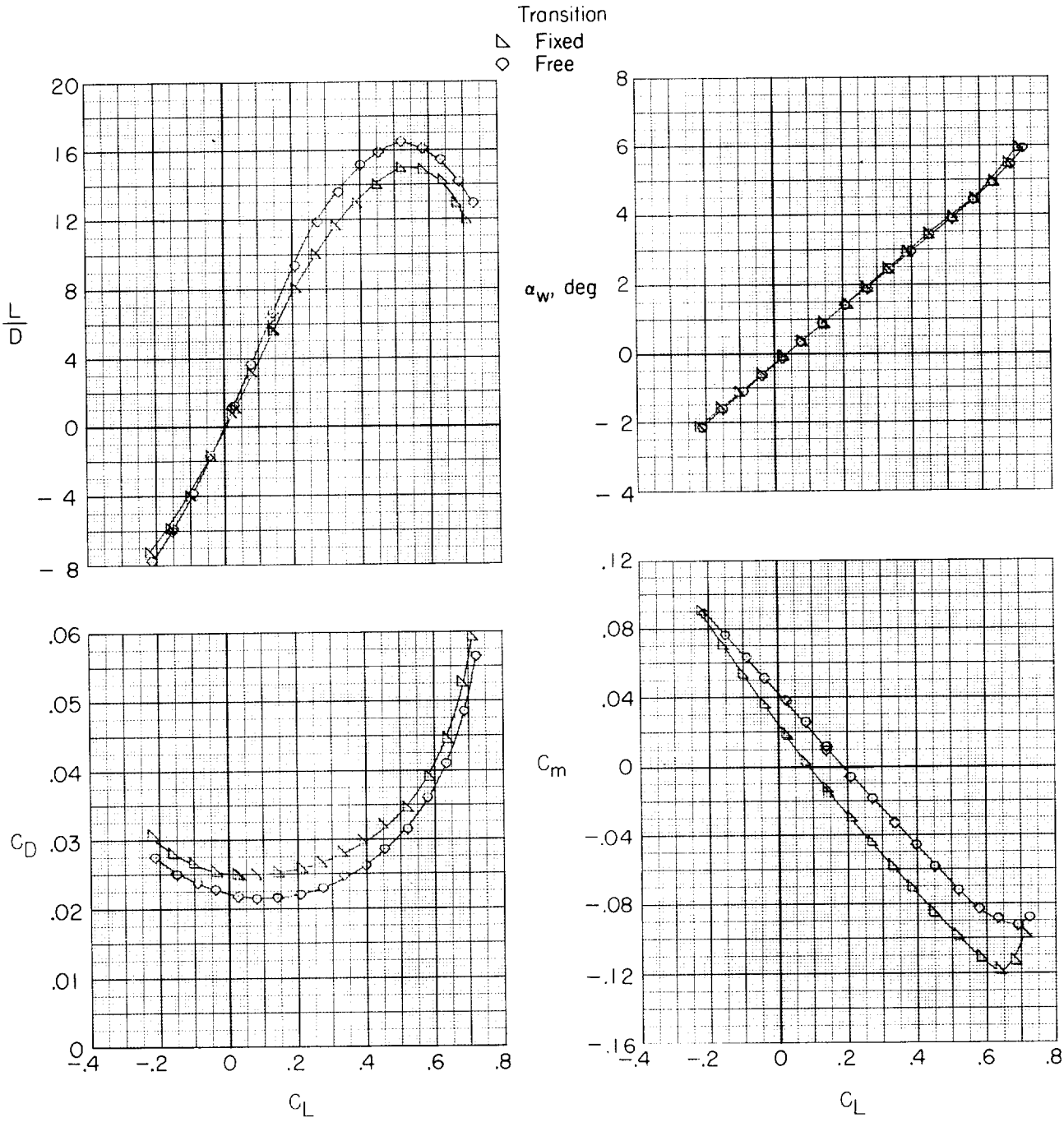

(c) M = 0.725.

Figure 13.- Continued.

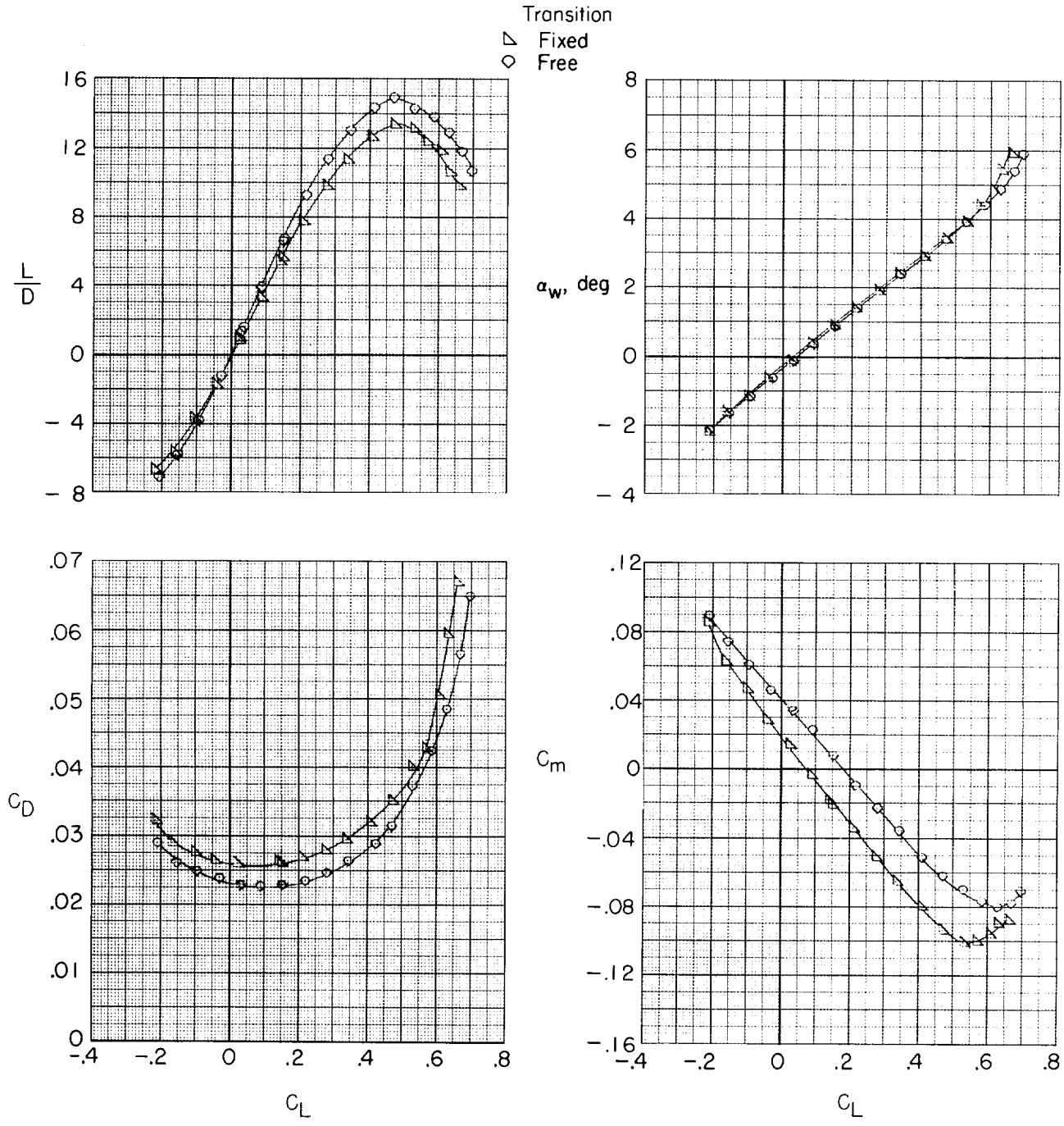

(d) M = 0.75.

Figure 13.- Continued.

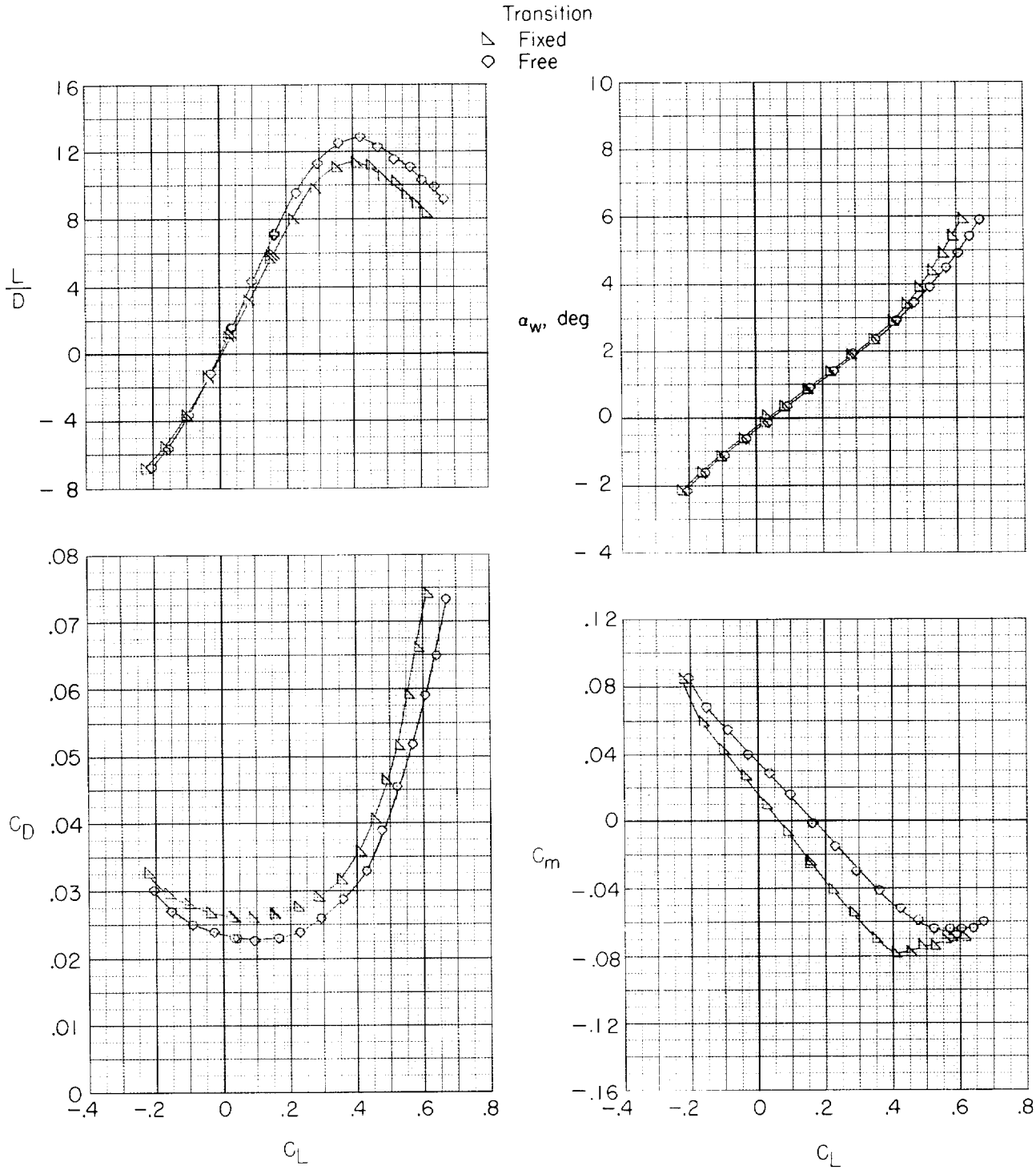

(e) M = 0.775.

Figure 13.- Continued.

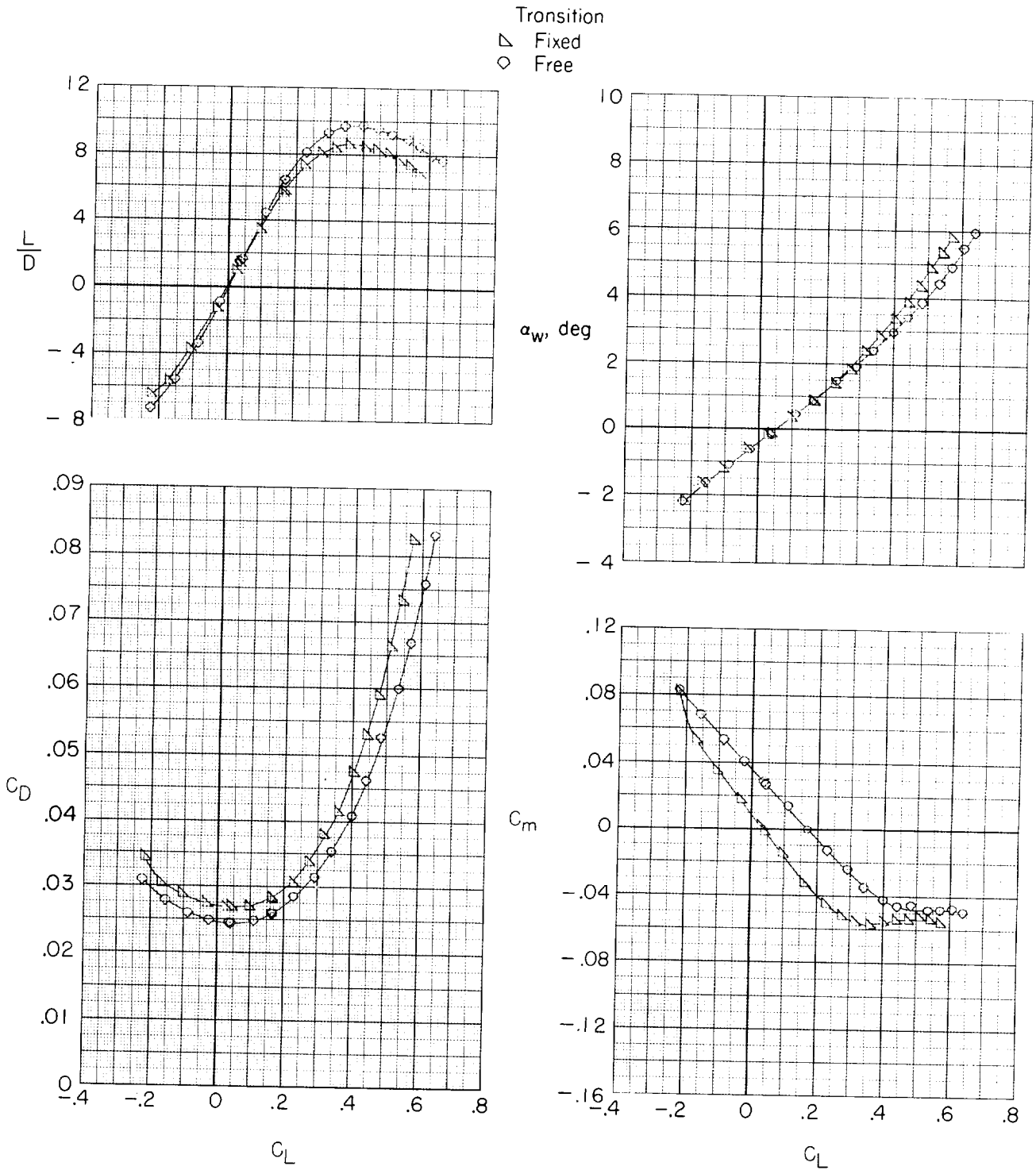

(f) M = 0.80.

Figure 13.- Continued.

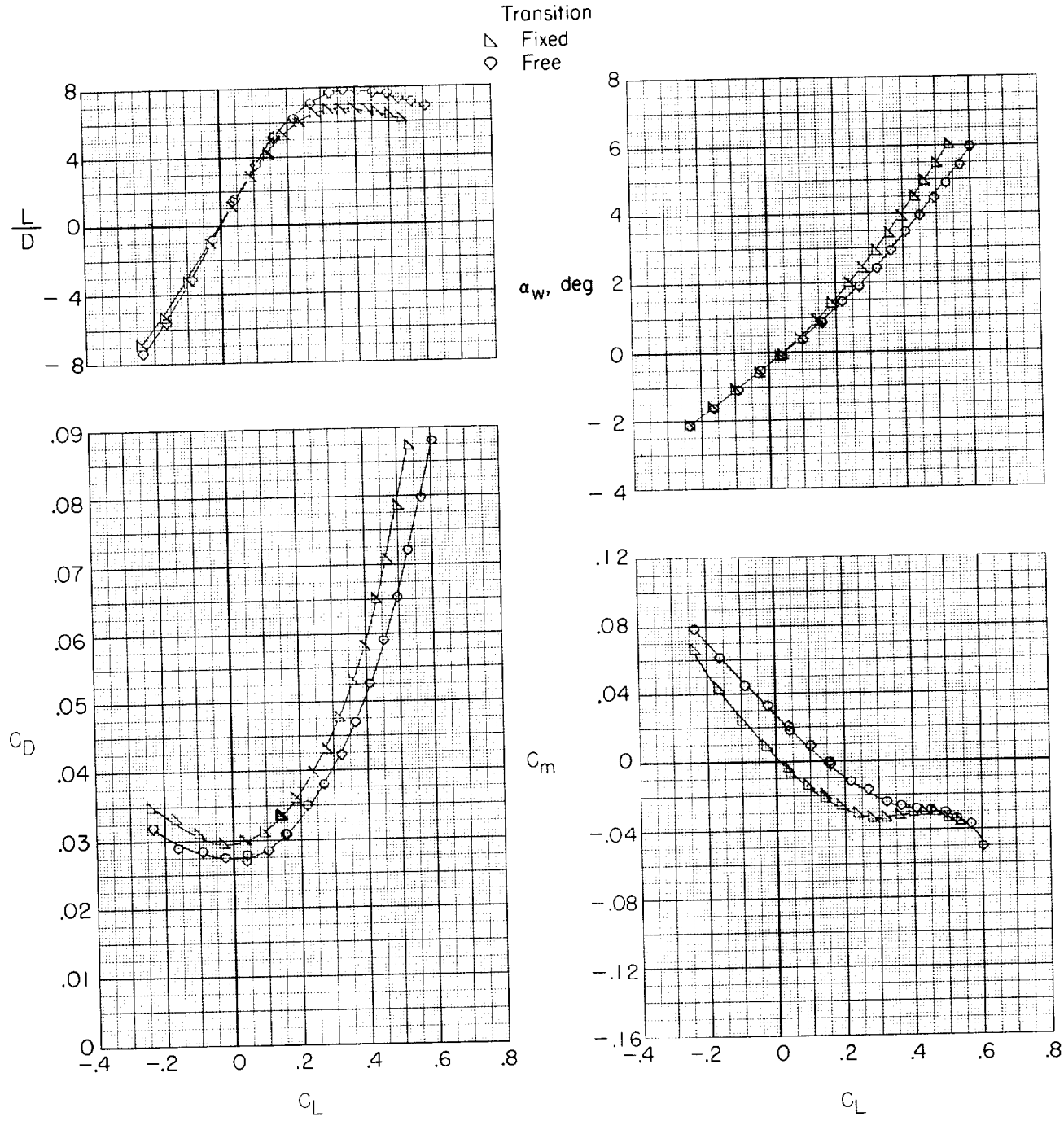

(g) M = 0.825.

Figure 13.- Continued.

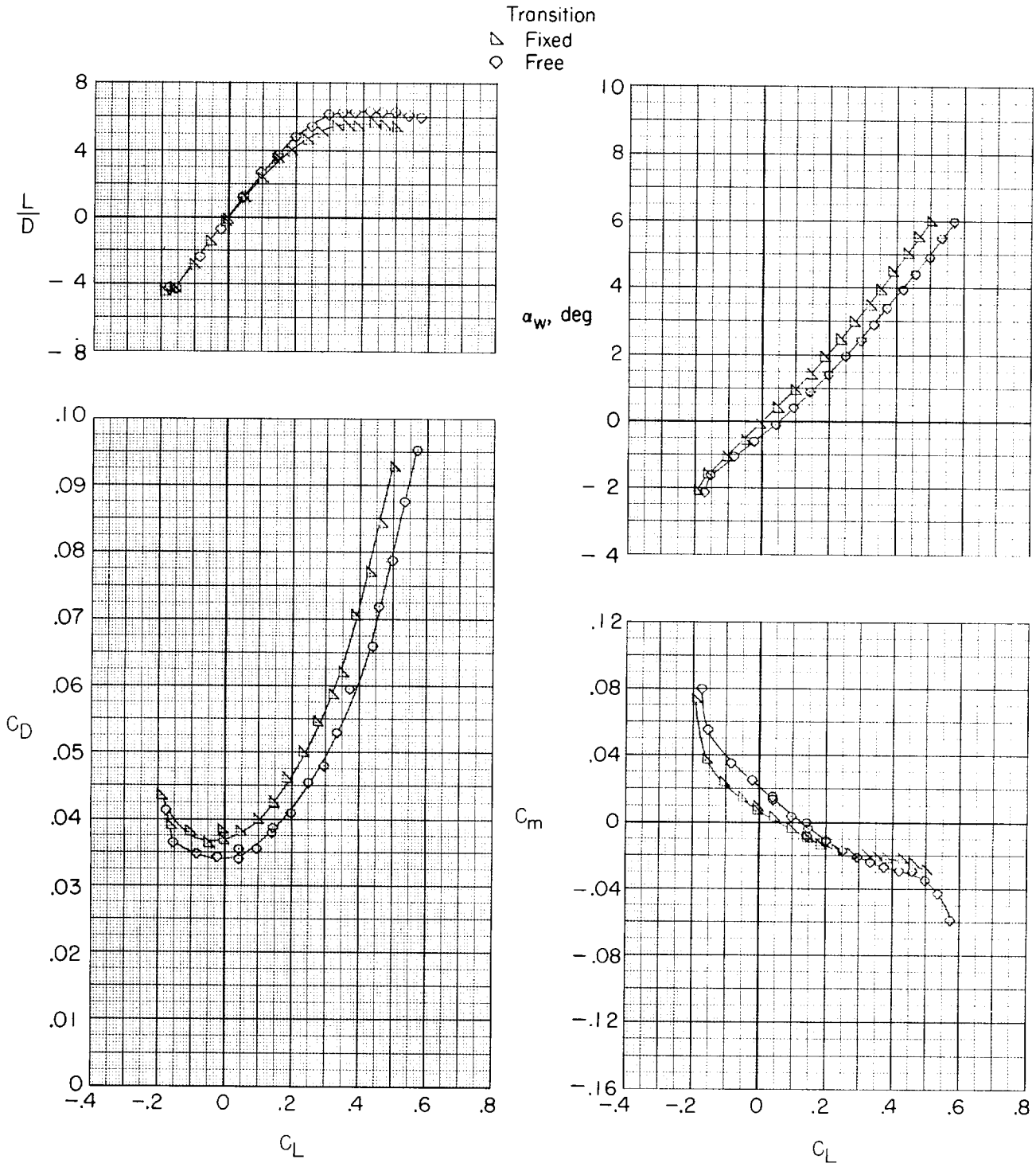

(h) M = 0.85.

Figure 13.- Concluded.

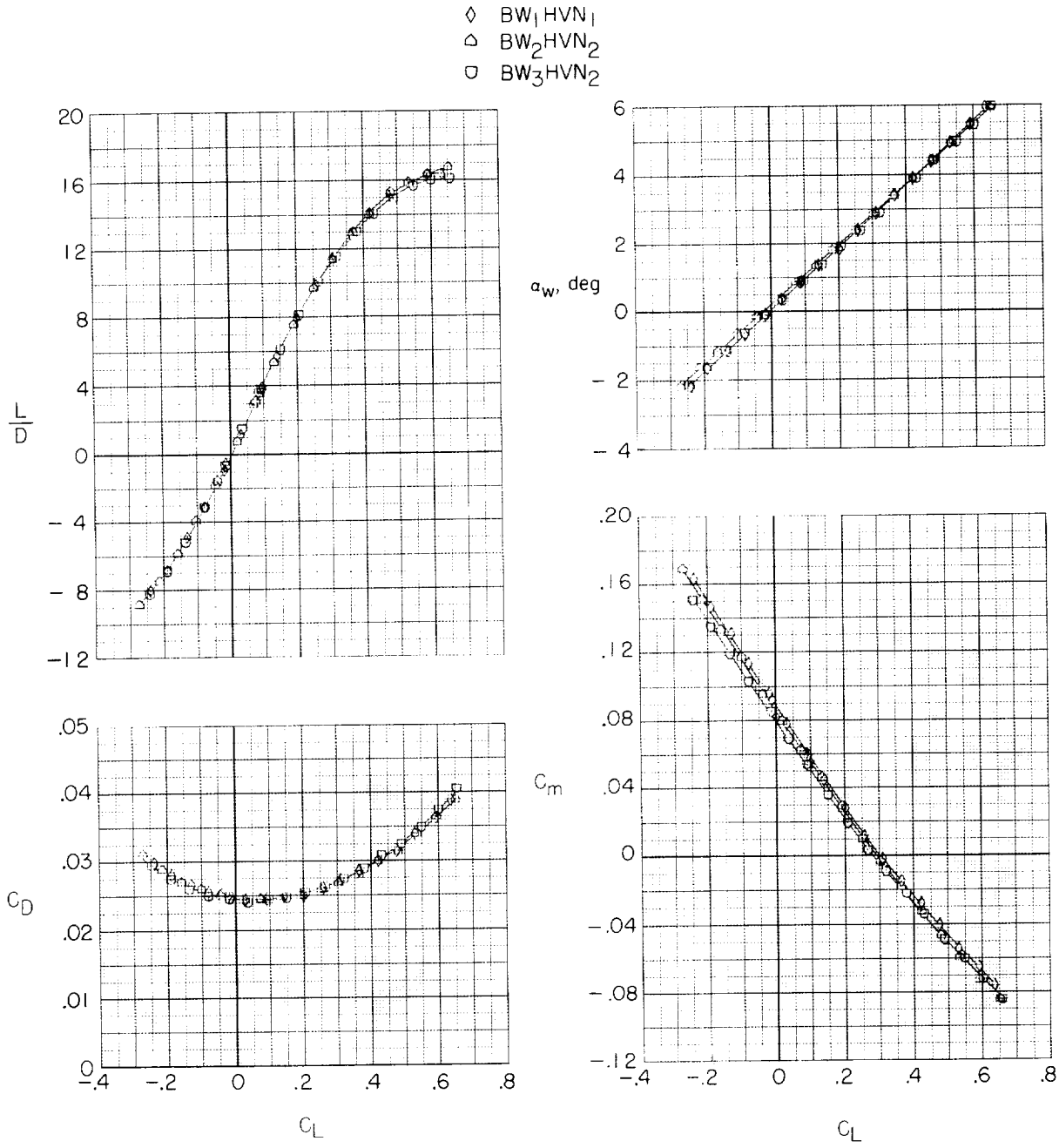

(a) $M_\infty = 0.55$.

Figure 14.- Longitudinal aerodynamic characteristics for configurations BW_1HVN_1, BW_2HVN_2, and BW_3HVN_2 with $\delta_h = -0.5^o$. Transition fixed.

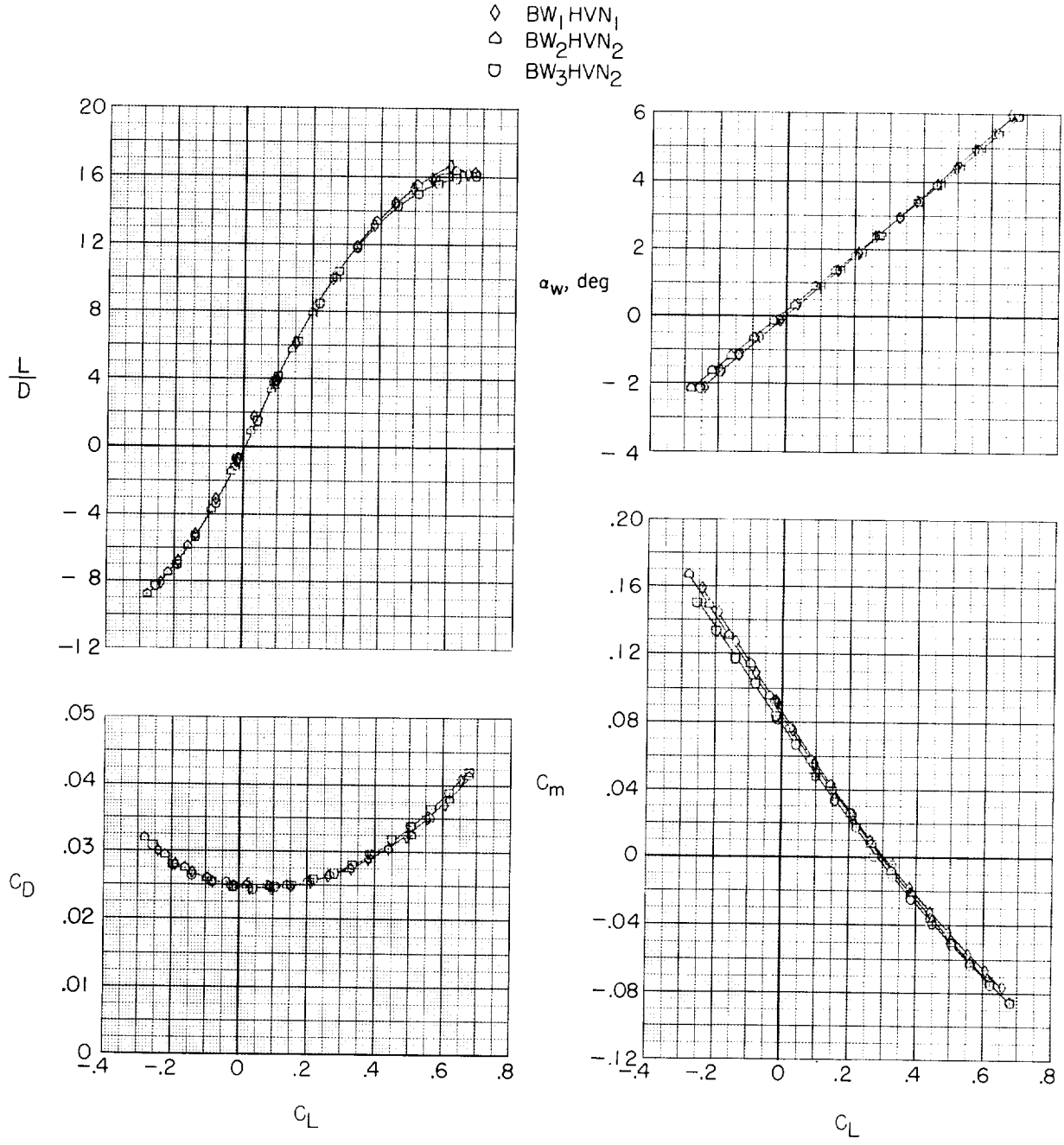

(b) M = 0.625.

Figure 14.- Continued.

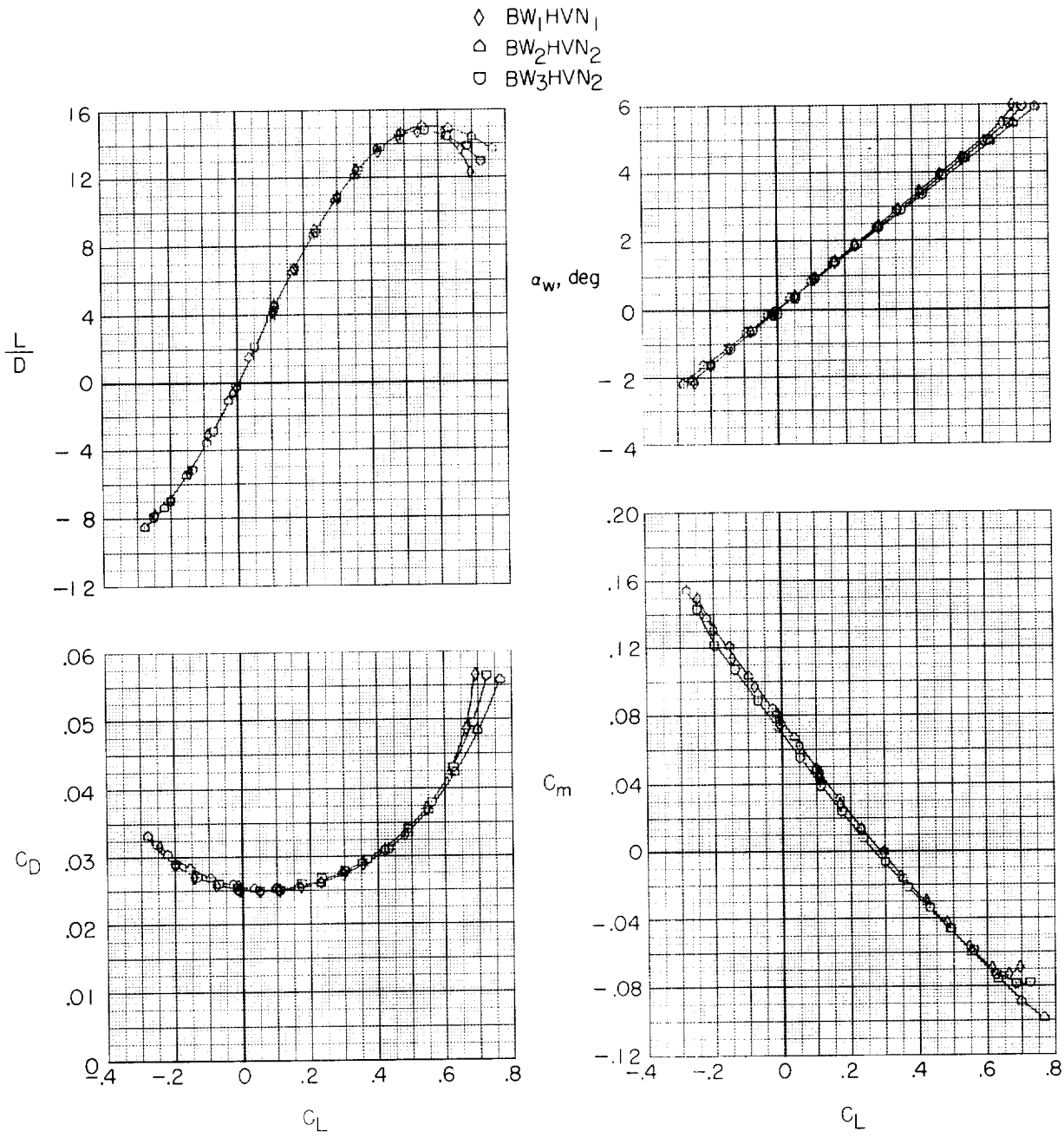

(c) M = 0.725.

Figure 14.- Continued.

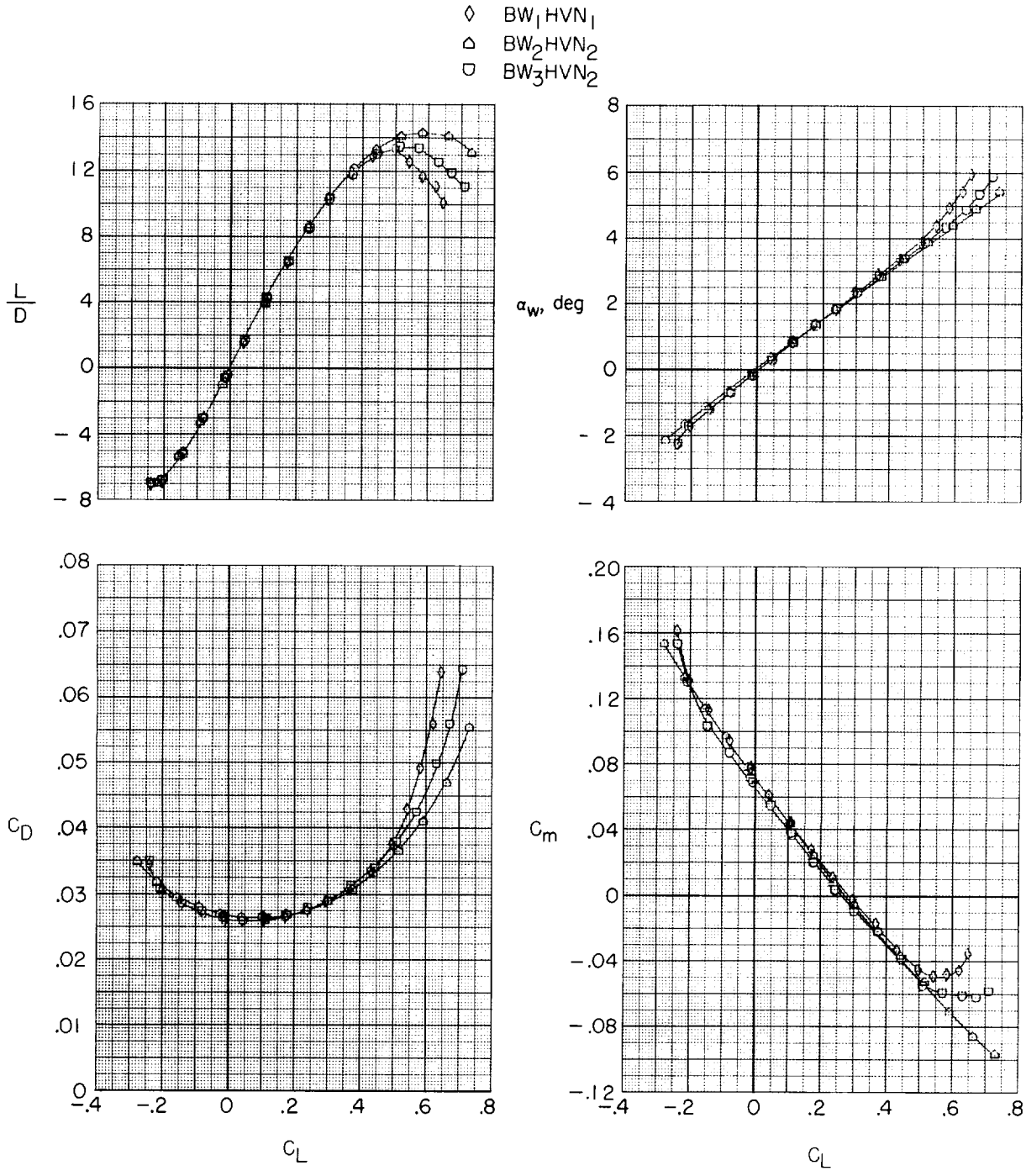

(d) M = 0.75.

Figure 14.- Continued.

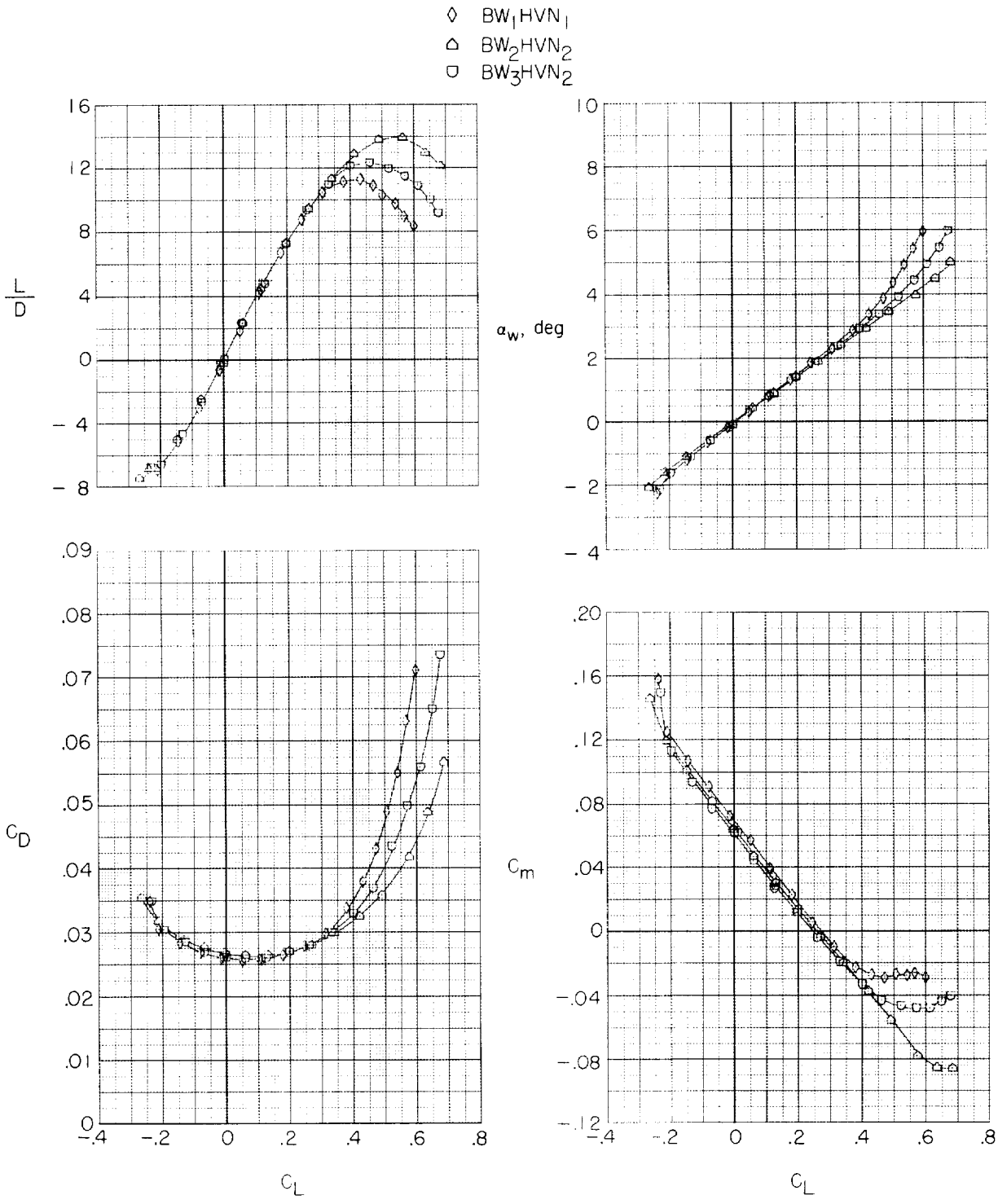

(e) M = 0.775.

Figure 14.- Continued.

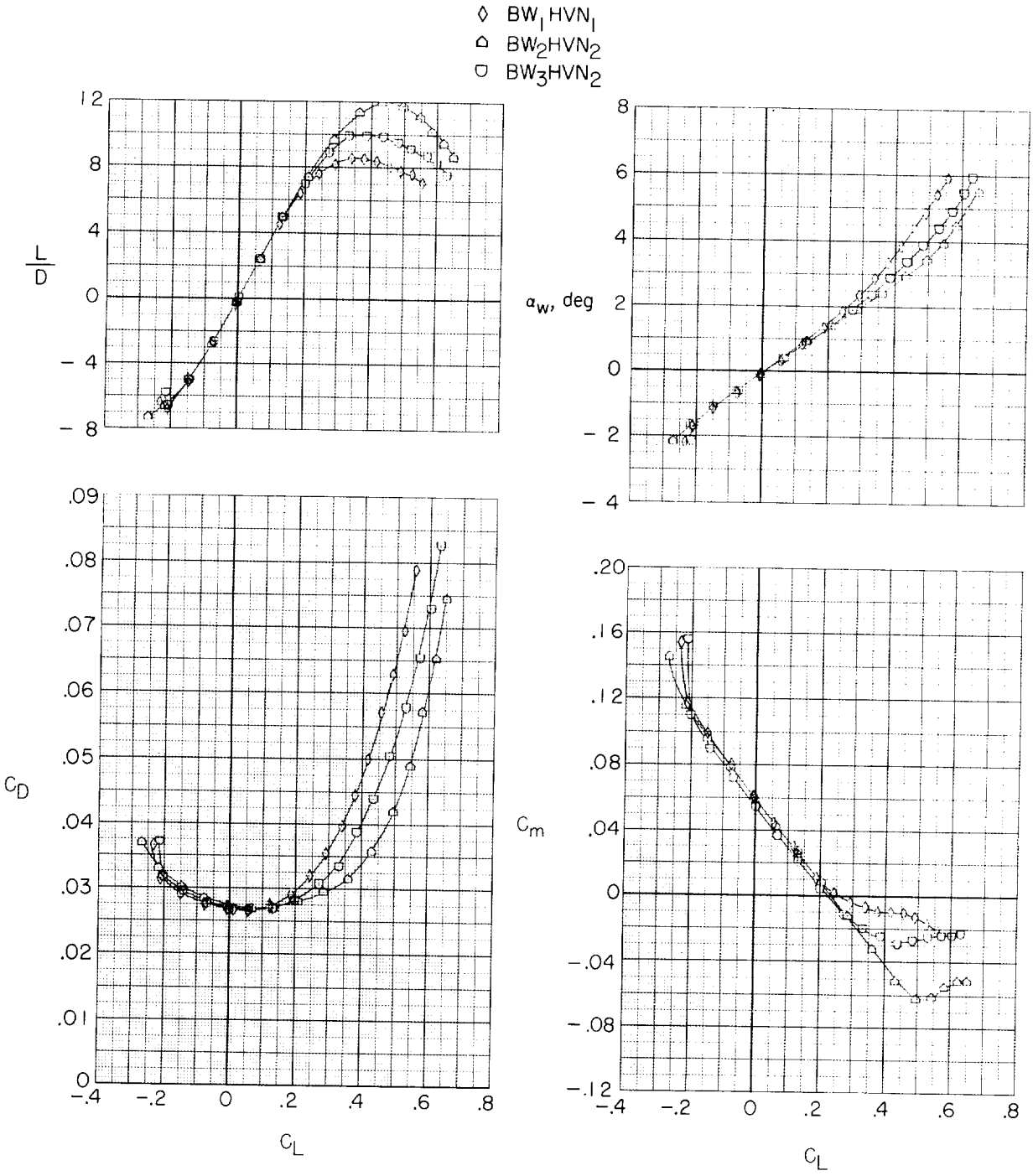

(f) M = 0.80.

Figure 14.- Continued.

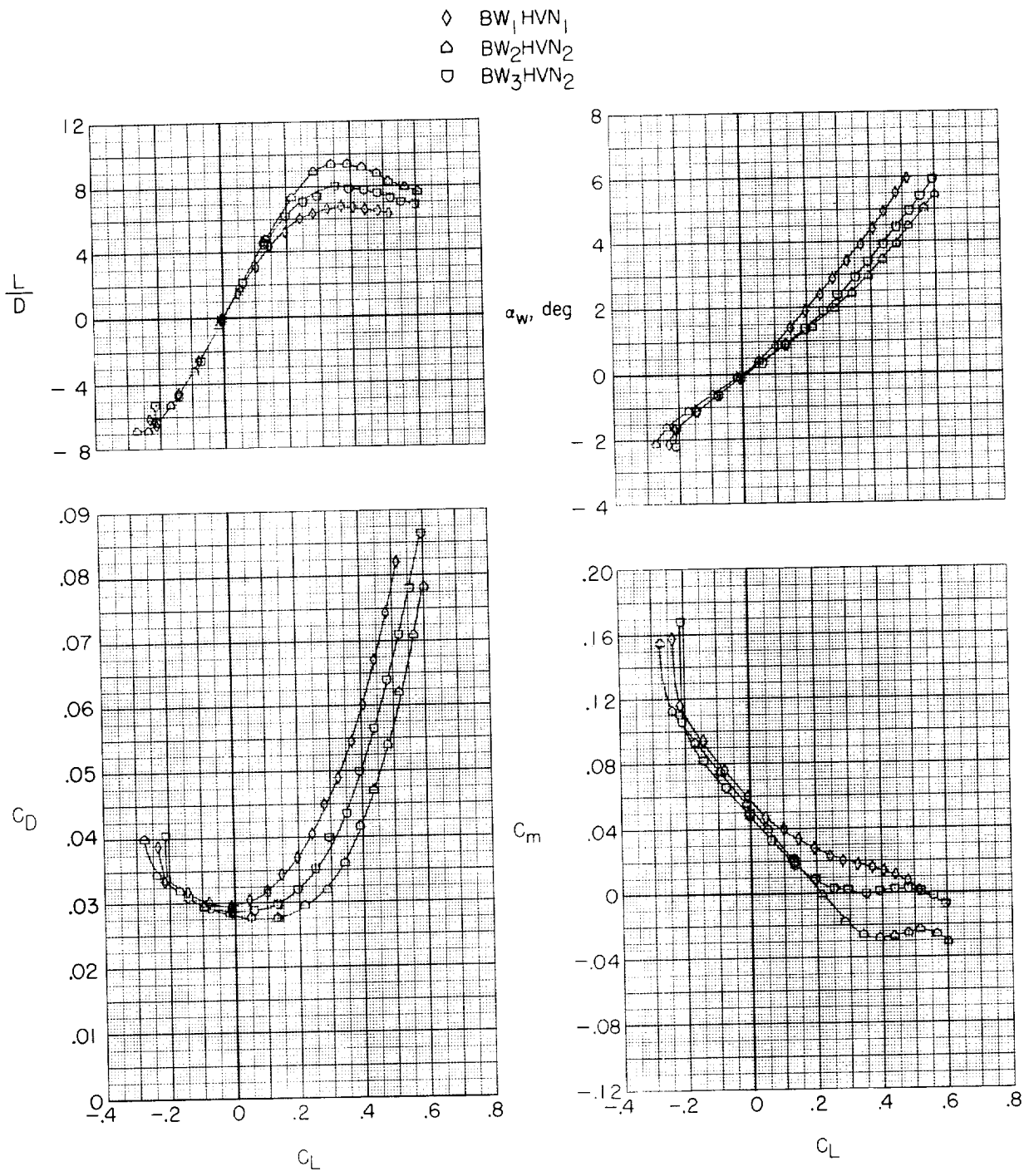

(g) M = 0.825.

Figure 14.- Continued.

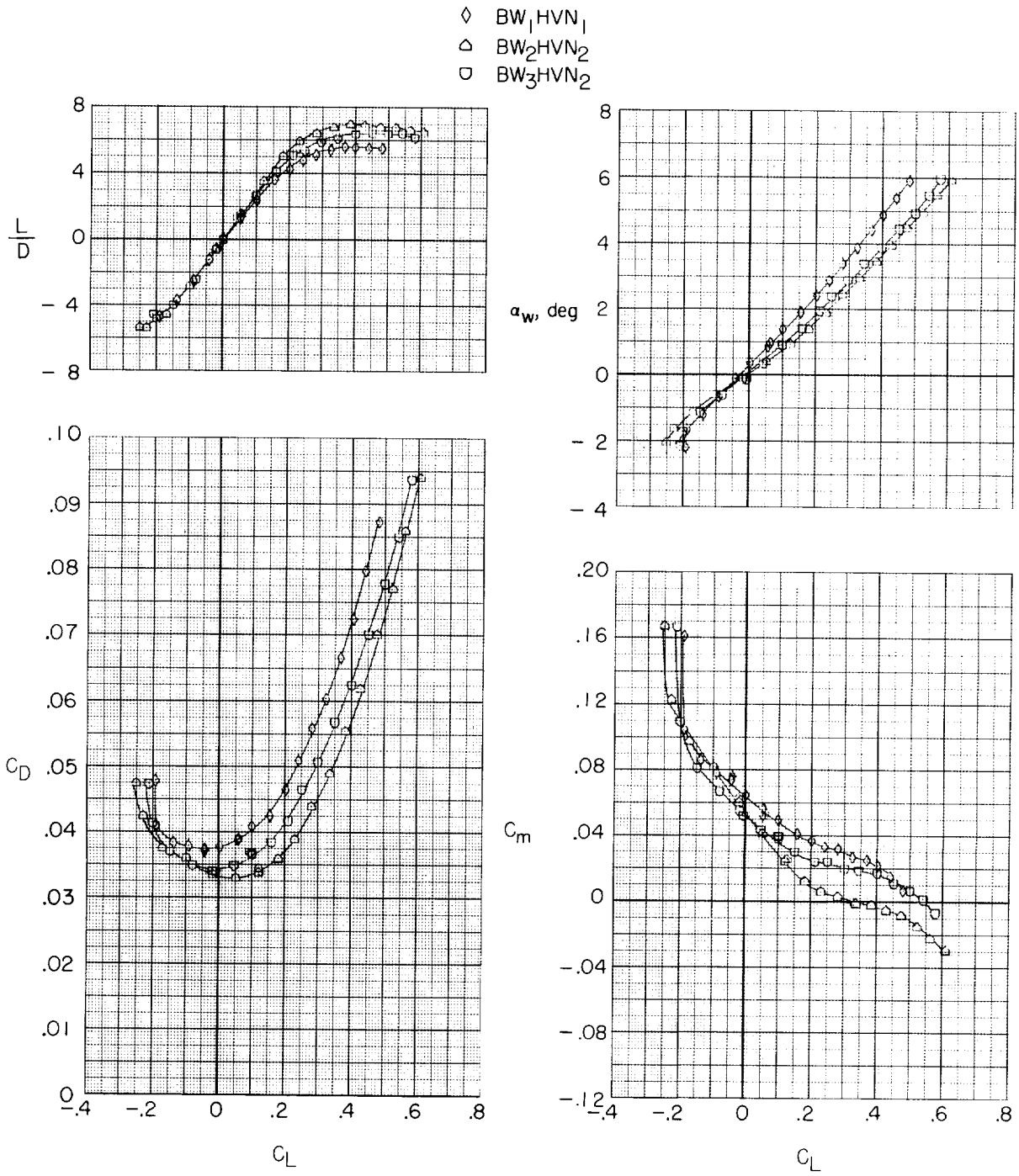

(h) M = 0.85.

Figure 14.- Concluded.

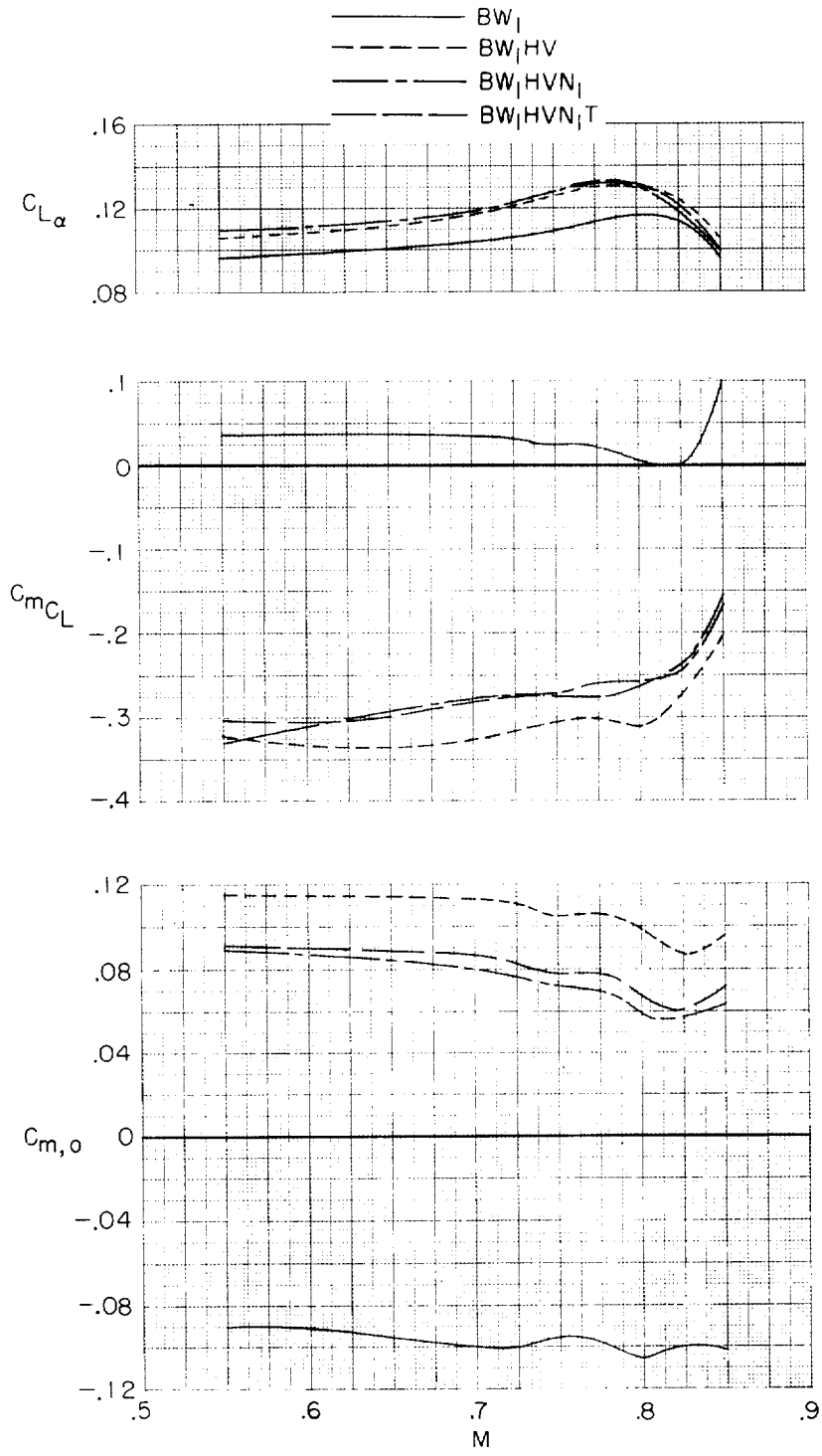

(a) Lift and stability characteristics.

Figure 15.- Effect on the aerodynamic characteristics of adding horizontal and vertical tails, nacelles and pylons, and flap-track fairings with $\delta_h = -0.5^o$. Transition fixed.

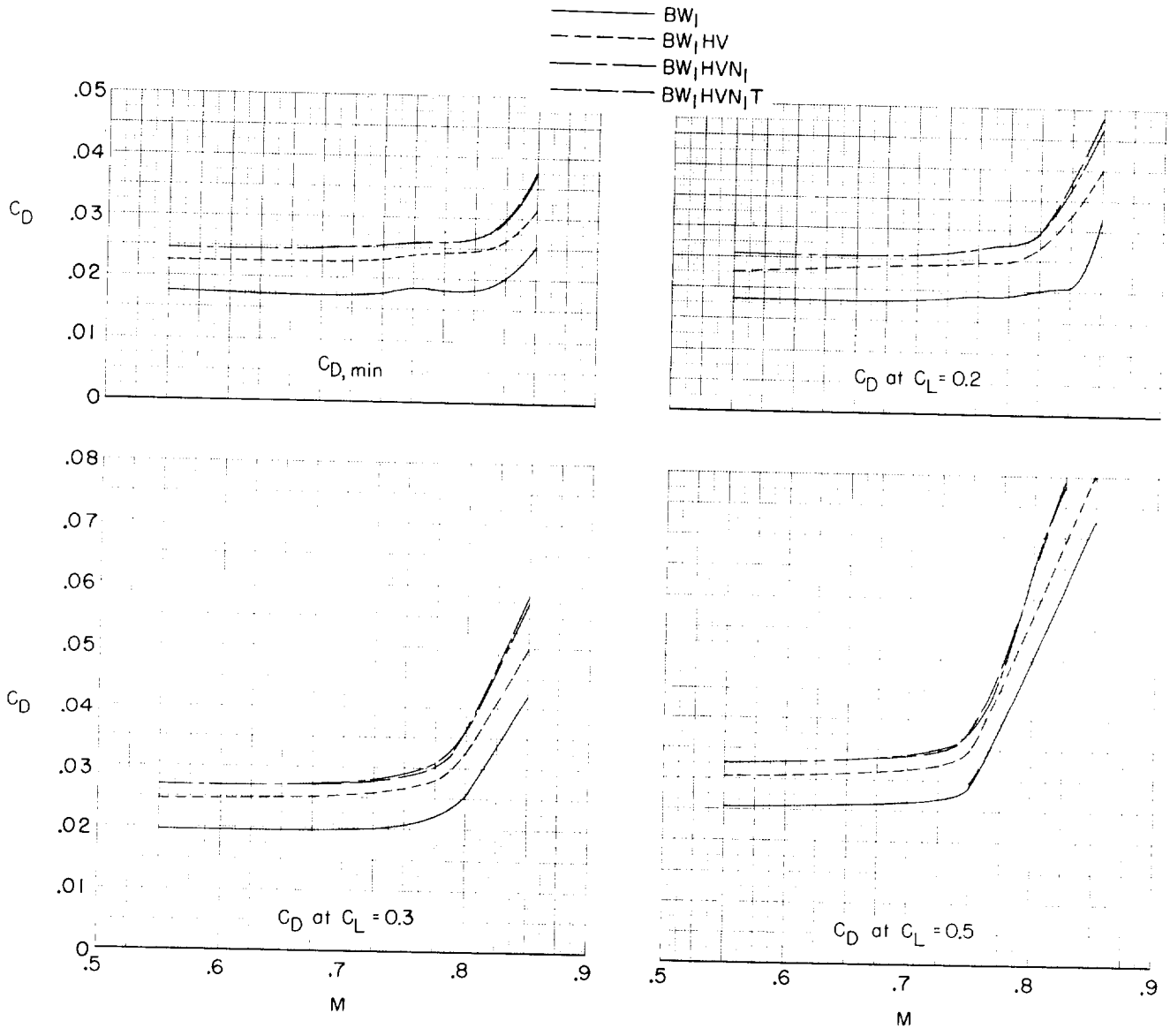

(b) Drag characteristics.

Figure 15.- Continued.

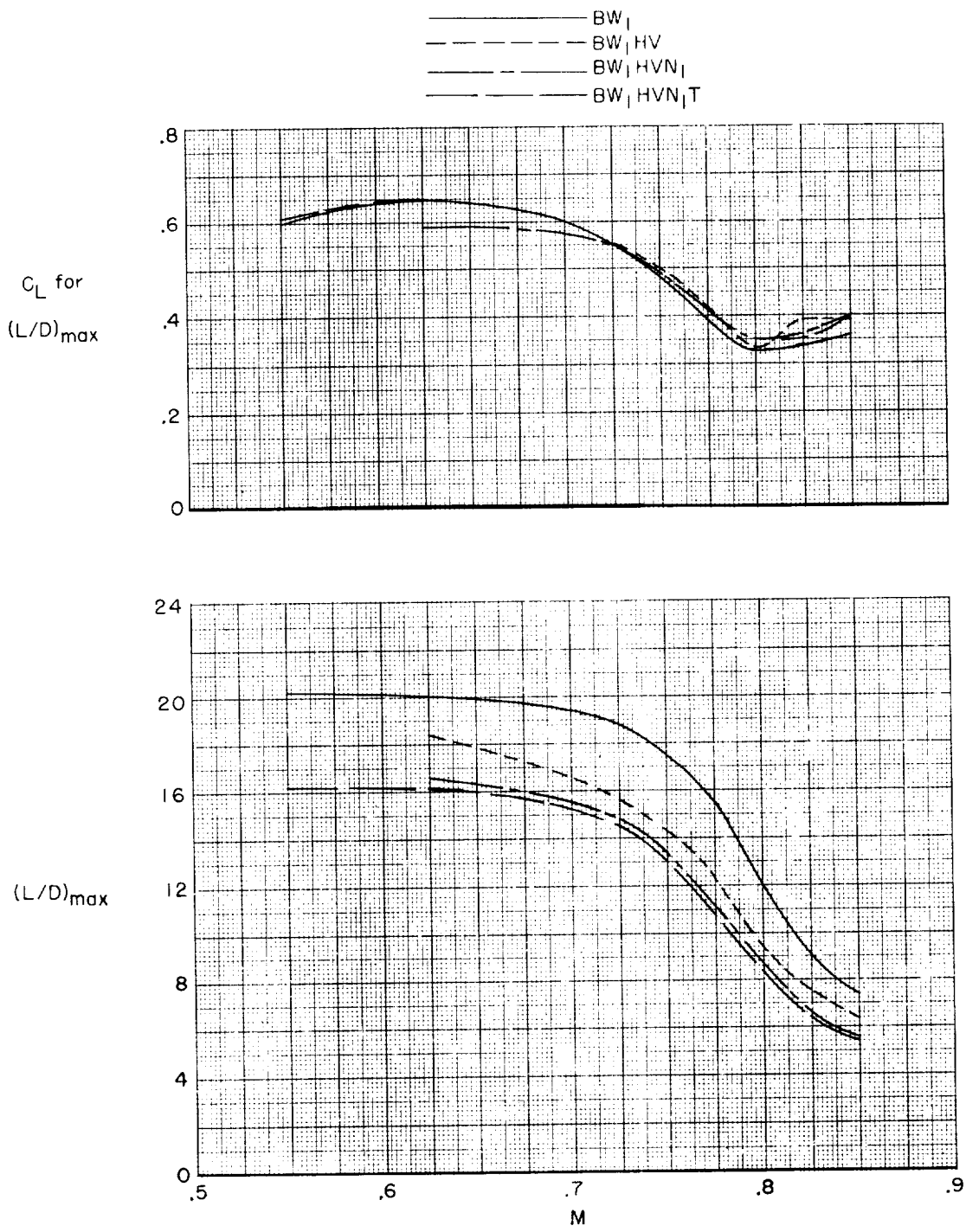

(c) Lift-drag-ratio characteristics.

Figure 15.- Concluded.

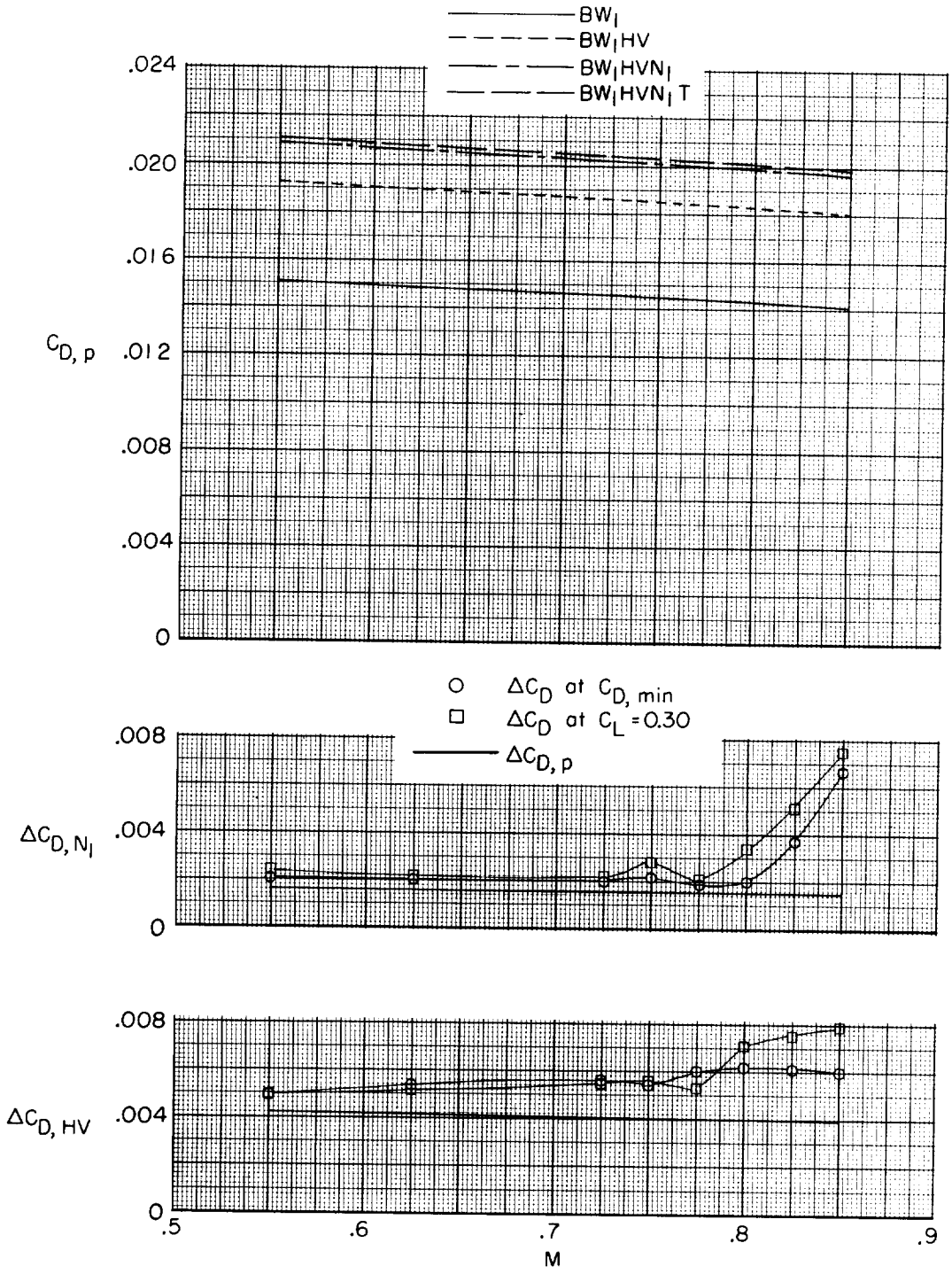

Figure 16.- Computed profile drag coefficients and measured incremental drag coefficients for the nacelles and tails.

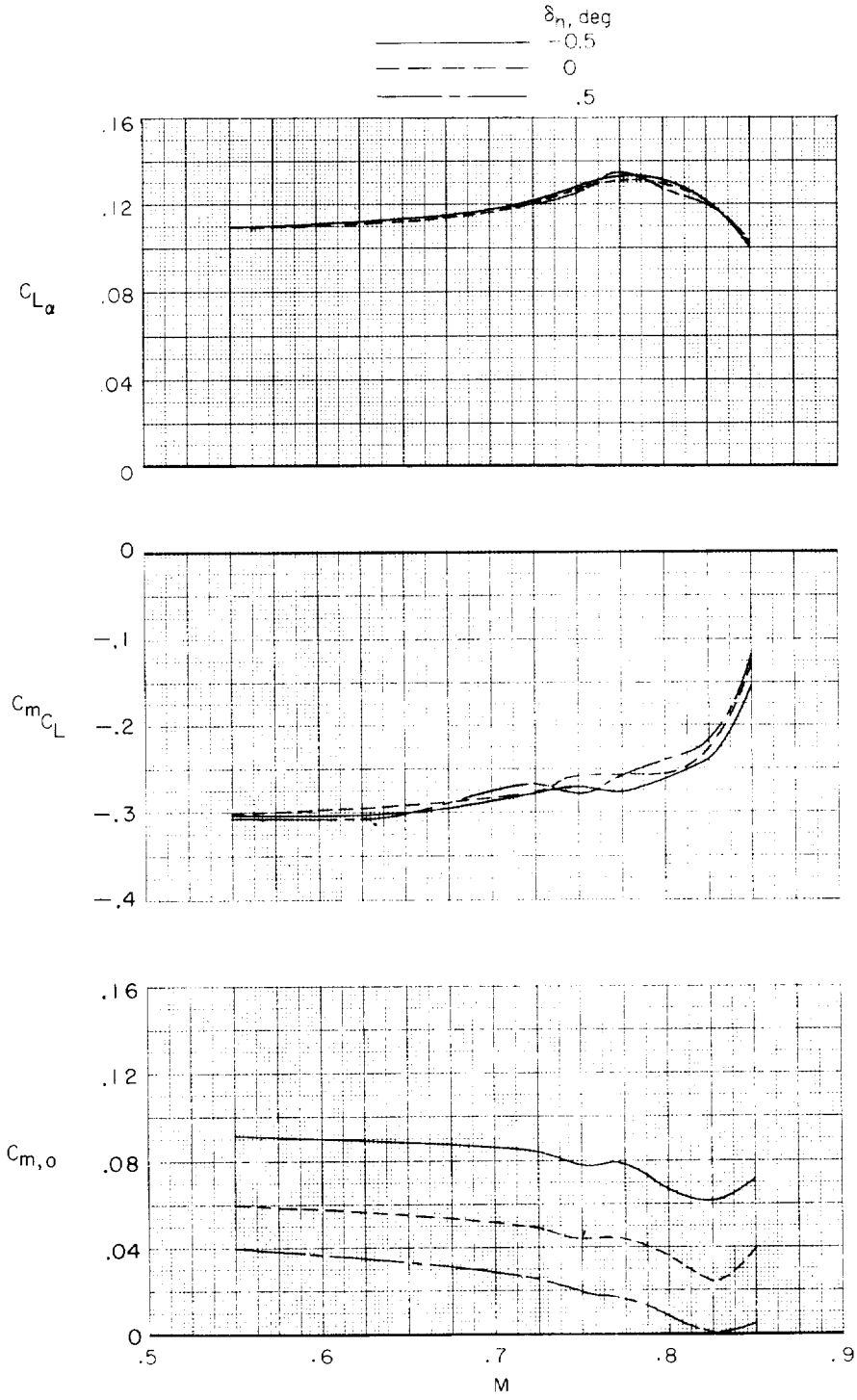

(a) Lift and stability characteristics.

Figure 17.- Effect on the aerodynamic characteristics of horizontal-tail deflection for configuration BW_1HVN_1T. Transition fixed.

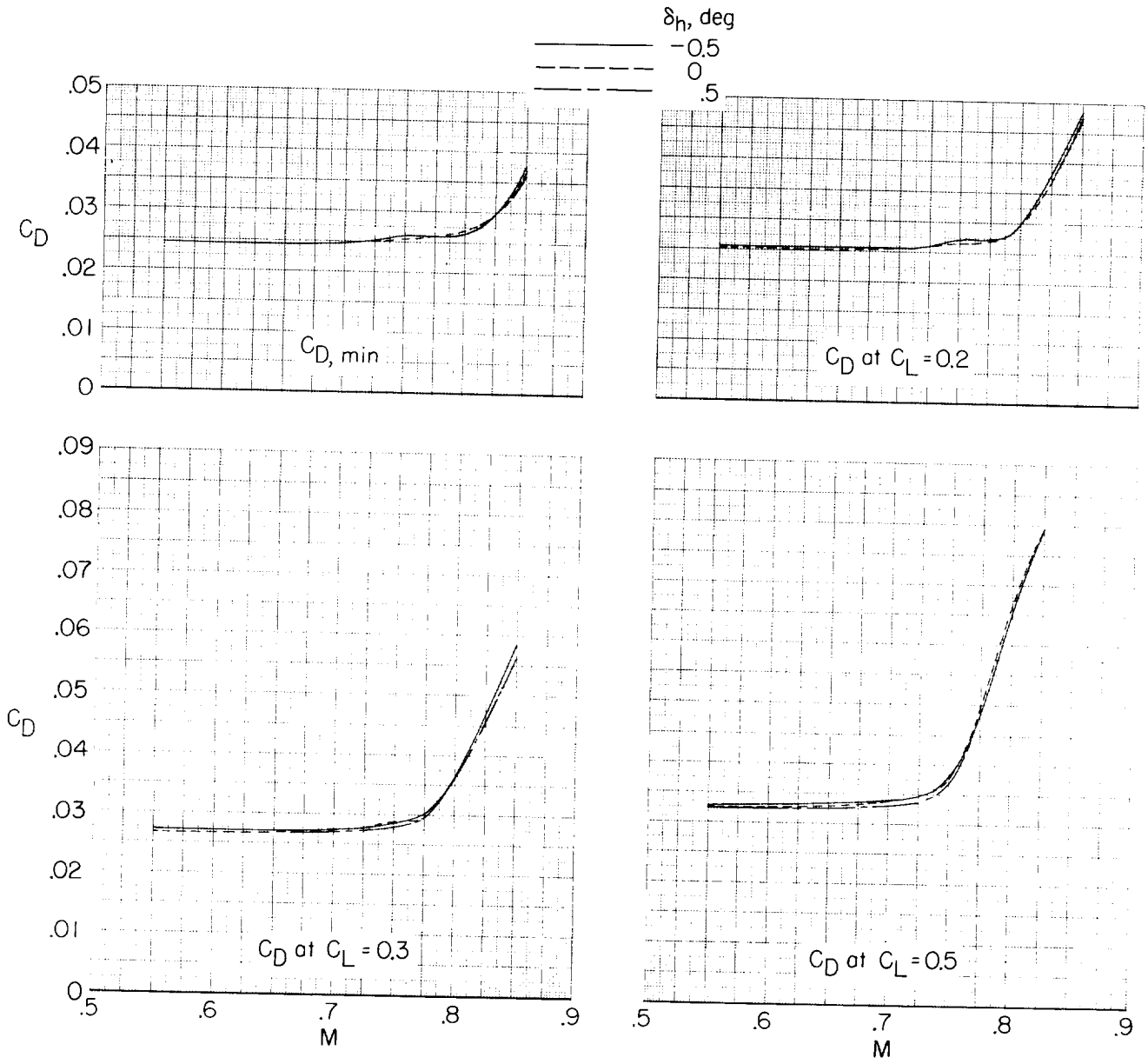

(b) Drag characteristics.

Figure 17.- Continued.

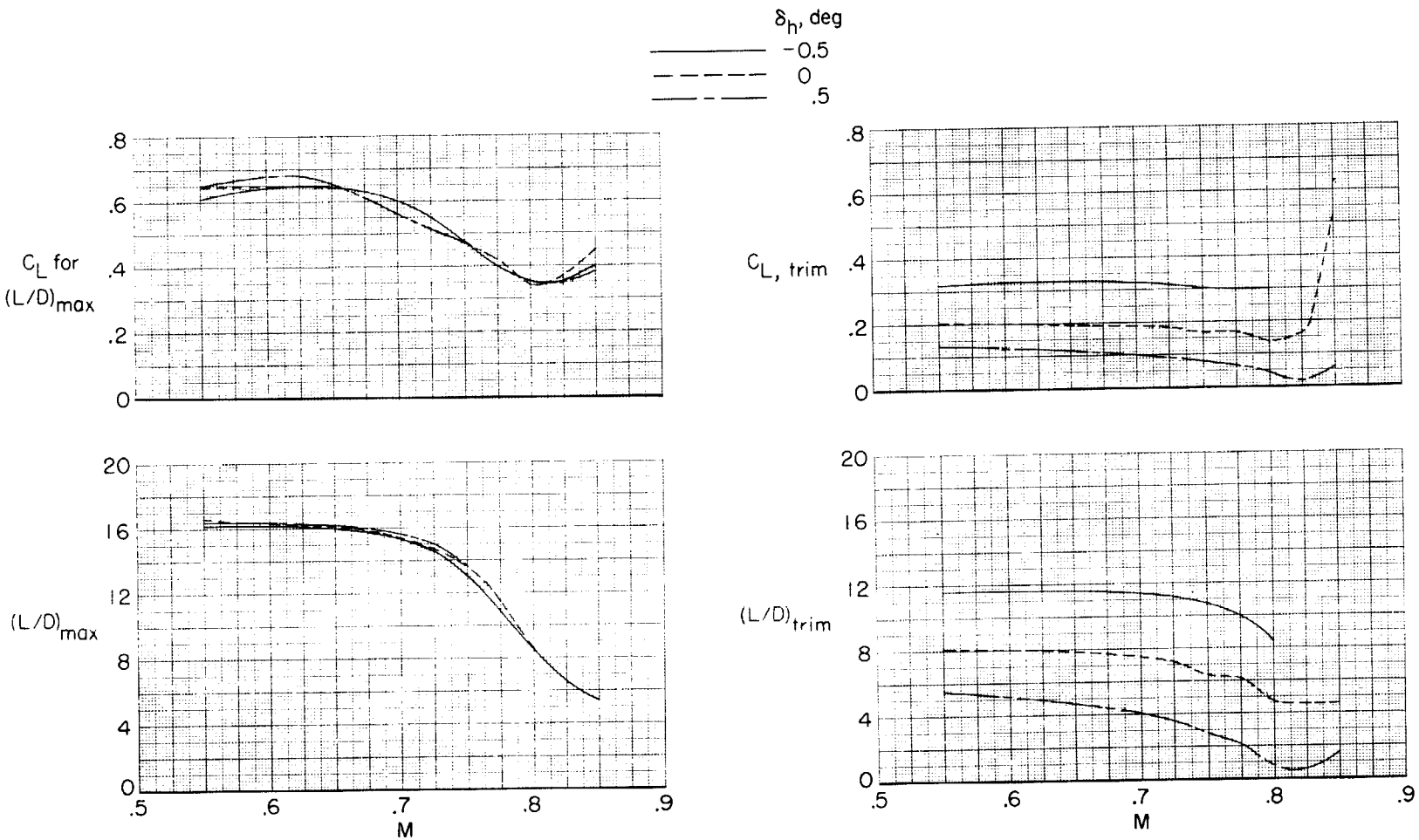

(c) Lift and lift-drag-ratio characteristics.

Figure 17.- Continued.

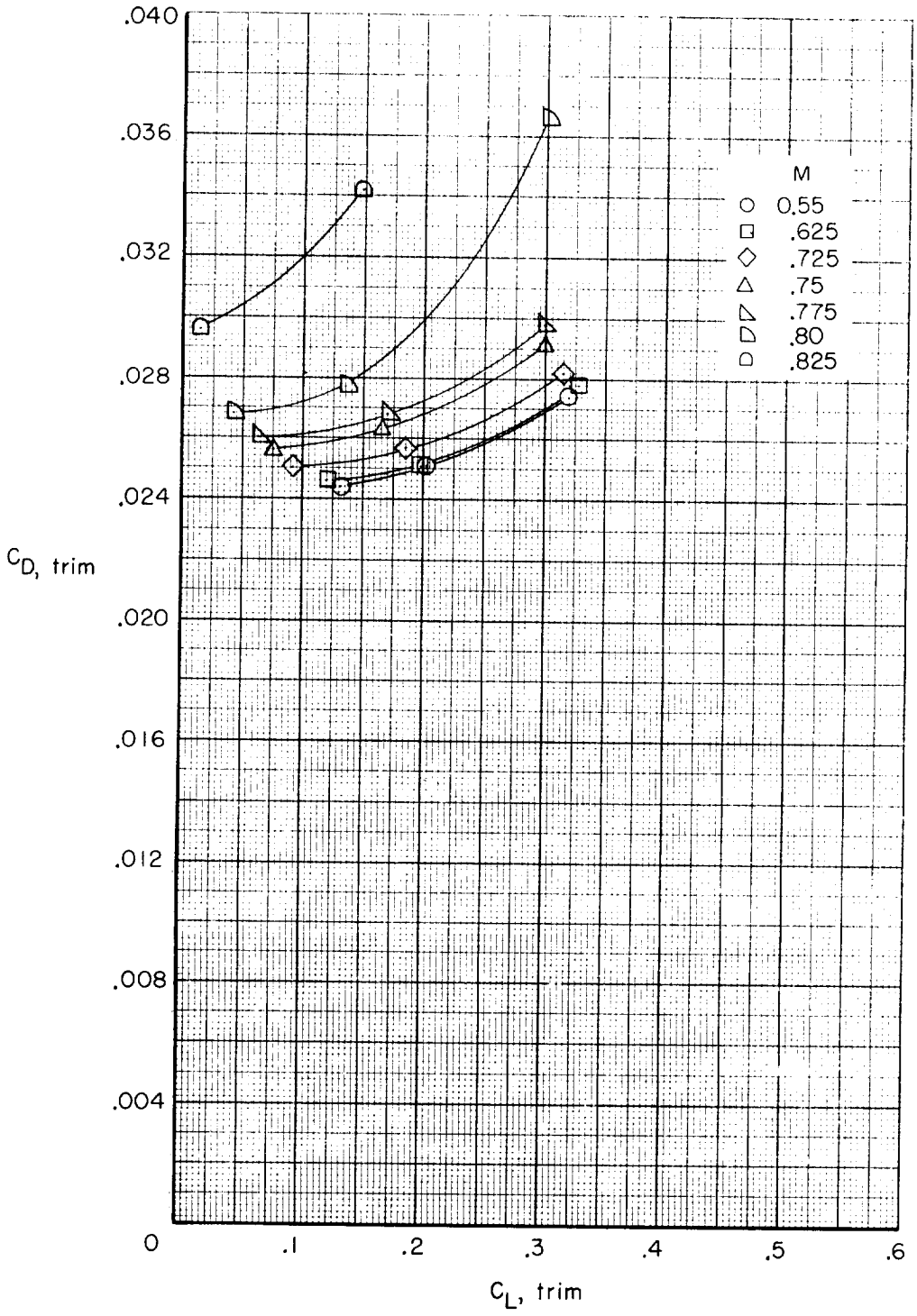

(d) Trimmed drag polars. Symbols represent trim points.

Figure 17.- Concluded.

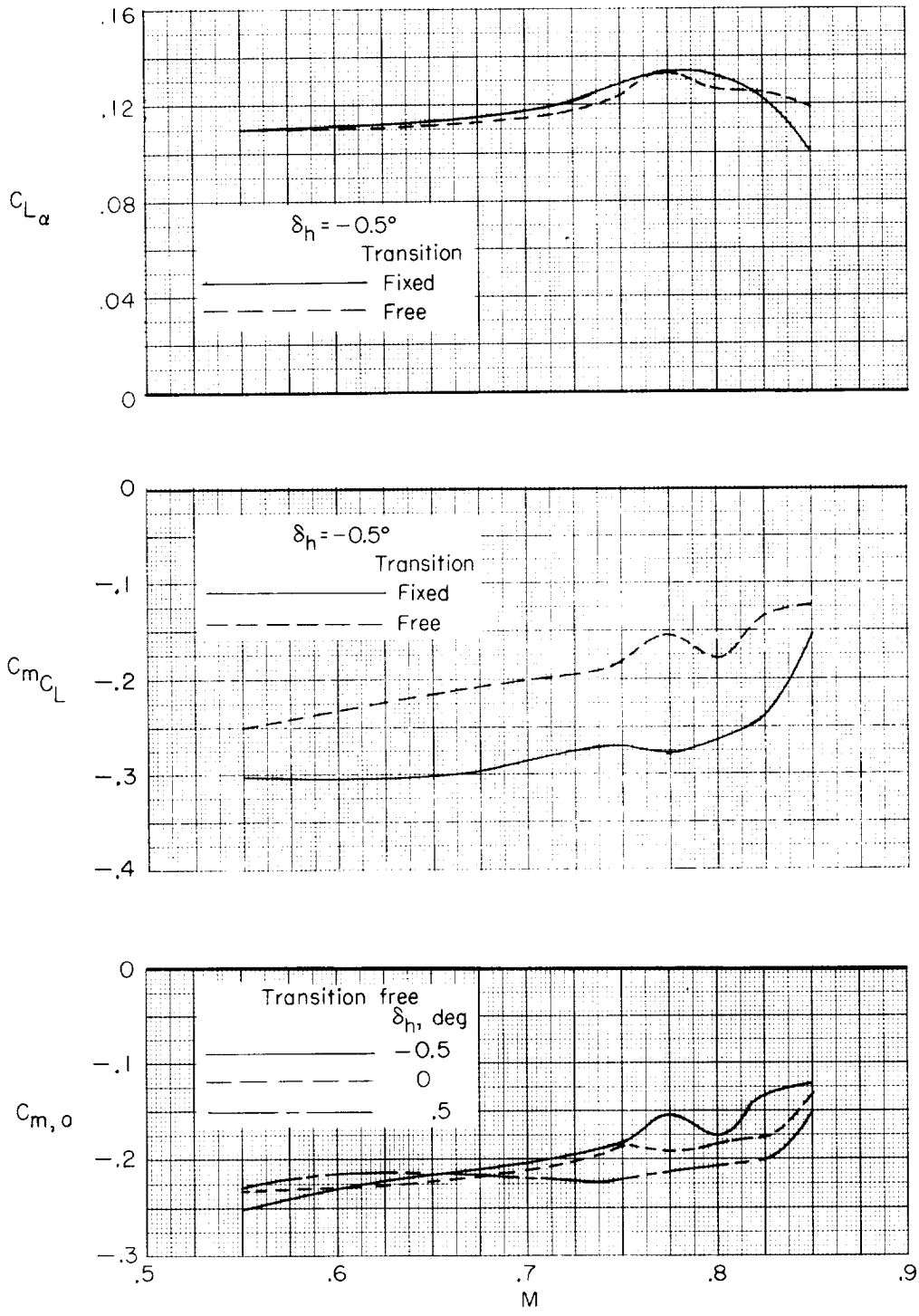

(a) Lift and stability characteristics.

Figure 18.- Effect on the aerodynamic characteristics of fixing transition for configuration BW_1HVN_1T.

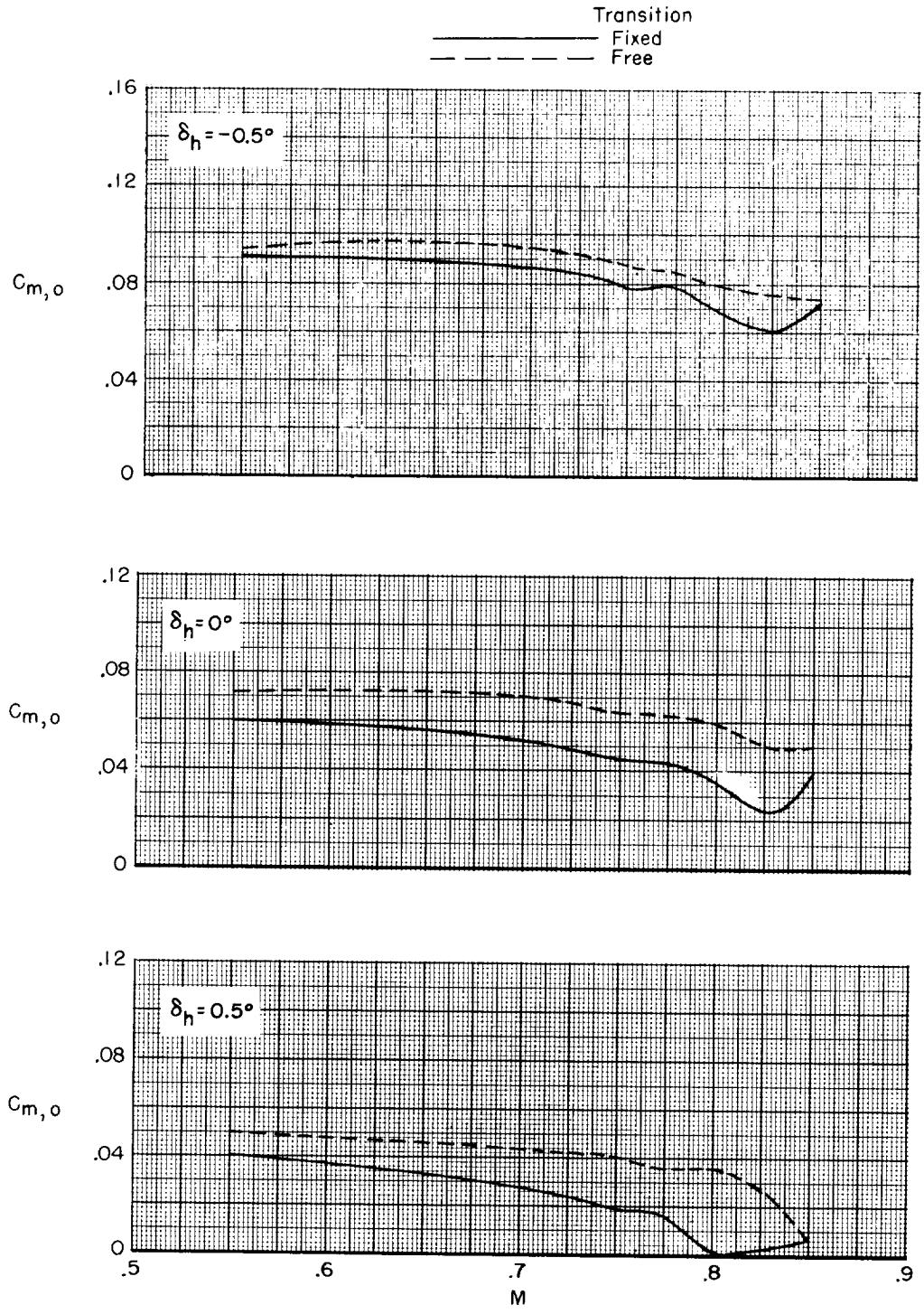

(b) Pitching moment at zero lift $C_{m,o}$.

Figure 18.- Continued.

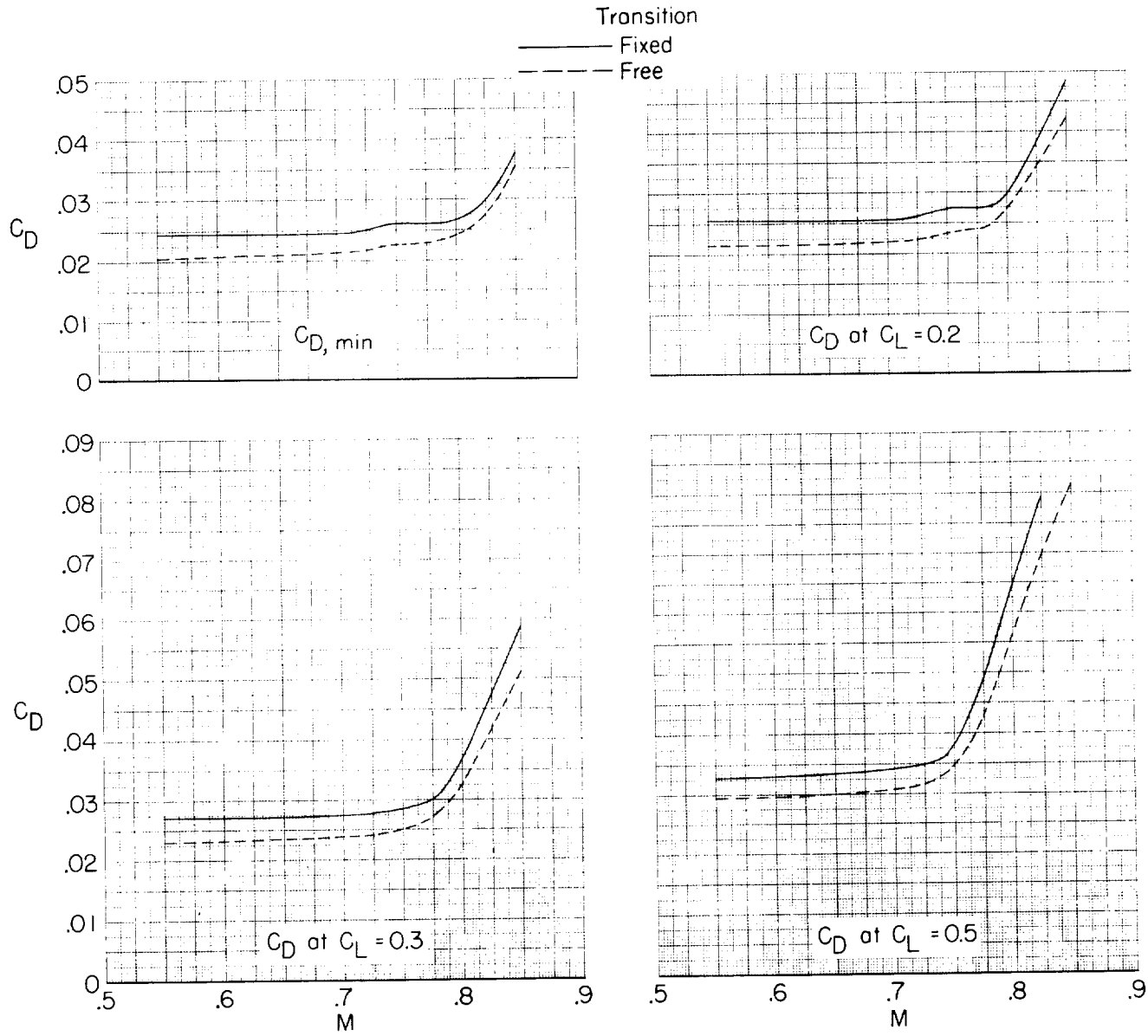

(c) Drag characteristics with $\delta_h = -0.5^0$.

Figure 18.- Continued.

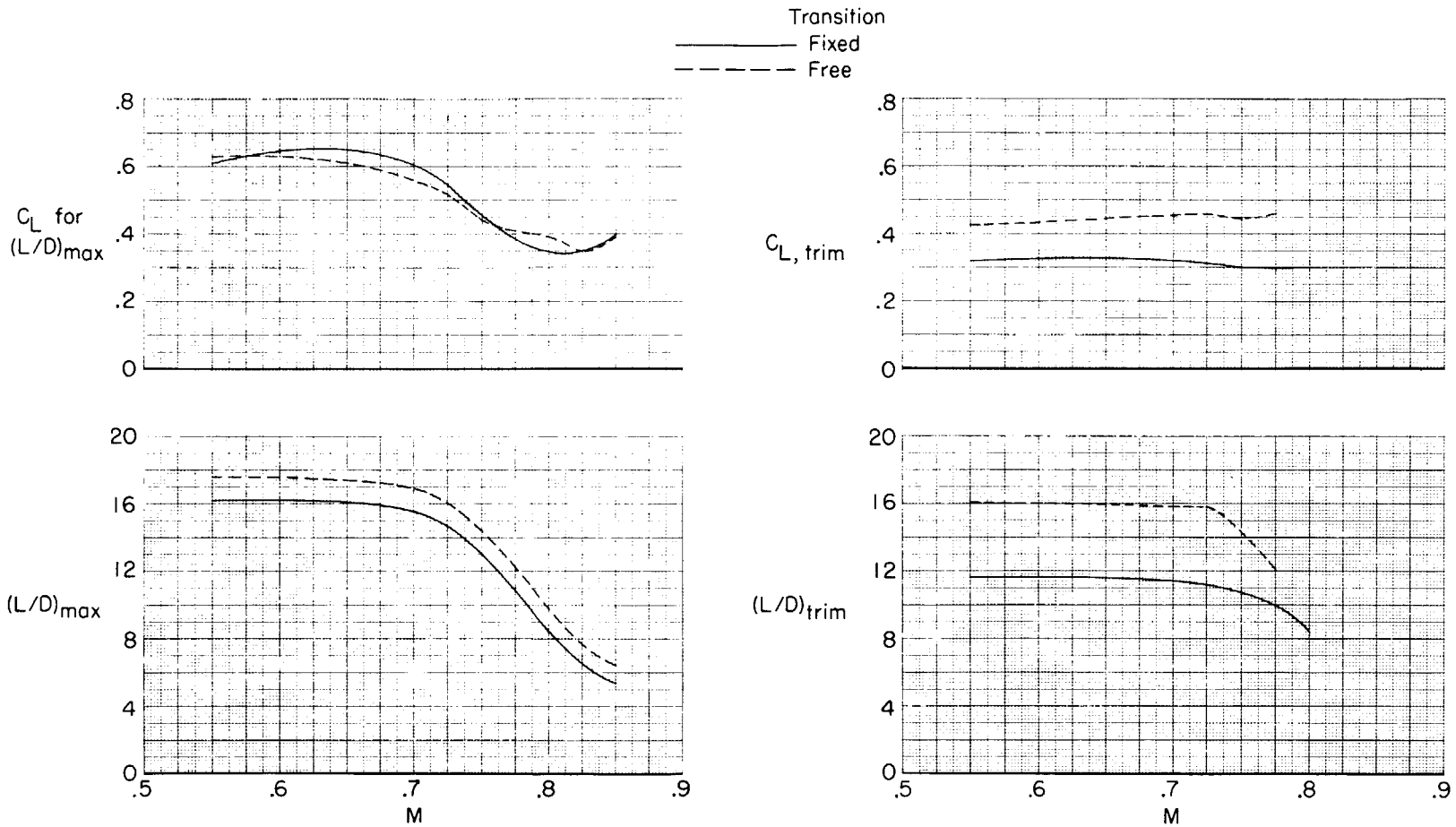

(d) Lift and lift-drag-ratio characteristics with $\delta_h = -0.5^0$.

Figure 18.- Concluded.

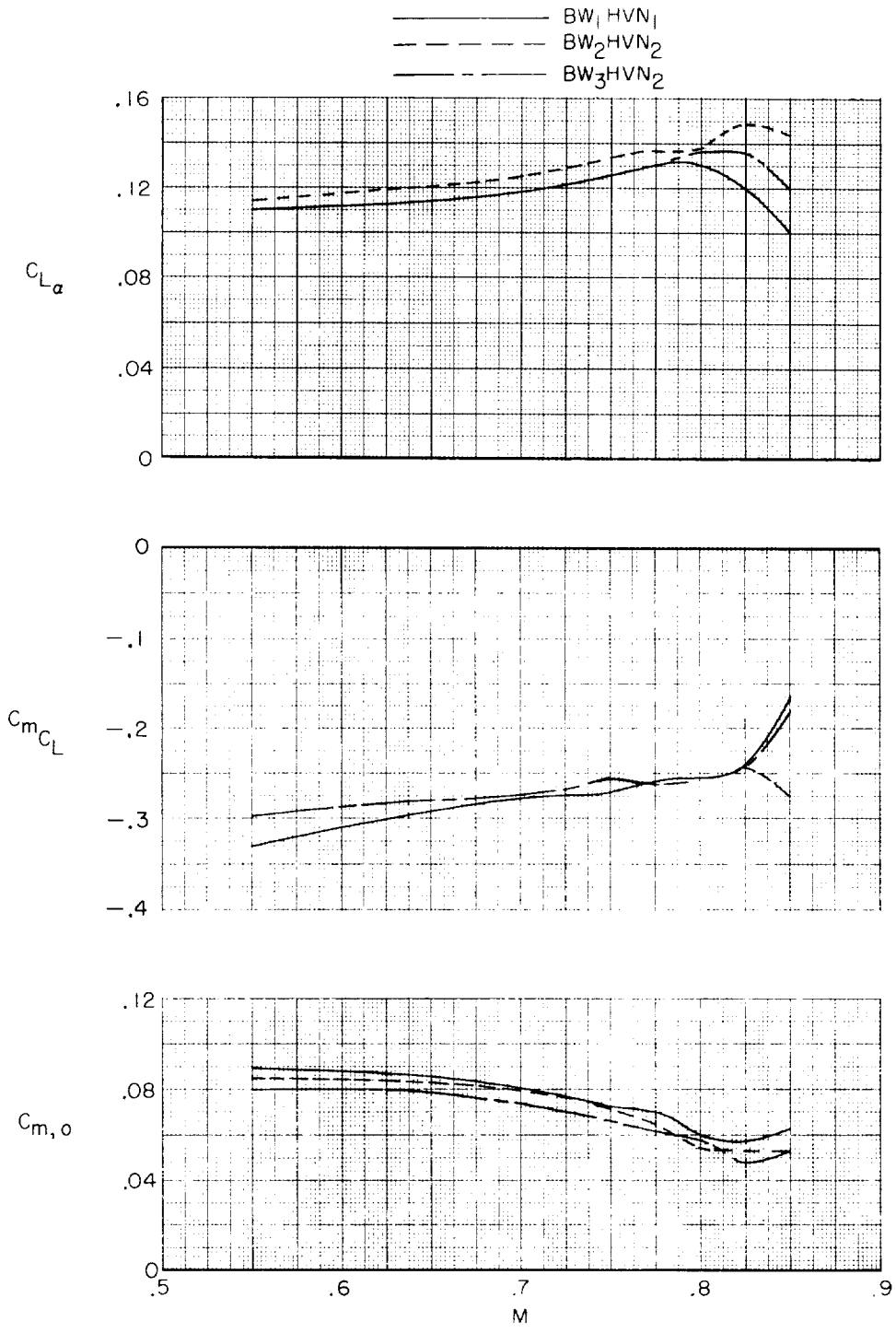

(a) Lift and stability characteristics.

Figure 19.- Effect on the aerodynamic characteristics of wing modifications with $\delta_h = -0.5^o$. Transition fixed.

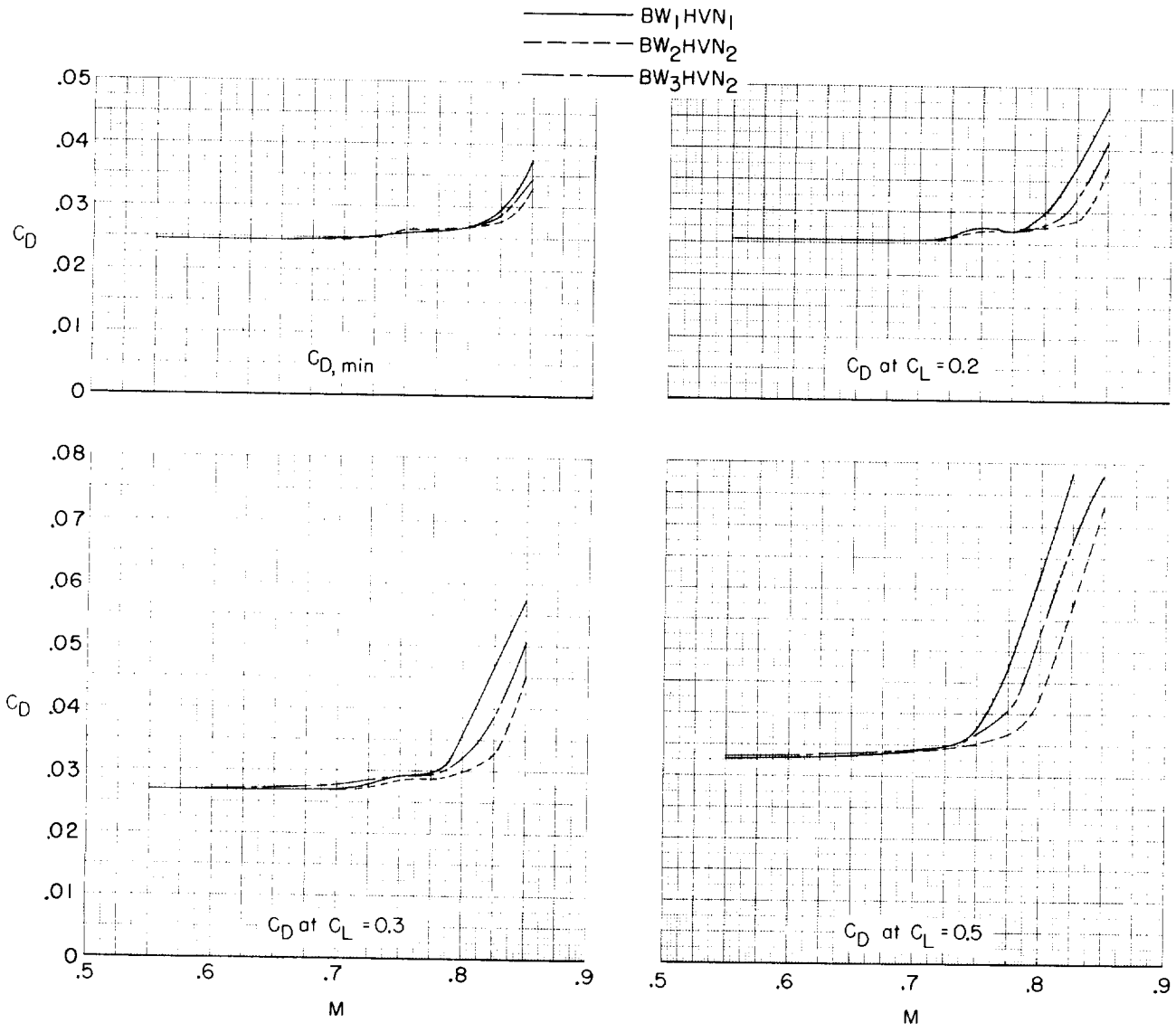

(b) Drag characteristics.

Figure 19.- Continued.

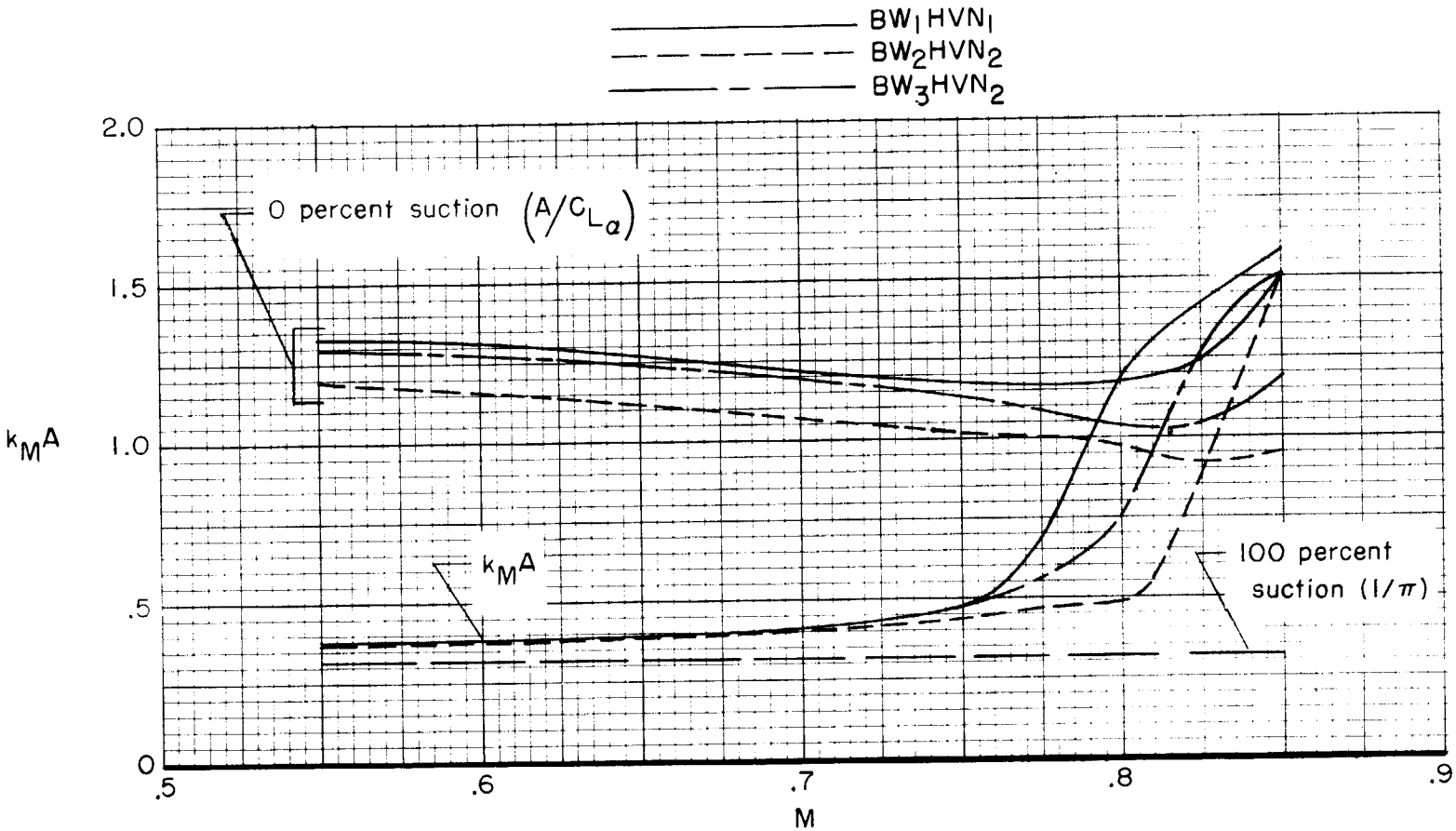

(c) Drag due to lift parameter.

Figure 19.- Continued.

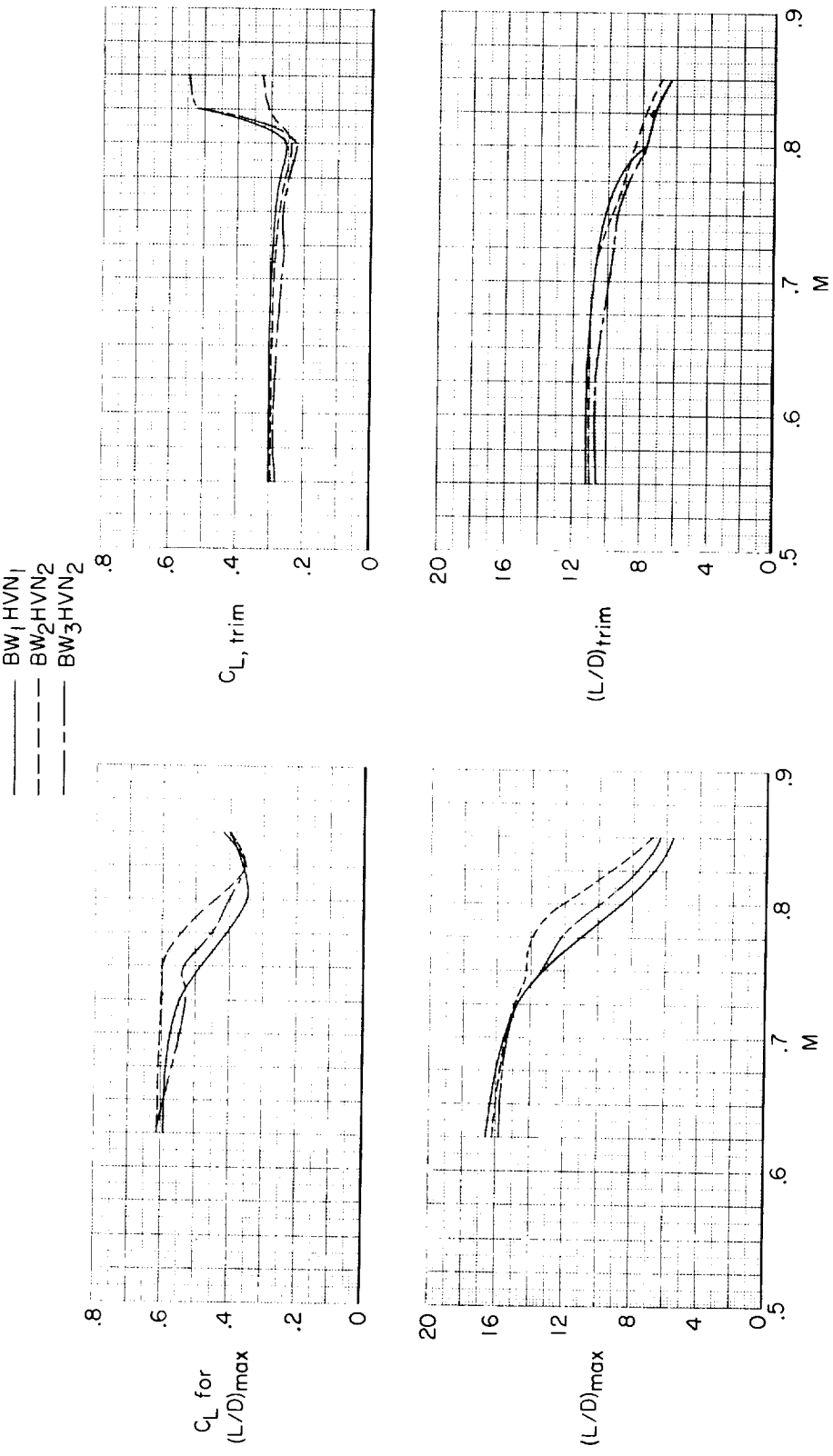

(d) Lift and lift-drag-ratio characteristics.

Figure 19.- Concluded.